THE ROLES OF NUCLEOPROTEIN AND PHOSPHOPROTEIN STRUCTURE ON MUMPS VIRUS RNA SYNTHESIS

by

JACQULINE RISALVATO

(Under the Direction of Biao He)

ABSTRACT

Mumps virus (MuV) is a negative-sense, non-segmented, RNA virus from the genus Rubulavirus and family *Paramyxoviridae*. A human pathogen, MuV causes acute enlargement of the parotid glands, fever, and fatigue (1). Being highly neurotropic, it is also capable of causing mild meningitis and severe encephalitis and is still the leading cause of virally acquired adolescent deafness worldwide. While mumps infection has been decreased significantly due to the introduction of the MMR vaccine in the late 1960's, there have been several large outbreaks in young, highly vaccinated populations in the 21st century (2-5). To better control and characterize these outbreaks, a better understanding of MuV replication and the roles its proteins in replication and infection is critical. There are three key proteins involved in MuV replication: the nucleoprotein (NP) which encapsidates the RNA genome, the large (L) protein which is essential for genome replication and transcription, and the phosphoprotein (P) which acts as a cofactor for both L and NP to allow their interactions (6). In this work, we examined the roles of NP and P structure on

viral RNA synthesis. Through mutational analysis of MuV NP based on the crystal structure of PIV5's NP, we discovered impacts on viral growth kinetics and developed a mutant virus capable of producing high levels of DI particles. Furthermore, mutational studies of MuV P determined that not only is P trans-complementary in its functions, but the N- and C-terminal domains exhibit chiral properties necessary for its structural stability and assist in its ability to form homodimers, heterodimers, and its hallmark tetramer of two homodimers oriented in antiparallel. This discovery assisted in the development of a novel method of determining dynamic sites, as well as a model for the MuV P coiled-coil polar ends. This work improves our understandings of how protein structure directly impacts MuV replication and growth and advance the development of next-generation antiviral therapies and vaccine candidates.

INDEX WORDS: Mumps; MuV; paramyxovirus; defective interfering particles; DI particles; nucleoprotein; phosphoprotein; anti-parallel tetramer

THE ROLES OF NUCLEOPROTEIN AND PHOSPHOPROTEIN STRUCTURE ON MUMPS VIRUS RNA SYNTHESIS

by

JACQULINE RISALVATO

BS, University of South Carolina, 2015

A Dissertation Submitted to the Graduate Faculty of The University of Georgia in Partial Fulfillment of the Requirements for the Degree

DOCTOR OF PHILOSOPHY

ATHENS, GEORGIA

2021

THE ROLES OF NUCLEOPROTEIN AND PHOSPHOPROTEIN STRUCTURE ON MUMPS VIRUS RNA SYNTHESIS

by

JACQULINE RISALVATO

Major Professor: Biao He
Committee: Melinda Brindley
Ming Luo
S. Mark Tompkins
Kaori Sakamoto

Electronic Version Approved:

Ron Walcott
Dean of the Graduate School
The University of Georgia
May 2021

DEDICATION

This work is dedicated to my husband, Frank Risalvato, for his constant love and support. Thank you for spending eleven years and counting with me. Thank you for believing in me always and pushing me to achieve my goals and to reach for the stars, no matter how far away those dreams may seem. I hope I have made you proud.

ACKNOWLEDGEMENTS

I would like to acknowledge and thank my major professor, Biao He, for his helpful advice and constant pushing for improvement. While not always appreciated in the moment, your guidance and constant presentation of countless opportunities to explore all ideas and options has helped me learn how to accept my mistakes and relish in my accomplishments.

I would like to thank my committee members Melinda Brindley, Ming Luo, Kaori Sakamoto, and S. Mark Tompkins for their support and guidance during this specific process and for all other curve balls life has thrown my way during my candidacy.

To the past and future members of the He lab, I thank you tremendously. Yuan Lin, Cristina Huertas-Diaz, Kelsey Briggs, Ashley Beavis, Mark Phillips, Huiling Wei, Zhuo Li, Mathew Abraham, Shannon Phan, Jimmy Zengel, and Adrian Pickar-Oliver, thank you for your encouragement, willingness to discuss projects, assistance, and friendship. To Lei Wang, I miss your jolly smile and laughter tremendously, and wish we could have had more time together.

Thank you to my parents, siblings, and grandparents for their support and being interested in my endeavors even when you did not fully understand what I was discovering. Your support, love, and efforts to understand my work and passion helped drive me to be a better communicator and develop my research.

Finally, although already dedicated to you, thank you Frank Risalvato for everything you have done for me during this journey. You moved across the country,

married me, adopted two dogs and one cat, and traveled the world for me. You push me to be my best self every day and to let my passion drive me. Thank you for strengthening my desire to create a better world.

TABLE OF CONTENTS

Page

LIST OF TABLES

Page

LIST OF FIGURES

Page

CHAPTER 1

INTRODUCTION

Mumps virus (MuV) is a negative-sense, single-stranded RNA virus in the family *Paramyxoviridae,* genus *Rubulavirus*. A human pathogen, MuV causes acute infection, with hallmark parotid gland enlargement, and is highly neurotropic (1). Widespread vaccination campaigns in the 1960s with the MMR (measles, mumps, rubella) vaccine using the Jeryl Lynn strain led to a significant reduction in the number of mumps cases. Since the turn of the twenty-first century, there have been several notably large outbreaks of mumps even within vaccinated populations (2, 3, 5). Currently, there is no approved antiviral therapy for mumps infection, and there is a growing concern that the existing MMR vaccine is not as efficacious in combating newer circulating MuV strains (7).

One antiviral target for combatting this issue is the process of viral RNA synthesis during infection. Both the phosphoprotein (P) and nucleoprotein (NP) of paramyxoviruses are heavily involved and partake in many roles during viral RNA synthesis (6). Phosphoprotein is a critical cofactor for L polymerase, the key enzyme for replicating the mumps viral genome. Additionally, P chaperones L to the NP-RNA genome template (8). Nucleoprotein protects and uncoils the RNA genome of mumps and is crucial in the budding process from host cells (9).

The hypothesis for this research is that the structure of NP and P are critical for transcription and replication of MuV RNA, and their interactions together can also shed light on the viral replication process. The following specific aims will be addressed:

Specific Aim 1: To determine how structure modulates function of MuV NP by mutating amino acid sites to those found similarly in parainfluenza virus 5 PIV5. A crystal structure of MuV NP has yet to be developed; however, PIV5 NP has been crystallized. Due to their high identity, the differences in PIV5 and MuV NP were determined and sites in MuV NP mutated to represent those found in PIV5 NP. The hypothesis is that by exchanging amino acid sites between similar paramyxovirus NP, the structure and function of specific domains of MuV NP may be determined.

The second arm of Specific Aim 1 is to determine how defective interfering (DI) particles can be innately developed by MuV due to the structural changes to the MuV NP. Using binding affinity and interference assays developed for this investigation, a novel MuV with a mutated NP domain is hypothesized to inherently produce high numbers of DI particles that inhibit viral replication due to affects in viral genome replication.

Specific Aim 2: To determine the role of the amino and carboxy terminal domains of MuV P (P_{NTD} and P_{CTD}, respectively) and how the structure of P affects viral RNA synthesis. We mapped the regions within MuV P that are important for its functions. Deleting the very ends of the P_{NTD} and P_{CTD} abolished function, but there is no data to show that they do not interact with NP. A novel minigenome assay was developed to investigate effects of an alanine screen in theorized NP-P binding domains in P_{NTD} and P_{CTD}. The working

hypothesis is that these amino acid substitutions will have impacts on replication protein interactions and structural stability of P, thus displaying how P's unique antiparallel tetramer structure affects MuV viral replication.

The investigation and development of these specific aims will provide increased understanding of the role of both NP and P in MuV replication. Characterization and expansion of the understanding of viral proteins and how their structure affects viral RNA synthesis will prove crucial in the development of successful antiviral strategies.

CHAPTER 2

LITERATURE REVIEW

History and classification

MuV is classified as a member of the family *Paramyxoviridae*, subfamily *Paramyxovirinae*, and genus *Rubulavirus* (1). The *Paramyxoviridae* family is divided into the *Paramyxovirinae, Pneumovirinae*, and unclassified paramyxovirus subfamilies. A few honorable mentions from the *Paramyxovirinae* subfamily are Newcastle disease virus, Sendai virus, and Measles virus. From subfamily *Pneumovirinae*, some well-known examples are human respiratory syncytial virus, Bovine respiratory syncytial virus, and Human metapneumovirus. J paramyxovirus and Beilong virus are two of the many viruses from the Unclassified paramyxoviruses subfamily (10). MuV is primarily a human pathogen possessing a nonsegmented, negative-sense, single-stranded RNA genome of 15,284 nucleotides (1). Parainfluenza virus 5 (PIV5), also in the *Paramyxovirinae* subfamily, is the most closely related virus to MuV genetically.

In the 5th century BC, MuV is believed to be first described in the first book of the *Epidemics* by Hippocrates. Hippocrates described symptoms and pathologies we still see due to MuV today – malaise, parotitis, orchitis, as well as hearing loss in both children and adults, predominantly male (11). This documentation helps support the theory that MuV entered and sustained transmission within the human population approximately 5,000 years ago based on anthropologic estimations of population densities at that time (12). It was not

until 1790, however, that the physician Hamilton associated the involvement of the central nervous system (CNS) with mumps disease progression (13).

Koch's postulates were originally developed during a time in which viruses had not yet been discovered, which made the determination of MuV as the etiological agent of mumps disease difficult (14). Once the discovery of "filterable agents" (viruses), during an experiment to determine the etiology of tobacco mosaic disease by Ivanofsky in 1892, came to the forefront, the use of bacteria-free filtrate to isolate viral etiology soared (15). This pioneering of viral research led to several studies by Johnson and Goodpasture to prove a virus to be the etiological agent of mumps disease in 1934. The first arm of their experiments demonstrated that Rhesus macaques inoculated with the filtered saliva from individuals with mumps disease led to the display of similar mumps clinical symptoms. Additionally, saliva from healthy individuals did not cause disease in the macaques. The researchers took their experiments one step further to fulfill Koch's postulates; virus from monkeys with mumps-like illness was used to infect naïve children, and the saliva from these children was then used to infect naïve monkeys, resulting in parotitis (16, 17). While these experiments would not ethically be performed today, they were critical to the understanding of the viral etiology of mumps.

MuV was then shown to be successfully isolated and propagated in embryonated chicken eggs in 1945 (18, 19). While this development in MuV research not only aided in characterizing MuV, it was also shown to be attenuated via serial passage in eggs, which would inevitably lead to vaccine development (20). Tissue culture eventually became the standard for MuV propagation and study in 1955 (21), and the first vaccine against MuV was developed in 1958 (22, 23).

Structure and Morphology

Microscopy of MuV was successfully done in the 1960s and found MuV virions to be enveloped and pleomorphic, ranging from 100 to 600 nm in size (24, 25). The matrix (M) protein of MuV forms a structured virion shell underneath the cell-derived lipid envelope. The small hydrophobic (SH) protein is embedded within the viral membrane, indicating a role in viral exocytosis (26). The outer glycoproteins of the virus, hemagglutinin-neuraminidase (HN) and fusion (F) protein, project up to 15 nm from the enveloped viral surface, thus giving MuV a "studded" appearance (24). Linked to the M protein on the inside of the virion is the ribonucleoprotein (RNP) complex, which is formed by the nucleoprotein (NP) and viral RNA genome. The genome is encapsidated by the NP to form a left-handed, helical nucleocapsid 0.98 μm in length (27). Thirteen NP subunits form one nucleocapsid ring, along with 78 nucleotides of the RNA genome, keeping true to the paramyxovirus "Rule of Six". The "Rule of Six" is where the viral genome is a multiple of six in order to maintain full encapsidation of the RNA genome by each NP subunit (each NP subunit binds to six nucleotides) (28-30). The nucleocapsid rings stack upon one another to form a long helical capsid with a total diameter ranging from 17 to 20 nm (27). An electron microscopy image and 3D illustration of MuV are provided in Figure 2.1 and 2.2, respectively.

Mumps virus genome

The nonsegmented, single-stranded, negative-sense, MuV RNA genome is 15,384 nucleotides in length. The genome is a series of seven transcriptional units: 3'-Leader Sequence-NP-V/P/I-M-F-SH-HN-L-Trailer Sequence-5' (visually depicted in Figure 2.3). These seven transcriptional units encode for a total of nine proteins, with three of these proteins being transcribed by the V/P/I gene (1, 31). The production of three different genes (V, P, and I) by the singular V/P/I transcriptional unit is done via RNA editing. V is considered to be the "true" transcript, and the insertion of either two or four non-template guanine (G) residue(s) into a G-rich coding region in the cysteine-rich open reading frame of V results in the formation of the P and I mRNA, respectively (32). In other words, the transcription of P is due to a +1-reading frame shift, and the transcription of I is due to a +2-reading frame shift. This shift is better examined visually in Figure 2.4. All three of these proteins possess the same amino (N)-terminus but different carboxy I-terminus regions due to this frame shift. The use of the V/P/I ORF in MuV is a prime example of how some viral genomes can encode for multiple proteins without increasing their size.

The MuV viral genome is led by a 3' leader region that is 55 nucleotides long and terminated by a 5' trailer region with 24 nucleotides. Transcription and replication levels of the virus are regulated by the order in which the transcriptional units are oriented 3' to 5' (proteins upstream in the genome are made in higher abundance than those downstream) and the untranslated regions between them. The gene start and end sequences at the beginning and end of the transcriptional unit, respectively, signal for mRNA synthesis polyadenylation and termination by the viral RNA-dependent RNA polymerase (vRdRp or L). The untranscribed regions between the transcriptional unit are referred to as intergenic

regions, as they are nucleotides between the genes that are unable to be translated to mRNA.

Mumps viral proteins

Nucleocapsid protein

The nucleocapsid protein (nucleoprotein or NP) is 549 amino acids in length, 61 kD in size, and is the most abundant protein of MuV as it is the first transcribed gene within the genome. There are two main domains of NP: the N-terminus and C-terminus or tail (33). The N-terminus is the largest of the two at 400 amino acids in length and has arguably the most important roles. The N-terminal domain is often referred to as the assembly domain, as it is responsible not only for the encapsidation of the RNA genome but also the formation of the nucleocapsid. Additionally, this domain is responsible for phosphoprotein (P) binding. This interaction with P is also what allows the viral polymerase to associate with NP and recognize the RNA genome for replication (34-36). While the N-terminus is conserved among paramyxoviruses, the C-terminus is reportedly hypervariable and intrinsically disordered in structure (27, 34, 37).

In a negative-strand RNA virus (NSRV), the primary function of NP is to encapsidate the viral genomic RNA by forming the nucleocapsid during viral replication. During viral RNA transcription and replication, the NP binds to both the viral genome and antigenome regardless of sequence specificity, making this ability of NP a hallmark for nonsegmented NSRVs (38). The NP structure is also nuclease-resistant, aiding in the protection of the viral RNA genome from innate immune defenses. For replication, the helical nucleocapsid is uncoiled by the N-terminus of MuV P, and this NP-P interaction allows the vRdRp to access the viral genomic RNA template (27, 39).

While primarily known for its structural functions, nascent NP (NP^0) without a RNA genome exists in a soluble form within the cell. During viral transcription, P binds to a NP monomer to form an NP^0-P complex. P then acts as a chaperone to prevent NP^0 from accidentally encapsidating cellular RNA in the cytosol (40, 41). Once enough NP^0-P complexes have accumulated, this triggers a "switch" from viral transcription to replication, and the NP^0 molecules then form a new nucleocapsid to encapsidate MuV RNA (42, 43).

Phosphoprotein

The phosphoprotein (P protein) of MuV is produced by an insertion of two non-template guanine nucleotide residues at the G-rich region of the V/P/I ORF. When translated, P is approximately 47 kD in size and 391 amino acids in length (6). As a cofactor of L and NP functions, P protein has several roles in both virus replication and transcription (44).

As the name suggests, the phosphoprotein of MuV is highly phosphorylated by host cell kinases at serine and threonine residues. This phosphorylation of P is believed to regulate aspects of MuV RNA synthesis (44). PLK1 (polo-like kinase 1) and RPS6KB1 (ribosomal protein S6 kinase beta-1) are two examples of human host cell kinases that phosphorylate phosphoprotein, and in turn induce a negative effect on MuV transcription and replication (45, 46). P protein is a key regulator of MuV transcription and replication.

While the P protein does not have intrinsic enzymatic activities, it interacts with NP and L as an adaptor for the RNP complex. P protein acts as a chaperone for L polymerase to access the NP and RNA template and allow genome transcription and

replication (47). Additionally, the P protein binds to NP within both its N-terminal and C-terminal regions (39, 48). P binding to NP is essential for successful MuV replication and transcription. Nascent NP self-assembly and accidental encapsidation of host cell RNA is prevented by P binding to NP (9, 40). It has also been shown that P binding to NP functions as an "anchoring" mechanism for the vRdRp to the NP-RNA template (39, 47). P's unique structure among paramyxoviruses as a tetramer formed by a pair of P dimers in anti-parallel orientation is believed to be essential to its stability and role in NP and L interactions and will be discussed further in this work.

V protein

At approximately 25 kD in size and 224 amino acids in length, the V protein of MuV is a non-structural protein produced during the infection phase of the virus life cycle (6). The V protein's mRNA is considered the "faithfully" transcribed mRNA by the V/P/I gene, whereas the P and I mRNA transcripts are made by RNA editing in a cytosine-rich region of the gene. Through this cytosine-rich region, V binds to MDA5 (melanoma differentiation-associated protein 5), thereby blocking both interferon (IFN) expression and interleukin-6 (IL-6) signaling by degrading STAT-1 and -3 (49-52).

The MuV V protein is known to be incorporated within MuV virions as seen similarly in PIV5. It is thought that this incorporation of V allows for MuV replication once inside the host cell by blocking innate immune pathways, thus playing a critical role in MuV pathogenesis (53). Additionally, V protein has been shown to interact with the MuV replication complex and, thus, is involved in the transcription and replication process (54).

V protein incorporation into the virion is hypothesized to be performed by NP interactions, as the N-terminal domain of P (which is also shared with V) is known to interact with NP.

I protein

The I protein of MuV (or C or W protein, as it has also been called) is produced due to a shift in the V/P gene ORF; in this case, the shift is due to the addition of one guanine residue at the same editing site that leads to the translation of P from the V transcript. The I protein is 19 kD and 171 amino acids in length, making it the smallest of the three proteins derived from the V/P/I transcriptional unit. While the role of the I protein remains indeterminate, I polypeptides have been detected in virus-infected cells (32, 55). Though not required for virus replication, through its shared N-terminal domain with V and P, the I protein could be involved in either immune-mediated responses (via interactions with V) or replication (via interactions with P) (56).

Matrix protein

The matrix (M) protein is essential for viral budding and assembly. The M protein is 40 kD in size and 375 amino acids in length (6, 57). M protein supports MuV particle structure by forming an inner layer beneath the external membrane, whereby the protein folding creates an external capsid surface of positively charged domains that bind on to and interacts with the negatively charged lipid membrane outer layer (58). M protein is required for MuV particle budding but only through its interactions with NP and F glycoprotein. In addition to its interactions with NP and P for assembly, M protein has been shown to recruit and interact with host proteins to assist in gathering viral components at

the plasma membrane to assemble the virion and bud from the cell (59-62). The late domains (named due to their role in the later stages of viral budding) FPVI and FPIV amino acid motifs in M protein of both MuV and PIV5, respectively, are essential in M's interaction with host proteins at the plasma membrane surface (60, 63).

Fusion protein

A type I transmembrane protein, fusion (F) protein facilitates virus-to-cell and cell-to-cell membrane fusion. F protein is first produced in an inactive precursor form, F_0, which is 74 kD in size and 538 amino acids in length. A glycoprotein, F_0 undergoes N-glycosylation in the rough endoplasmic reticulum before it is then cleaved by host endoprotease furin in the Golgi apparatus. This cleavage at amino acid residues 98-102 (RRHKR) yields the F_1 and F_2 subunits, which are linked via disulfide-bonds (64-66). This formation of a F_1+F_2 heterodimer is required for F to be actively fusogenic.The F_1 subunit is the larger of the two at 61 kD, while the F_2 subunit is 16 kDa. This cleavage exposes a hydrophobic domain within the N-terminus of F_1.

Hydrophobic residues within fusion proteins have been found to be relatively conserved among paramyxoviruses. Heptad repeats of hydrophobic residues are found in the F_1 ectodomain of MuV. Heptad repeats 1 and 2 (HR1 and HR2) form a stable six-helix bundle which is involved in MuV fusion, however, the precise mechanisms of this HR1 and HR2 stability formation have yet to be elucidated (67-69). What is known is that the HR domains of F act to assist in the joining of the viral and cellular membranes and, thus, have an essential role in viral-to-host membrane fusion (70, 71).

Small Hydrophobic protein

Small hydrophobic (SH) protein is the smallest protein of MuV, named both for its size (6 kD and 57 amino acids long) and numerous hydrophobic residues (72). The orientation of SH protein is not widely conserved among paramyxoviruses; MuV SH has its C-terminal domain facing the cell cytoplasm, while PIV5 SH has its N-terminal domain facing the cytoplasm (73).

While this type 1 membrane protein is nonessential for MuV replication, it is involved in mediation of host immune responses, and its absence has been found to increase NFκB activation and apoptosis in L929 cells. Experiments in which SH was deleted from the MuV and PIV5 genomes showed that SH protein inhibits TNF-α (tumor necrosis factor alpha) signaling and increases NFκB activation (74). rMuVΔSH, when infected intracranially in infant rats, displays attenuation and reduced neurotoxicity (75).

Though the SH protein is influential in MuV growth and pathogenicity, its gene is hypervariable to the degree that the SH nucleotide sequence of MuV is used to identify different MuV strains (26, 76, 77). However, varying success of complete extraction of the SH nucleotide sequence from MuV infected individuals in the field due to its small size and low expression levels can make identification of some circulating strains difficult (26).

Hemagglutinin-neuraminidase protein

A type II transmembrane glycoprotein, the hemagglutinin-neuraminidase (HN) protein is 80 kD in size and 582 amino acids in length. During viral entry, HN recognizes sialylated glycoconjugates, as it is capable of binding sialic acid as a receptor, making HN responsible for MuV attachment to the cell surface (78-81). The binding of HN to cell

surfaces has been attributed to pathogenicity, with a mutation of E335K in the Urabe vaccine strain being attributed to increased neurovirulence and affinity for α2,6-sialic acid linkages that are found in greater abundance on the membrane of human neuroblastoma cells (82, 83).

Additionally, HN has enzymatic activity as a neuraminidase via removal of sialic acid groups from budding virus particles, making HN essential for viral release. The removal of sialic acid molecules for viral progeny minimizes aggregation by interactions between potential virus receptors and glycoproteins that would limit viral spread (84).

The HN protein is also essential for the activation of F so that fusion between the host cell and viral membranes can be completed. Studies have shown that proteolysis of HN results in attenuated fusion activity by F protein (85).

Large protein

The largest of the paramyxovirus and MuV proteins, the Large (L) protein is 200 kD in size, 2,261 residues in length, and has low expression in MuV-infected cells due to it being the transcriptional unit farthest from the leader sequence in the viral genome. While L protein is responsible for enzymatic activities of initiation, elongation, and termination of RNA synthesis, it is L and cofactor P together that comprise the vRdRp (86). Other enzymatic activities of L include the addition of the 5’ cap to the 3’-poly(A) tail of transcribed viral mRNA and methyltransferase activity (86-89).

Due to its critical role in viral transcription and replication, mutations within L protein can be catastrophic to viral replication. Additionally, L protein’s large size makes it prone to mutations during transcription. There are six conserved domains separated by

variable regions in the L protein. Domain II has a potential RNA binding site and is positively charged, and Domain III is possibly an active site for phosphodiester bond formation – Domains II and III together constitute the polymerase component of L protein (90, 91). Domain V is responsible for 5' capping of mRNA, while Domain VI has methyltransferase activity (87-89, 92). The individual functions of Domains I, II, and IV remain unclear; however, mutagenesis studies have suggested that they may be involved in regulating the switch from transcription-to-regulation functions of the polymerase (93).

For vRdRp function, the complex of P-L is critical. The N-terminal of P binds to L and facilitates the docking of L to the NP and vRNA template for genome synthesis. Without its chaperone, P, L becomes uncoordinated in its ability to successfully perform replication and transcription, as it can no longer secure its attachment to the NP-vRNA template (94-97). This dynamic between P and L has been found in almost all paramyxoviruses, including SeV, PIV5, hPIV3, MeV, and VSV. Many of the functions of L are conserved among paramyxoviruses, but the binding sites of L to other replication proteins (NP and/or P) for some of these viruses remains to be elucidated (86).

Viral entry

To enter the target cell, MuV HN protein binds to sialic acid on the cell surface to initiate viral-to-host cell membrane attachment. The binding of HN to the receptor induces a conformational change in the F protein, which leads to the fusion of the viral membrane to the cell membrane (71, 84). Once the virion's membrane has fused to the cell surface, the MuV helical nucleocapsid and genetic material are released into the cell cytosol (6). This type of viral entry is referred to as membrane fusion and is seen among a variety of enveloped viruses and is the predominant mode of viral entry for paramyxoviruses.

Viral replication and transcription

To begin viral replication, the proteins NP, P, and L are needed to form the replication complex. These three proteins are packaged within the virion and are thus present upon MuV entry and release of intravirion contents within the cell. The MuV RNA genome is associated with NP to form the ribonucleoprotein (RNP) complex, which functions to both protect the genome from degradation and expose the genetic template for replication when prompted by vRdRp binding. The genes within the MuV genome are defined by an upstream start and a downstream end signal sequence. The intergenic regions between these transcriptional units are short and not transcribed; however, they do contain *cis*-acting signals for viral transcription (98). It is believed that the process of transcription is begun first, and the genome is replicated later in the life cycle, but the regulation of this switch by the vRdRp remains unclear (99-101). Some proposed mechanisms are P phosphorylation levels or that a "critical mass" of P production is reached, as P can interact with both RNP and nascent NP (9, 34, 35, 39).

Synthesis of all the viral mRNA transcripts is initiated at the 3' leader sequence; it is here that the vRdRp transcribes the viral genome into mRNAs with a 5' cap and 3' poly(A) tail. As the vRdRp moves down the genome and across the intergenic regions, it is reinitiated downstream at the sequential gene's start site. Failure of the polymerase to successfully reinitiate this process causes the 3' to 5' gradient of mRNA transcripts, and gene order in the MuV genome thus reflects viral protein amounts (102, 103).

The vRNA genome is replicated by first producing a positive-sense (or anti-genomic) RNA. The anti-genome is then replicated into the negative-sense vRNA by the vRdRp at the 5' trailer sequence. The MuV ribonucleocapsid can hold both the negative- and positive-sense vRNA genomes. However, only encapsidated RNA can be transcribed, which makes the MuV RNP exhibit anti-termination functions by forcing the vRdRp to ignore transcription signals in the intergenic regions of the genome to successfully produce a full-length RNA genome (6).

Structure of the NP, P, and L proteins are critical to their function in viral transcription and replication. While the NP of paramyxoviruses share similar genetic identity, their structures vary between viral species. Some of these differences include the number of NP units required to make one full ring of the helical capsid, the width of the helical capsid, and the distance between the turns of stacked NP rings (104). Each nuance of NP structure can impact access to the RNA template by the polymerase and RNA stability. Additionally, the P protein of paramyxoviruses has variability in their tertiary structures and domain(s) where NP and L bind. The kinases and degrees of phosphorylation of P among paramyxoviruses are also variable (44, 45, 48, 105). The impact of MuV NP and P structure on its replication will be discussed further in this work.

Viral assembly and budding

Newly synthesized negative-stranded RNA genomes are encapsidated by the NP, where it then associates with the P-L complex in the cytoplasm. Simultaneously, mRNAs are translated and viral proteins are transported via the exocytic pathway to the inner plasma membrane. The matrix protein then binds to the NP, cytoplasmic tails of F and HN, and then organizes and assembles these proteins along the lipid membrane. M, NP, and F proteins have previously been shown to be essential for efficient viral assembly and virion production, with M being the key coordinator of the budding events and linking the viral envelope to the RNP for incorporation into the virion (60, 106). F protein is the major contributor of the two glycoproteins in virion egress, while HN does not significantly increase particle budding from the host cell, as it functions primarily in viral entry. Cell-to-cell fusion to form syncytia, however, requires the expression of both F and HN within the same cell, so HN does play a role in syncytia formation, a paramyxovirus hallmark (85, 107). Additionally, HN protein's neuraminidase activity may function in the prevention of self-aggregation of virus particles – a unique characteristic of MuV and parainfluenza viruses in the paramyxovirus family (71, 78, 85, 108). A figure demonstrating the MuV life cycle from viral entry, to replication and transcription, translation, assembly, and finally budding can be seen and is described in Figure 2.5.

Nucleoprotein – the role of structure and function in MuV replication

Though NP is an essential protein for paramyxovirus replication, the morphology of these proteins exhibits some commonalities, as well as differences, that set several paramyxoviruses apart. The number of NPs required to make a ring structure, the distance between these rings, how many rings, and so on impacts the way the RNA genome of each virus is accessed by its respective polymerase complex and its stability (104).

Characterization of the MuV nucleocapsid complex was achieved using an *E. coli* expression system. When co-expressed with P, NP-RNA rings were formed with 13 NP subunits, and these rings did not require the presence of RNA. As predicted, when RNA was incorporated into the expression system, it was found that each NP ring encapsidated 78 nucleotides, which matched the expected size to maintain the paramyxovirus rule-of-six. Further detailed analysis using cryo-electron microscopy of purified nucleocapsid revealed a traditional herringbone structure that is seen in many paramyxoviruses (27, 47).

To better understand the NP-P interaction, the aforementioned researchers co-transfected RNP components and interactions were visualized. Only when the C-terminal domain of P was expressed alongside NP was there little change in the nucleocapsid structure, leading to a hypothesis that the C-terminal of P plays a role in stabilizing NP for docking L to the NP-RNA template. Uncoiling of the NP structure was observed when the N-terminal domain of P was expressed alongside NP, which was suggestive of the P N-terminus being important for accessing the RNA by the vRdRp during genome synthesis. Further analysis using a minigenome system, which is described in Figure 2.6 and has shown to be critical in ongoing research into the mechanisms of protein structure in MuV

replication, revealed that both the N- and C-termini of P were required for vRNA synthesis (39, 48).

While the structure of MuV NP has yet to be crystallized, the PIV5 NP has. At approximately 60% similarity to MuV NP, the PIV5 NP crystal structure has been useful in predictive analysis and understanding of how MuV NPs structure possibly affects its replicative function. MuVs NP cryo-EM structure (10.4-Å) was modeled using the crystal structure of PIV5 NP (109, 110). Since the cyro-EM MuV NP structure lacked the RNA genome, but the RNA genome was crystalized with PIV5 NP, it was difficult to determine if the residue differences interacted with RNA or L. However, the lack of RNA emphasized an opening of a RNA binding groove thought to be needed for the vRdRp to access the RNA template during synthesis (110). The C-terminal tail of NP is highly unstructured, and while no structural information was obtained from this model about this tail, it was found to not be required to form nucleocapsid structures (34, 37). Though not required for structure, if the C-terminal tail of NP is removed, there is no activity in the minigenome system, which suggests the region acts as a template for RNA synthesis either by interacting with the RNA genome or the vRdRp (27, 110).

Altering the structure of NP has various possible implications, as NP plays numerous roles in protecting the vRNA genome, exposing the RNA template for vRdRp transcription, holding the anti-genome and exhibiting anti-termination functions for vRdRp genome replication, encapsidating newly synthesized vRNA genomes correctly, and virion assembly and chaperoning of other viral proteins to the host cell surface for budding. Elucidating how NP structure affects replicative function would aid in understanding the

virus life cycle and provide useful information in developing novel viral targets for therapeutics.

Defective interfering particles

Defective interfering particles (DIPs) and defective viral genomes (DVGs) were first described by Preben Von Magnus in the 1940s while he was working with influenza A virus. After a high titer passage, he noticed a loss in viral titer throughout these high MOI (multiplicity of infection) passages. Von Magnus theorized that virions of "incomplete" virus were produced only when influenza virus was expanded at a high titer, and these particles also interfered with infective virus replication (111). His discovery was referred to as the "Von Magnus phenomenon" and the viral particles "Von Magnus particles" (112). His follow-up experiments showed that these particles developed independently of the number of infective virus particles used in the infection; it is instead dependent on the ratio of infectious (ID_{50}) to noninfectious particles within the original stock (113). "Von Magnus particles" were then found in Rift Valley fever virus, vesicular stomatitis virus (VSV), and Sendai virus (SeV) infections in the 1950s and 60s (114-117).

In the 1970s, Alice Huang and David Baltimore used advanced techniques to characterize and coin the term "defective interfering particles". Huang and Baltimore defined them as particles that "contain normal viral structural proteins…[and] part of the viral genome" and can replicate "in the presence of helper virus". Additionally, they described the interference by these DIPs as "specifically with the intracellular replication of nondefective homologous virus" (118).

In the 1970s and 80s, it became evident that DI particle presence correlated with establishment of persistently infected cells *in vitro* and *in vivo*. Mice infected with DI particles had increased survival rates, and DI particle infections increased production of interferon (112, 116, 119). By the 1990s, poliovirus, rabies, measles, human parainfluenza virus, Semliki Forest virus, Ebola, Sinbis virus, and respiratory syncytial virus (RSV) had become some of the many RNA viruses found to be capable of producing DI particles when grown at high MOIs (112, 120-123).

DIPs characteristically are virus particles biochemically and morphologically comparable to the standard virus particle, but they harbor deletions in their genomes and contain DVGs (defective viral genomes). DVGs often have significant heterogeneity when it comes to the type, structure, deletion location, and size of their genomes, they must retain the initiation and termination elements to allow them to be replicated by intact viral polymerase. RNA viruses in particular have an intrinsic ability to generate DVGs and DIPs throughout a normal course of propagation due to the error-prone nature of the RdRp. Once formed, the DVG can be replicated and packaged into particles to form DIPs, which have the same ability to bud and enter a new host cell as a standard or helper virus. However, the replicative advantage of DVGs is that when in the same cell as a helper virus, DIP production will predominate due to the shorter length of DVGs and increased promotor strength and packaging efficiency (112, 124, 125).

It has been established that, as a basis, DVGs form when the viral polymerase loses its processivity by falling off the template and reattaching elsewhere along the genome to complete replication. This is exacerbated further by paramyxoviruses, for example, as their NP can hold both the sense and anti-sense genomes and create the high heterogeneity and

complexity of DVGs. Truncated viral genomes are categorized as three primary forms: the deletion, copyback, and snapback (126). When the polymerase detaches and reattaches downstream, DVGs are made that share 3' and 5' ends with the full-length viral genomes and the deletion DVG is formed. The copyback DVG is synthesized when the polymerase detaches and reattaches to the nascent (antigenome) strand of RNA, thereby creating a complementary end to the 5' vRNA end, but this rejoining occurs at a nonhomologous region, which creates a nonhomologous loop structure flanked by complementary ends. A third major type of DVG is the snapback DVG; compared to copyback DVGs, they do not have as much of a "loop" in its structure and is mostly complementary, sometimes with as little as one noncomplementary nucleotide at the breakpoint. It is thought that for snapback DVGs, the polymerase falls off of the template at the breakpoint and reattaches quickly to the nascent strand at a nearby rejoin point and begins to make a copyback-esque DVG but without a large, nonhomologous loop (122, 125, 127). The mosaic DVG, a fourth DVG that sometimes occurs, describes a genome that is mixture of deletion, copyback, and/or snapback components. Figure 2.6 provides a visual representation of the three major types of DVGs and how they form. These truncated genomes with promoters of increased RdRp polymerase affinity have biased competition for viral components, and interference with the standard viral genome occurs (125, 126).

Influenza viruses are arguably the most explored virus in the field of DIPs and DVGs, primarily because their segmented genome encourages recombination and reorganization of the viral genome (112, 128). For paramyxoviruses, Sendai virus (SeV) is probably the most extensively studied in terms of defining DIPs and DVGs of this virus family (49, 129). Mononegaviral replication spontaneously produces errors and is prone to

making DVGs (130). Persistent infections with mononegaviruses, including SeV, have showcased intercalating waves of DI genomes, which showed that the accumulation of DI genomes in excess interferes with replication of the authentic genome, causing a decrease in infective virus replication (126). Once this occurred, a reduction in DI genomes also occurred, since replication of DVGs requires intact helper virus replication machinery. These waves repeat during persistent infection and are thought to allow long-term viral infection (112, 125).

SeV has been studied extensively for the characterization of virus-host interactions during innate immune responses. DVGs of SeV have been identified as major type I interferon inducers, primarily interferon-beta (IFN-β), by stimulating the RIG-I pathway (49, 131, 132). This finding of innate immunity triggering by SeV DVGs has assisted in the discovery and characterization of other paramyxovirus DVGs and DIPs, as well as helped in defining mechanisms of DVG production during viral replication and maintenance of persistent infection (122, 129). Yoshida *et al*. recently found that a single amino acid substitution in the N protein, D153Y, induced a heterogeneous virus population with cobyback DIPs predominating. Mice inoculated with this mutant SeV exhibited less pathogenicity and increased IFN-β production. This spontaneous N mutation is hypothesized to weaken the NP-NP interaction within the helical capsid, potentially increasing template switching by the vRdRp and allowing for exposure of the RNA genome to innate immune detection systems within the host cell (129, 130, 133, 134). Better understanding of how NP's structure can affect viral replication and DVG production is needed to help in the development of novel live recombinant vaccine vectors that could provide both antigen and adjuvant functionalities.

The role of phosphoprotein structure in MuV replication

The phosphoproteins of paramyxoviruses contain three primary regions: the N-terminal, oligomerization, and C-terminal domains, along with flexible linkers between these domains. P self-associates via oligomerization, an observed common feature of negative-stranded RNA viruses (NSRVs). This oligomerization occurs through a centralized coiled-coil domain. Through the interactions of hydrophobic side chains as the α-helix interface of oligomerized coiled coils, P monomers can form dimers, trimers, or tetramers (135). Recent crystallization studies have supported differing oligomer formations and suggest that the predominating structure of MuV P is a tetramer (47).

Sendai virus phosphoprotein structure and functions

Crystallization of a paramyxovirus P protein was first done on the oligomerization domain of SeV P and revealed the orientation to be a parallel coiled-coil tetramer. A parallel coiled-coil tetramer indicates that each monomer is in a similar orientation/polarity of their N- and C-terminal domains within the tetramer. Other paramyxovirus P oligomerization domain crystallization has revealed tetrameric P structures for mumps virus, measles virus, and human metapneumovirus.

Alterations of the P domains of SeV to determine their function have been performed without affecting other domain functions. Only when the oligomerization domain of SeV P is deleted, however, is transcription and replication of SeV vRNA inhibited. The inhibition of viral replication upon the deletion of the SeV P oligomerization domain demonstrates that the self-association of P monomers is essential for viral

reproduction (136). While larger than the MuV P at 568 amino acid residues in length, SeV P is similarly divided into an N-terminal domain (head) and C-terminal domain (tail). Similarly to MuV, a N-binding domain of P is found in the N-terminus to function as a chaperone to prevent NP assembly without nascent viral genome (137). The C-terminal residues 479-568 of SeV are also predicted to bind to the NP, which reflects what has been found in other paramyxovirus phosphoproteins (135, 136, 138).

The SeV P oligomerization domain (residues 320-446) houses the SeV L binding site at residues 412-445. When SeV P binds to L to form the vRdRp, P is hypothesized to migrate down the NP-RNA template in sections of six nucleotides, while the SeV NP protein encapsidates six nucleotides per monomer. It has been proposed that to allow the L protein to progress over the RNA template one nucleotide at a time, the SeV P protein "cartwheels" over the NP-RNA template during L transcription. This proposed mechanism would mean that the P and L interactions are constantly broken and restored. Measles virus RNA synthesis is believed to follow a similar model of P-L interactions. This model was further supported by measles virus NP-P interaction analysis, which revealed "fast" binding kinetics and weak binding affinity, ideally to allow for the "cartwheeling" of P and constant breaking and rejoining of vRdRp (135, 139). The ability of vRdRp to travel rapidly along the NP during genome synthesis is necessary for successful viral propagation, and the replication complex kinetics would assist in this mechanism.

Rhabdovirus phosphoprotein structure and function

Vesicular stomatitis virus (VSV) P protein crystallization revealed a parallel dimer formation held by hydrophobic residue interactions. This feature of P dimerization by

rhabdoviruses sets it apart from other paramyxovirus P proteins. A hallmark of paramyxovirus P proteins, the oligomerization domain where P self-associates is also a necessity for replication of VSV (9, 140, 141). The N-terminal domain of rabies virus phosphoprotein interacts with both nascent NP and L, and the C-terminal domain binds to the NP-RNA template. Unlike VSV and SeV P, however, the rabies virus P is an anti-parallel dimer, meaning that the N- and C-terminal domains are oriented on the same side rather than on opposite poles (142-144). Crystallization of the rabies virus P also revealed a helical hairpin between two α-helices for each P monomer, which is thought to allow interactions between the N-terminal helix of one monomer with the C-terminal helix of another monomer (145). Reasons for this "interaction gateway" between the helices of the N- and C-termini of P could aid in maintaining structural stability of the dimer as well as allowing fast and flexible kinetics of P-NP to P-L interactions during viral transcription and replication.

Parainfluenza virus 5 phosphoprotein structure and function

Like other paramyxoviruses, the parainfluenza virus P has a binding site for nascent NP in the N-terminus, self-associates and interacts with L polymerase at the oligomerization domain, and associates with the NP-tail in its C-terminus. Similarly to SeV, PIV5 P can form either dimers or tetramers, and its monomers are arranged in homo-parallel fashion (109, 146, 147).

Recently, in 2020, the parainfluenza virus 5 phosphoprotein was crystallized, focusing on the oligomerization domain of P bound to L polymerase. Crystallization allowed for the discovery of many mechanisms, including two independent bindings sites

for L and NP in the C-terminus of PIV5 P that may provide stable contact between L and the NP-RNA template to prevent premature release of the L from the NP. Ultimately, a unique conformation of the methyltransferase domain and C-terminal domain of L and its relation to the C-terminal of P was proposed. The researchers hypothesized that during transcription, the C-terminus of P captures a N monomer empty of genomic RNA to keep in proximity for recapturing recently transcribed template RNA emerging from the exit channel in L. For genome replication, the C-terminus of P captures the recently released N monomer and is used to coat the new viral RNA (146).

Mumps virus phosphoprotein structure and function

The mumps virus P oligomerization domain is defined as amino acid residues 213 to 277 and has been crystallized. The MuV P tetramer is unique, in that it is comprised of two pairs of parallel α-helices that are positioned anti-parallel to each other. This means that in MuV P, there are two N-terminal and two C-terminal domains on either end of the oligomerization domain, and this is believed to have functional and structural significance (47). Mediation of binding to the NP is within the last 49 amino acid residues of MuV P (residues 343-391), which coalesces with the extreme C-terminal NP-binding domain (NBD) found in other paramyxovirus phosphoproteins (148). Nucleocapsid binding for MuV P is not just limited to the C-terminal domain, but the N-terminal domain is also capable of this interaction (47). The N-terminal domain of P was revealed by electron microscopy to be responsible for the uncoiling of the helical nucleocapsid. This uncoiling by P_{NTD} resulted in improved viral RNA synthesis in a minigenome system (39).

Since both N-terminal and C-terminal domains of MuV P bind to NP, its novel tetramer organization may be responsible. Minigenome system analysis showed that without the oligomerization domain, MuV N- and C-terminal domains alone did not result in viral replication. Only when paired with the oligomerization domain were the N- and C-terminal domains, when transfected together, capable of viral replication (39, 48). This trans-complementarity of MuV P and how structure stability affects replication function will be discussed further in this work.

Transmission and Prevention

The natural hosts of MuV infection, humans can spread the disease through direct contact, contaminated fomites, or respiratory droplet spread. This highly contagious disease propagates in the upper respiratory tract and then spreads to draining lymph nodes. Once in the lymph nodes MuV infection becomes viremic and disseminates into all tissues and organ systems during the two- to three-week incubation period (149). A hallmark of MuV infection is inflammation of the parotid gland (a symptom by which mumps disease received its name). MuV is also highly neurotropic, and central nervous system invasion occurs in approximately half of all clinical cases, with aseptic meningitis and/or encephalitis in up to 10% of patients with nervous system signs (1, 150). In both the pre- and post-vaccination era, MuV infection has been the leading cause of acquired adolescent deafness. About a third of infected persons may have mild to no symptoms of MuV infection (149, 151).

Currently, there is no approved antiviral therapy treatment for MuV infection. Treatment is focused primarily on the alleviation of symptoms. In the US, mumps

vaccination is a part of the childhood vaccination program regimen as a component of the trivalent measles, mumps, and rubella (MMR) vaccine. Children are recommended to be vaccinated initially by 12-15 months of age and boosted by 4 to 6 years of age (152). The MMR vaccine uses the Jeryl Lynn strain of MuV (JL), which was isolated from an infected patient in 1963 and attenuated by serial passage in chicken eggs and chick-embryo cell cultures. There has been a 99% reduction of mumps cases since the introduction of the MuV vaccine and since the introduction of the two-dose MMR vaccination program in 1989 (153, 154).

While safe and efficacious, recent outbreaks in the US and worldwide have brought the relevance of the JL mumps vaccine to the forefront. Almost six-thousand cases of mumps and infection in ten US states were reported during an outbreak at a university in Iowa in 2006. Outbreaks have continued to occur throughout the decade, primarily among adolescents in confined areas (college campuses, sports teams, and detention centers). Interestingly, vaccinated and young persons appear to be the dominant demographic of these outbreak cases, which raises concerns as to whether the current program for mumps vaccination in the US is still as efficacious as it was when introduced (7, 154-156).

Standardization of the efficacy of the current MMR vaccination program has proven difficult, as there is no established MuV neutralizing antibody titer predictive of protection. Since the JL strain of MuV used in the MMR vaccine is from genotype A and the outbreaks strains are from genotype G, there could be antigenic differences between the vaccine and outbreak strains leading to the decreased vaccination efficacy. It is also debated among the epidemiological community if a third dose of the MMR vaccine provides enough boosting immunity to protect the patient long-term. The lack of consistent

immune correlates of protection for MuV makes determining if the JL strain is enough to provide effective immunity against the new genotype resurgence questionable (2, 3, 5, 155, 157, 158). There is a growing need for better immune correlates and animal models to improve characterization of MuV and disease pathogenesis.

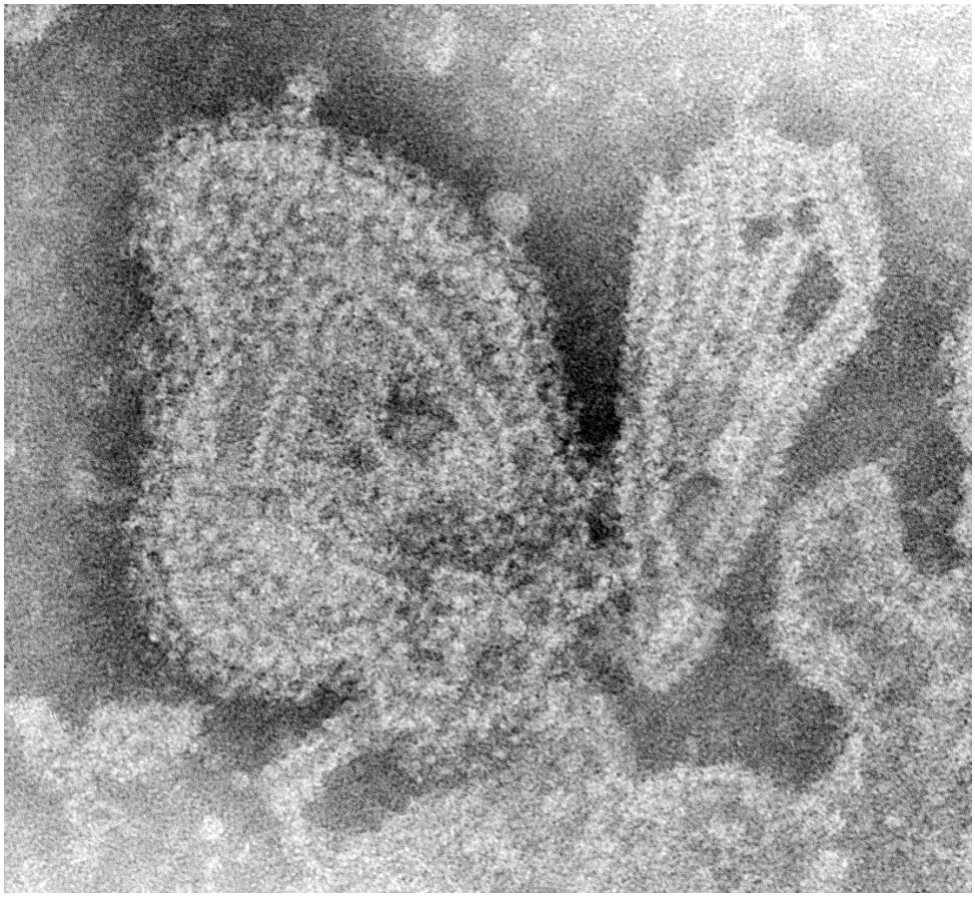

Figure 2.1. Electron microscopic image of MuV virion. This image displays the pleomorphic morphology exhibited by MuV. The virion in this case has ruptured and allowed some of the nucleocapsid's RNP to escape (on the right). This image was taken using a high-powered, transmission electron microscope (SEM) in 1976. Modified from the CDC Public Health Image Library ID# 1874 (159).

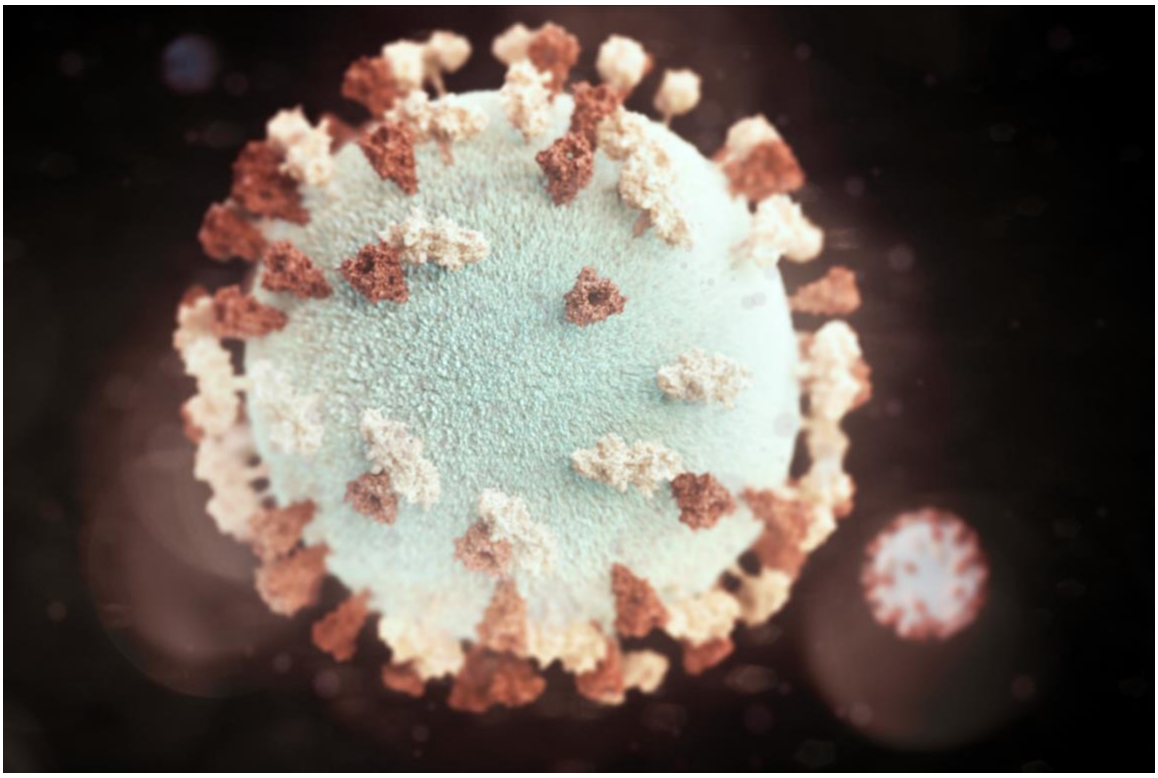

Figure 2.2. Three-dimensional graphical illustration of the MuV particle. This illustration represents the spherical shape of the MuV virion and highlights the glycoprotein tubercles that "stud" the outer surface. The F protein is represented by the reddish-brown tubercles, and the HN protein by the beige tubercles. Modified from the CDC Public Health Image Library ID# 21073 (160).

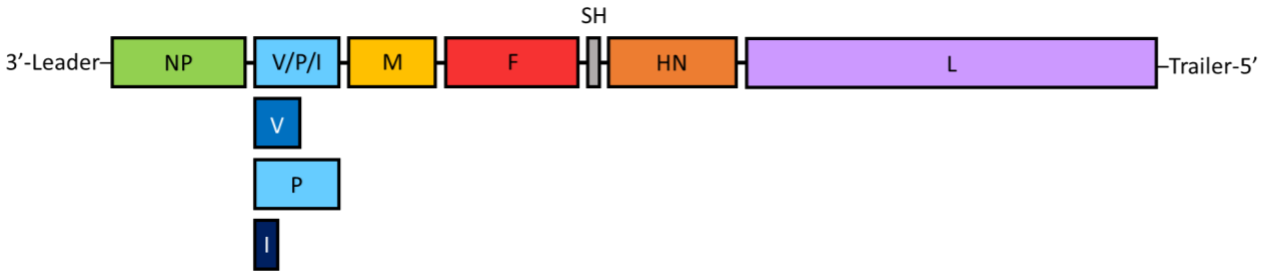

Figure 2.3. Illustration of the MuV genome. The figure represents the orientation and order of the transcriptional units of the MuV genome. Since MuV is negative sense, the genome reads from 3' to 5'. First is the leader sequence, followed by the 7 genes that encode for 9 proteins: NP (nucleoprotein), V/P/I (phosphoprotein), M (matrix protein), F (fusion protein), SH (short hydrophobic protein), HN (hemagglutinin-neuraminidase protein), and L (large protein subunit of the vRdRp). After the L ORF is the trailer sequence. The V, P, and I proteins are all produced from the V/P/I gene via RNA editing and displayed based on their respective sizes beneath the V/P/I ORF.

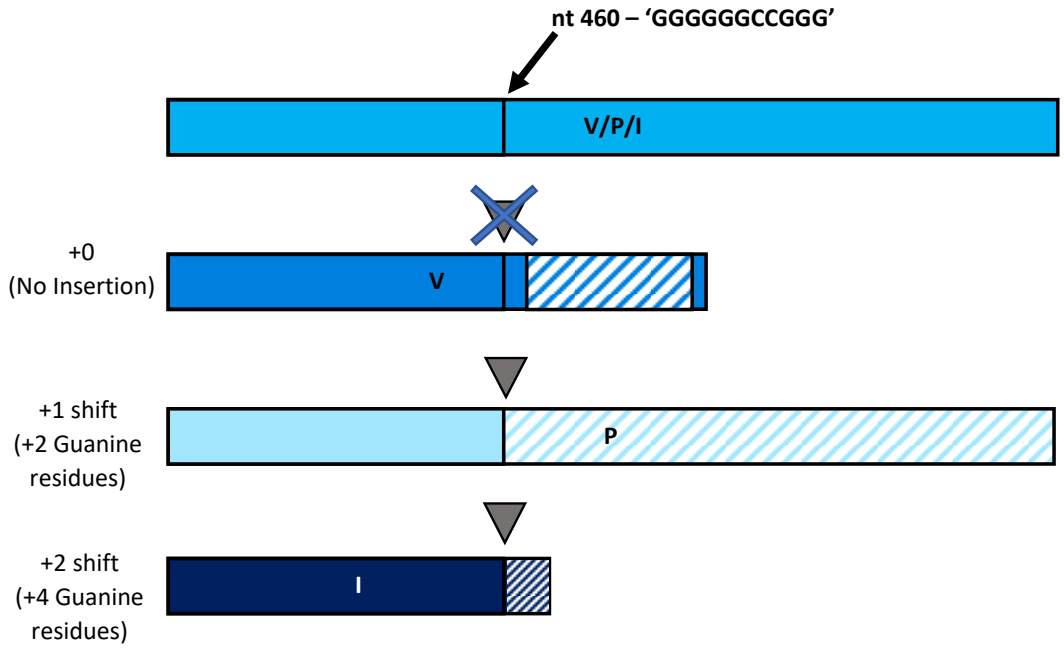

Figure 2.4. V/P/I RNA editing open reading frame (ORF) shift. The diagram describes the how the insertion of +2 or +4 Guanine residues at a specific region in the V/P/I gene leads to a +1 or +2 ORF shift, respectively. The region common to V, P, and I is shown by the vertical line where the insertion occurs. This figure is inspired by "RNA Editing by G-Nucleotide Insertion in Mumps Virus P-Gene mRNA Transcripts" by Reay G. Paterson and Robert A Lamb, Journal of Virology, 1990 (32).

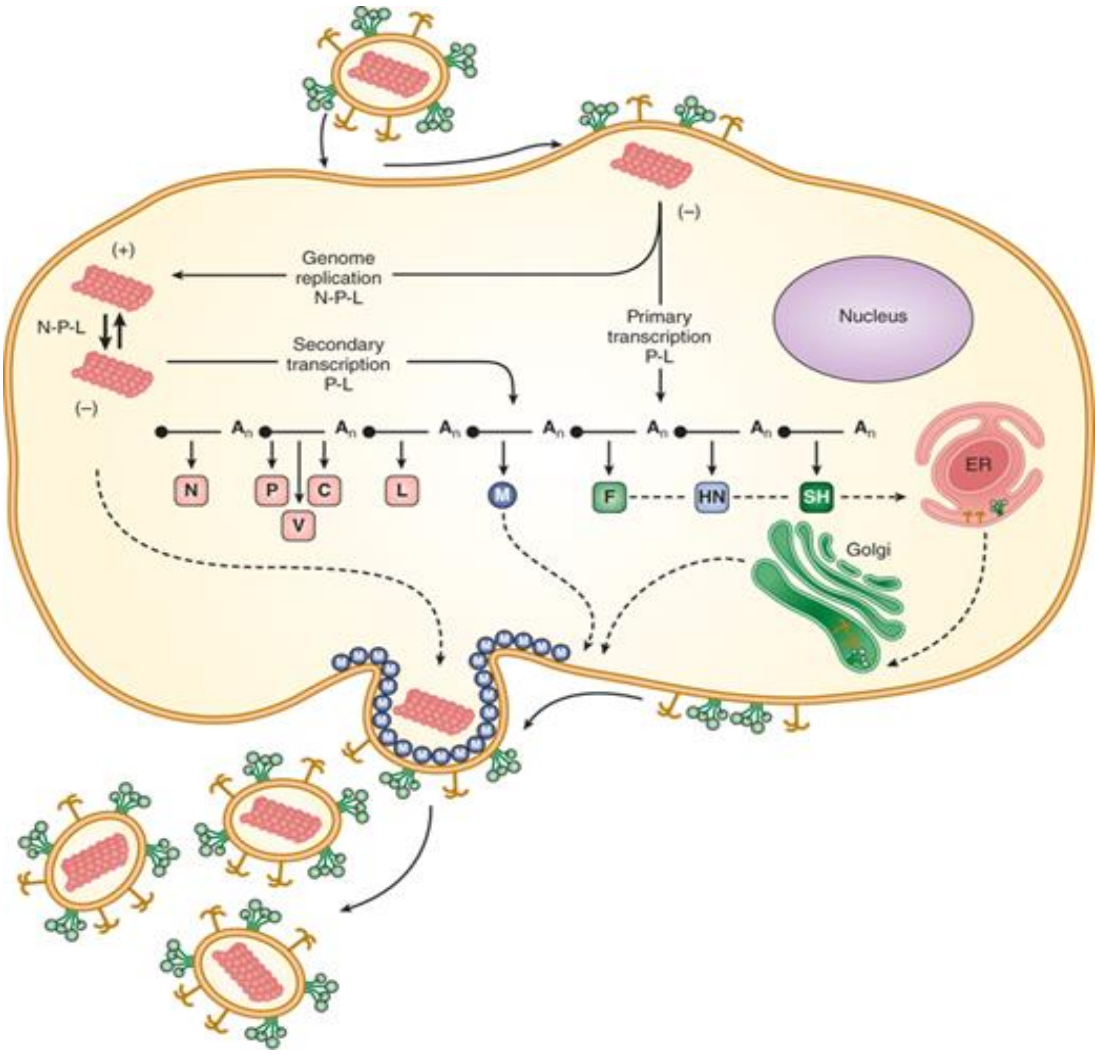

Figure 2.5. Paramyxovirus life cycle. The figure represents an illustration of the paramyxovirus and MuV life cycle involving the N/NP, P, V, C/I, L, M, F, HN, and SH proteins. First, MuV HN binds to the host cell surface and F fuses the viral envelope to the cell membrane. The helical capsid and vRdRp is then released into the cytosol, where transcription of the negative-sense vRNA genome and synthesis of the anti-sense vRNA genome simultaneously occurs to replicate the negative-sense genome. This newly synthesized copy of the vRNA genome is also used for secondary transcription by the vRdRp. mRNAs are translated and recruited to the host cell surface by M. The particle then

buds from the cell to infect a new host. Modified from Medical Microbiology, 27th Edition, © McGraw-Hill Education (161).

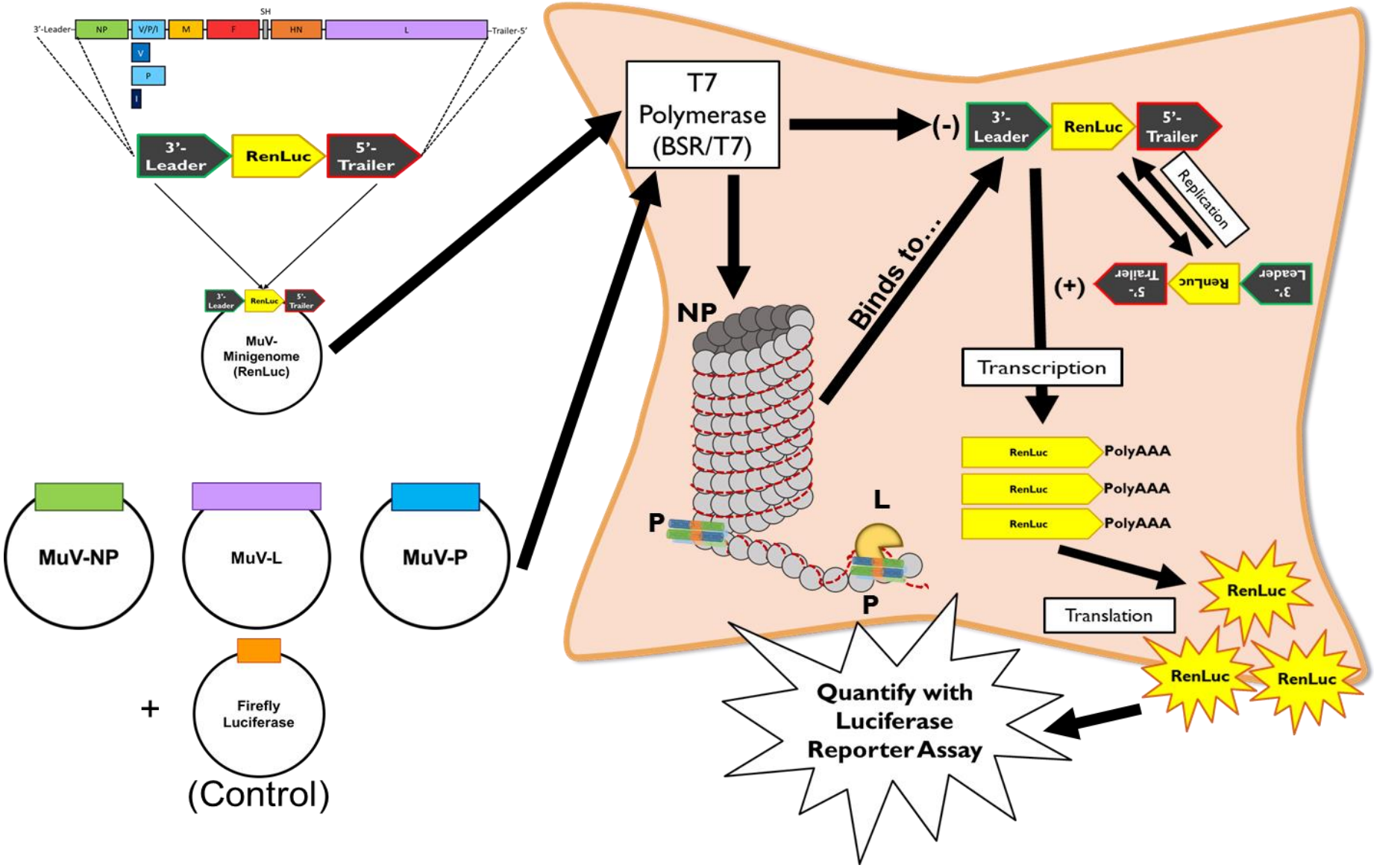
3'-Leader
NP
V/P/I
M
SH
F
HN
L
Trailer-5'
V
P
I
3'-Leader
RenLuc
5'-Trailer
MuV-Minigenome (RenLuc)
MuV-NP
MuV-L
MuV-P
+
Firefly Luciferase
(Control)
T7 Polymerase (BSR/T7)
Binds to…
NP
P
L
P
(-)
3'-Leader
RenLuc
5'-Trailer
Replication
(+)
Transcription
RenLuc PolyAAA
RenLuc PolyAAA
RenLuc PolyAAA
Translation
RenLuc
RenLuc
RenLuc
Quantify with Luciferase Reporter Assay

Figure 2.6. Mumps virus minigenome replication system. This figure represents the minigenome system used for evaluating the effects of the MuV replication proteins NP, L, and P on MuV replication. The 3' leader and 5' trailer sequences of the MuV genome are cloned into a pCAGGS plasmid, with a *Renilla* Luciferase expression gene between the leader and trailer. This plasmid is referred to as a "minigenome plasmid", as it includes the leader and trailer sequence of the MuV full-length genome with a *Renilla* Luciferase protein sequence in-between. The MuV minigenome plasmid and pCAGGS plasmids encoding for MuV NP, L, and P are transfected, along with a Firefly Luciferase control pCAGGS plasmid, into BSRT7 cells. As BSRT7 cells express T7 polymerase, the T7 promoter in the pCAGGS plasmids is recognized and NP, P, and L proteins are transcribed. The NP, P, and L recognize the leader sequence of the minigenome plasmid and begin transcribing *Renilla* Luciferase. Thus, the more *Renilla* Luciferase that is detected by the luciferase assay once the cells are lysed, the more "viral" replication that has occurred. As the minigenome plasmid also expresses a T7 promoter, the Firefly Luciferase plasmid that has a T7 promoter is used as a control to compare "basal" cell level expression of Firefly Luciferase to that of *Renilla,* which would include both T7-based and NP, P, and L-based expression.

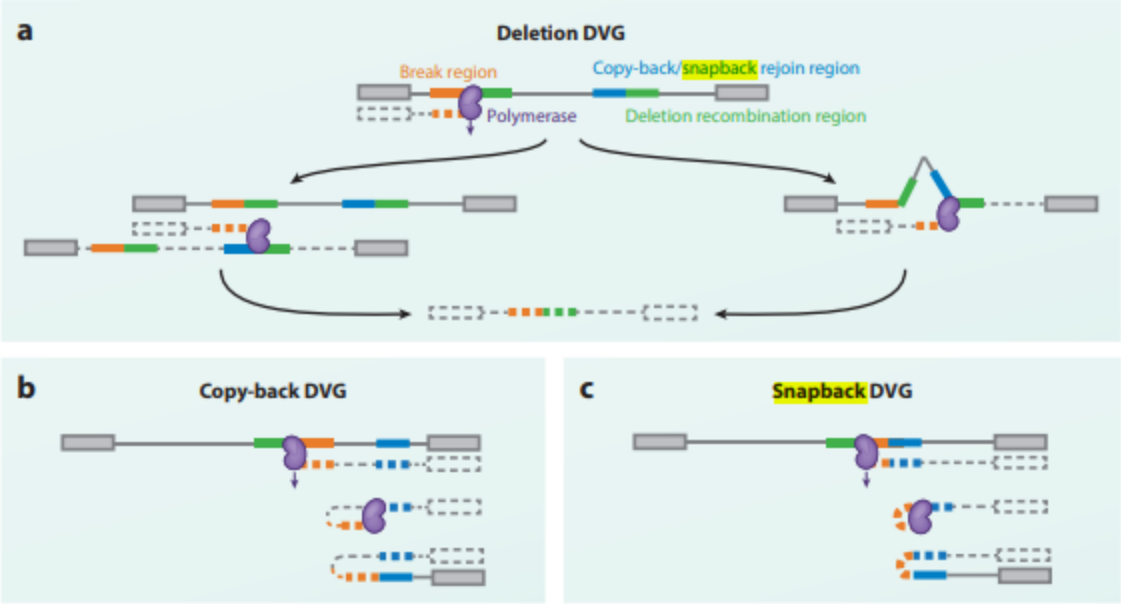

Figure 2.7. Types of DVGs and how they are formed. In panel (a), a deletion DVG is shown to be generated when the RdRp falls off the template antigenome strand at what is called a "break" region and then either continues along the same template strand skipping internal regions or switches to a new template strand at a "region" point. The latter scenario is how copyback and snapback DVGs are formed. In panel (b), a copyback DVG is shown to be generated by the polymerase when it detaches from the template strand and rejoins the nascent strand at a nonhomologous region, thereby creating a nonhomologous loop structure with complementary ends. In panel (c), a snapback DVG is shown to be generated in a manner like the copyback DVG, but significant nonhomologous regions are absent as rejoin points are proximal to the breakpoints. Modified from "The Impact of Defective Viruses on Infection and Immunity" – a Review by Emmanuelle Genoyer and Carolina B Lopez, 2019 (125).

CHAPTER 3

MUMPS VIRUS NUCLEOPROTEIN DOMAIN "TOP" AFFECTS DEFECTIVE INTERFERING PARTICLE PRODUCTION[1]

[1] Risalvato J., Zengel J., Beavis, A., Luo, M., He, B. Submitted to Journal of Virology XX/XX/20XX.

Abstract

Mumps virus (MuV) is a negative-sense, single-stranded RNA virus belonging to the family Paramyxoviridae. A human pathogen, MuV is responsible for acute infection of the parotid glands and can cause severe cases of encephalitis, meningitis, and deafness. The nonsegmented RNA genome of MuV is encapsidated by the nucleocapsid protein (NP), which forms the ribonucleoprotein (RNP) complex; this which serves as a template for RNA synthesis. To make RNA accessible to the viral polymerase, a conformational change within NP must occur. Crystal structure analysis of the NP of parainfluenza virus 5 (PIV5), a paramyxovirus closely related to MuV, indicates that an α-helix close to the RNA genome becomes flexible when RNA is removed. This region of the NP is likely responsible for the conformation change that allows the polymerase to access RNA for transcription and replication. To examine the functionality of MuV's NP point mutations were made in MuV NP protein corresponding to PIV5 at sites G185P, A197Q, Q200R, and groups denoted as Top (N63G, P139D, A197Q), Tip (P109E, N121G, A124R), and Bottom (G21S, S29T, P43N, R93Q, R304Q). Only MuV mutants "185", "197", and "Top" were able to be rescued. The "Top" MuV mutant exhibited normal growth kinetics at low multiplicity of infections (MOIs); however, at high MOIs the virus could not efficiently replicate. Further analysis indicates that production of defective interfering particles (DI particles or DIPs) was enhanced in the mutant virus. Understanding the production of DI particles, which can lead to increased interferon production, will invariably lead to a better understanding of MuV pathogenesis as well as its replication/transcription process.

Significance

Mumps virus (MuV) is a reemerging human pathogen. The nucleoprotein (NP) of MuV and all other paramyxoviruses is essential for RNA synthesis and viral replication. By exchanging amino acid sites between similar paramyxovirus NP, the structure and function of specific domains of MuV NP may be determined. These findings will help lead to a greater understanding of MuV genome replication and potential antiviral targets.

Introduction

Mumps virus (MuV) is a single-stranded, non-segmented, negative-sense RNA virus that is a member of the *Paramyxoviridae* family and genus *Rubalavirus* (1). This human pathogen causes mumps, a disease that can be transmitted through the upper respiratory tract or conjunctivae by droplet transmission among individuals (4, 162). Infection typically results in malaise and the hallmark swelling of the parotid glands. In severe cases, infection can result in meningitis, encephalitis, and deafness. Additionally, in post-pubescent males, one in four will develop orchitis, with about 13% of patients developing subfertility (163, 164). Up until the introduction of mass vaccination of the MMR (Measles, Mumps, and Rubella) vaccine in the 1960s, mumps was the leading cause of acquired sensorineural deafness in children (165). After the introduction of a nation-wide, two-dose, MMR vaccination program in 1989, by 2001 mumps was considered nearly eliminated with less than 0.1 mumps cases per 100,000 people (166, 167). However, recent outbreaks in the past decade among younger, vaccinated populations indicate the need for the development of new strategies for outbreak control and MuV research.

For MuV to replicate, there are three key proteins involved: nucleoprotein (NP), phosphoprotein (P), and the large protein L (6, 168). NP forms a helical capsid that supports and protects the RNA genome (39, 169). P is bound to NP by the amino-acid terminal (NTD) and carboxy-terminal domains (CTD). While the P-NTD plays a role in unraveling the NP so that L may access the RNA genome for replication, P-CTD is responsible for transporting L to the NP-RNA template (48). L is responsible for the transcription of the RNA genome, as well as the 5' capping and addition of the poly(A) tail on the 3' end of viral mRNA (6, 48). Together, these three proteins form the vRNP (viral ribonucleoprotein) complex. The vRNP is a well-established feature of paramyxoviruses, with the NP structure between different viral species being relatively conserved (168, 170).

There are some unique features of MuV's vRNP complex. For example, MuV's P forms a unique tetramer in which two parallel homodimer pairs arrange at an oligomerization domain in an anti-parallel orientation, leading to two NTDs and two CTDs on both ends of the tetramer. This construction allows for both the NTD and CTD of MuV to interact with NP (39, 45, 48, 171). Parainfluenza virus 5 (PIV5)'s P tetramer is a parallel orientation with only the NTD directly interacting with its NP (8, 146, 147).

The NP of MuV, and all other paramyxoviruses, plays a crucial role in the formation of the vRNP complex and its functions. Since the crystal structure of MuV NP has yet to be determined, defining how NP interplays with L and P, as well as the RNA genome, has been a challenge. MuV NP forms a helical capsid with 13 subunits, and like most paramyxoviruses, holds the RNA on the outside of its capsid. This, and the fact that NP does not exhibit specificity when it comes to encapsidating RNA of various lengths, suggests that MuV's RNA is less protected by the NP as compared to other negative

stranded RNA viruses (6, 109). There is significant similarity of MuV's NP to PIV5's NP structure. Given what we do know about both virus' NP interactions with other viral proteins during replication, an exchange of amino acid sites within MuV NP to PIV5 was useful in better understanding MuV NP's role in viral pathogenesis and replication.

To determine key differences between the residues and structure of MuV NP and PIV5 NP, we developed a theoretical 3-D model for MuV NP using PIV5 NP's crystal structure as a template. In doing this, 3 point and 3 regions of interest were determined: Y185P, A197Q, Q200R, "Top" (N63G, P139D, A197Q), "Tip" (P109E, N121G, A124R), and "Bottom" (G21S, S29T, P43N, R93Q, R304Q). Sites 197A and 200Q are within an alpha helix in the MuV NP that is shifted so L may access the RNA, and 185Y lies within the hinge region of this helix. "Top" and "Tip" of MuV NP may interact with the carboxy-terminus (CTD) of P, and "Bottom" lies on the non-RNA interacting side of NP and may affect NP integrity. To evaluate these differences, a minigenome assay was utilized to estimate the effects of these mutations in MuV NP on MuV replication. These mutations were also inserted into a full-length MuV, and growth kinetics were measured for mutant MuVs "185", "197", and "Top".

In this work, we show a novel MuV mutant capable of inherently producing DI particles without the need for induction by high multiplicity infection and environmental pressures. The MuV mutant, "Top", exhibited growth kinetics at both high and low multiplicities of infection that were inhibitory over time. Additionally, "Top" when co-infected with a reporter wild-type MuV was capable of inhibiting said virus' growth. "Top" possesses mutations within a domain hypothesized to interact with the CTD of P and is thus crucial to L binding to the RNA properly for replication. It is also possible that this

mutated domain causes a misfolding of the RNA within its pocket in the NP, making it so that L cannot produce correct copies of the vRNA. MuV DI particles have not been cited outside of persistent infection and other environmental factors (172-174), making the development of a virus that produces DI particles conventionally an opportunity for better understanding of paramyxovirus replication and pathogenesis.

Materials and Methods

Mapping of MuV NP onto PIV5 NP

Swiss-Model (169, 175) was used to create a theoretical model by taking the amino acid sequence of the MuV NP and using the PIV5 NP crystal structure (4XJN.1.C) as a template (109) to build MuV's NP amino acid sequence onto.

Molecular cloning

Plasmids used in these experiments were constructed using standard molecular cloning techniques (details and files available upon request). Mumps virus isolated in Iowa from 2006 (GenBank: JN012242.1) was used as a basis for plasmid sequences (171). MuV helper plasmids NP, P, and L have been previously cloned into the pCAGGS expression vector (53, 75). Firefly luciferase (pFF-Luc) and a MuV minigenome plasmid expressing *Renilla* luciferase flanked by MuV-IA trailer and leader sequences under a T7 promoter (pT7-MG-RLuc) were also previously described (44).

Cell culture and transfections

Vero and 293T cells were maintained in Dulbecco's modified Eagle medium (DMEM) with 5% fetal bovine serum (FBS) and 1% penicillin-streptomycin (P/S) (Mediatech Inc., Manassas, VA). BSR-T7 cells were maintained in DMEM supplemented with 10% FVBS, 1% P/S, and 10% tryptose phosphate broth (TPB). Cell lines were incubated at 37ºC with 5% CO_2. Cells were passed at an appropriate dilution one day prior to use in order to obtain 60-90% confluency upon transfection or infection. JetPRIME transfection reagent (Polyplus Transfection Inc., New York, NY) was used to transfect cells following the manufacturer's protocols.

MuV minigenome system and dual-luciferase assay

BSR-T7 cells at 60-80% confluency in a 24-well plate were transfected with pCAGGS-P (80 ng), pCAGGS-L (500 ng), pT7-MG-RLuc (100 ng), pFF-Luc (1 ng), and various amounts of pCAGGS-NP (wild type or mutant at 0, 25, 50, or 100 ng) using jetPRIME (Polyplus Transfection, France) according to the manufacturer's protocol. pCAGGS-GFP (green fluorescent protein) was used to maintain a constant amount of total plasmid transfected per well and served as a positive control for successful transfection. After 48 hours, the medium was removed, and 100 µL of passive lysis buffer (Promega, Madison, WI) was added to each well. The plates were then shaken on an orbital shaker for 20 minutes. 40 µL of lysate was then transferred to a white, flat-bottom, 96-well plate, while the remaining 60 µL of lysate was frozen at -20ºC for analysis via Western blot. A dual-luciferase assay (Promega) was performed according to the manufacturer's protocol. A GloMax 96-microplate luminometer (Promega) was used to detect luminescence. The ratio of Renilla to firefly luminescence was determined for each well as the "relative

luciferase activity", and the average and standard error of triplicates was calculated. For Western blot analysis, mouse monoclonal anti-MuV NP and P antibodies were used together to detect NP and P expression, respectively, as previously described (39).

Virus rescue

293-T cells at 60-80% confluency were transfected in a 6-well plate with pCAGGS-NP (200 ng), pCAGGS-P (320 ng), pCAGGS-L (1250 ng), pCAGGS-T7 (200 ng), and full-length MuV genome (2500 ng) using JetPRIME (Polyplus). After 48 hours, the cells were co-cultured with Vero cells at a ratio of 1:2 in a 10-cm dish, and supplemented with DMEM with 5% FBS and 1% P/S. After 24 hours, the media was replaced with DMEM with 2% FBS and 1% P/S. Cells were observed for an additional 2-7 days after co-culture until CPE was observed, at which time single plaques were isolated and expanded in Vero cells in 6-well plates to establish passage 1 (P1). The P1 titer was then determined by plaque assay, then passaged again (P2) in T75 flasks at a multiplicity of infection (MOI) of 0.01. Virus was collected after 72 hours into aliquots and stored at -80ºC with sucrose phosphate glutamate (SPG). Plaque assays were performed to determine the viral titer. Virus sequence was confirmed by RT-PCR and sequencing.

Immunoblotting of Virus

Viral supernatant was collected and diluted to a titer of $3.0x10^6$ PFU/mL. Virus samples were then diluted 3:1 with 4X Laemmli Sample Buffer (Bio-Rad Laboratories, Hercules, CA) plus β-mercaptoethanol at 9:1, then heated at 95ºC for 5 minutes. Samples were loaded into a 4-20% Mini-PROTEAN® TGX (Bio-Rad Laboratories, Hercules, CA)

polyacrylamide gel, and proteins were size-separated by gel electrophoresis. The proteins were then transferred to a polyvinylidene difluoride (PVDF) membrane (GE Healthcare, Piscataway, NJ). The membrane was then incubated with mouse anti-MuV-NP antibody (1:2000 dilution), followed by incubation with Cy3-conjugated goat anti-mouse IgG secondary antibody (1:2500 dilution) (Jackson ImmunoResearch, West Grove, PA), and scanned using a Typhoon 9700 imager (GE Healthcare Life Sciences, Piscataway, NJ).

Growth curves

Confluent Vero cells in a 6-well plate were infected with MuV (wild type or MuV-NP Y185P, A197Q, or Top mutant) at a MOI of 0.01 or 2 in 1 mL of DMEM - 2% FBS - 1% P/S for 2 hours in triplicate. Cells were then washed three times with media, and 2 mL of DMEM - 2% FBS - 1% P/S was added to the cells. An initial sample was taken immediately after the DMEM was added to the cells and labeled as 0 hours post infection (hpi). For the high MOI of 2, samples were collected at 0, 12, 24, 36, 48, and 72 hpi. For the low MOI of 0.01, samples were collected at 0, 24, 48, 72, 96, and 120 hpi. All samples were supplemented with SPG and stored at -80ºC.Viral titers were determined by plaque assays on Vero cells. Each experiment was repeated for confirmation. Significance was determined by two-way analysis of variance (ANOVA).

Hemagglutination assay

Whole cockerel erythrocytes were obtained from the Poultry Diagnostic Research Center (Athens, GA, USA) as a gift from Brent Lovern. The red blood cells (RBCs) were centrifuged at 4ºC for 10 minutes at 150 rcf. After the centrifugation, the serum was

removed, retaining the RBC pellet, and PBS was added back to the original volume. This washing process was repeated a total of four times to create a 5% stock solution, viable for up to 7 days. The washed RBCs were then diluted to a 0.25% concentration in phosphate buffer saline (PBS). In a 96-well V-bottom plate, MuV was diluted with PBS in sequential 1:2 dilutions in a total volume of 50 µL per well, to which 50 µL of 0.25% RBCs were added to each well in addition. The plates were incubated at 4ºC for 90 minutes, and agglutination patterns were observed.

Viral reduction of infectious yield assay

Vero cells were grown to confluency in 24-well plates in DMEM – 5% FBS – 1% P/S. MuV-*Renilla* Luciferase was prepared at a MOI of 5. MuV or mutant MuV was diluted to MOIs of 2, 0.1, 0.01, or 0.001. The MOI groups were halved, with one half being treated with UV light (UV Stratalinker 1800) at 10 x 10^3 µJ x 100 five times. Cells were then infected with MuV-Renilla Luciferase, and then with either the UV-treated or untreated MuV or mutant MuV at various dilutions in addition. Cells with virus were incubated for 2 hours at 37ºC with 5% CO_2 with a total volume of 250 uL of DMEM – 2% FBS – 1% P/S and virus. After incubation, cells were washed twice with DMEM – 2% FBS – 1% P/S, then covered with 500 uL of media.

At 24 and 48 hours the media was removed, and cells were washed with PBS, then lysed with *Renilla* Luciferase Assay Lysis Buffer (Promega) according to the manufacturer's protocol, with shaking on an orbital shaker for 30 minutes. The cell lysates were then collected and added to a white, flat-bottom, 96-well plate. The *Renilla* Luciferase Assay Protocol (Promega) was then followed according to the manufacturer, and

luminescence was measured using the GloMax 96-well plate luminometer (Promega). An average between triplicates was taken for luciferase activity, and the data was normalized to the activity of MuV-*Renilla* Luciferase infection alone. Experiments were done in triplicate and repeated twice for consistency.

RT-PCR of DI particles

Viral RNA was extracted from cell culture supernatants using a QIAamp Viral RNA Mini Kit (Qiagen Inc., Valencia, CA). Reverse transcription (RT) was performed with random hexamers and SuperScript III reverse transcriptase (Life Technologies). The cDNA templates along with four unique leader and trailer specific primers and one control primer pair specific to the F and HN genes of the MuV genome were used to amplify DI particles and fragments of the MuV and mutant genome by PCR. PCR products were examined by electrophoresis on a 1% agarose gel and then gel extracted and column purified using the QIAquick Gel Extraction Kit (Qiagen Inc., Valencia, CA).

TOPO cloning and sequencing

Purified RT-PCR products were cloned into the pCR™ 2.1-TOPO® TA vector using the TOPO® TA Cloning Kit (Invitrogen, Carlsbad, CA). Reaction products were then bacterially transformed into TOP10 E. *coli* cells (Invitrogen, Carlsbad, CA). Five bacterial colonies from each cloning experiment were selected, grown overnight in culture at 37ºC, and their plasmid DNA extracted using the QIAprep Spin Miniprep Kit (QIAgen Inc., Valencia, CA). Primers for the M13F (5'-GTAAAACGACGGCCAG-3') and M13R (5'-CAGGAAACAGCTATGAC-3') regions of the pCR™ 2.1-TOPO® TA vector were

used for Sanger sequencing by Genewiz (South Plainfield, NJ). Sequences were analyzed using Geneious 11.1.5 (Auckland, New Zealand).

Analysis of chromatogram peak variance.

Background peak variance to quantify the heterogeneity of mutant and wild-type virus samples that were Sanger sequenced was calculated using the following formula:

$$100\times\frac{\text{Variant Base Peak Height}}{\text{Primary Base Peak Height + Variant Base Peak Height}}$$

This formula was adapted from the ThermoFisher Scientific Minor Variant Finder Software v1.0 User Guide and computational program (176, 177).

Statistical analysis

Statistical analysis was performed using Graphpad Prism software version 5.04 for Windows (Graphpad Software, La Jolla, CA). Student's *t* test was used to calculate *P* values.

Results

Identification of the Differences between MuV and PIV5's Nucleoprotein

To investigate the structural characteristics of MuV NP, we constructed a theoretical model of MuV NP based on the crystal structure of the PIV5 NP (169, 175) (Figure 3.1). There were six key amino acid differences between PIV5 and MuV's NP within the "core" of MuV, residues 1 to 379 (Table 3.1). The N-tail was not included as it has not been shown to be utilized in replication nor is essential for NP formation *in vitro* for cryo-EM modeling (110). Three of these differences were singular sites (MuV to PIV5):

Y185P, A197Q, Q200R. The latter three differences were grouped into regions based on their structural location in NP: “Top” (N63G, P139D, A197Q), “Tip” (P109E, N121G, A124R), and “Bottom” (G21S, S29T, P43N, R93Q, R304Q). To assess these differences and how they might affect the structure and function of the RNP, sites in MuV’s NP were mutated to represent those in PIV5.

In Figure 3.1C, the different single point mutations from MuV-like to PIV5-like residues were Y185P, A197Q, and Q200R and are structurally represented. MuV L is hypothesized to open the helical structure of NP at amino acids 180 to 202 in order to expose the RNA genome; however, this region is poorly conserved between MuV and PIV5. To examine the roles of Y185P, A197Q, and Q200R on the MuV NP, these residues were mutated. Amino acid sites 197 and 200 are thought to be on the NP helix, which needs to be shifted during a P-initiated conformational change for L to access the RNA, while 185 is thought to be on the hinge region upstream of the helix, and may play a role in this region’s flexibility (27, 39, 110).

In Figure 3.1D, the domains of interest: “Top”, “Tip”, and “Bottom”, are represented in the MuV NP theoretical structure. The “Top” and “Tip” domains are hypothesized to be the regions of NP that would interact with the carboxy-terminus (CTD) of P. Since PIV5’s NP does not interact with the CTD of its P, but MuV’s NP does, mutating these regions to evaluate if these proposed domains do in fact interact with the P_{CTD} and the consequences of their mutations was of high interest. The “Bottom” domain’s role is unknown, but it does consist of residues exposed on the non-RNA interacting side of the NP, which may mean that this domain is important to the NP’s structural integrity (39, 110).

Effects of NP Mutations on MuV Replication in a Minigenome System

To characterize the effects mutations in MuV NP to PIV5 NP amino acid sites, mutations were made to the MuV NP and tested in a minigenome system. The minigenome system is a transfection-based experiment that allows us to evaluate the direct effects of mutations in the NP, P, or L of the vRNP on viral genome replication. A plasmid containing a *Renilla* luciferase gene flanked by the leader and trailer sequences of the MuV genome is transfected along with NP, P, or L from MuV. The RNP forms in culture and transcribes *Renilla* luciferase via recognition of the MuV leader and trailer sequences, which can then be quantified using a luminometer. Should a mutation in one of the proteins negatively affect transcription, *Renilla* luciferase activity should decrease. This value is normalized against Firefly luciferase, which is also transfected at a constant amount.

It was found that mutants Y185P and Q200R had significantly decreased minigenome activity (Figure 3.2A) but were expressed (Figure 3.2B). Furthermore, mutant A197Q had noticeably reduced activity, with comparable protein expression levels to wild-type NP. When evaluating NP mutants with mutated domains, “Top” had reduced replication activity, but “Tip” and “Bottom” had almost none (Figure 3.2C). This observation was reflected in their expression levels, with “Tip” having very little protein expression, but increased NP degradation product, and “Bottom” having reduced expression (Figure 3.2D). Taken together, it was hypothesized that should mutations be made to the full-length viral genome, the NP mutations A197Q and “Top” would most likely yield viable virus if rescued.

Successful Rescue and Phenotype Determination of MuV mutants

Following the results from the minigenome experiment, mutations were made in the full-length MuV genome to evaluate their viability and phenotypic differences. As predicted, A197Q and "Top" were viable for virus rescue, but interestingly, so was Y185P (Table 3.2). After propagating the mutant viruses, RT-PCR of the whole virus genome followed by Sanger sequencing (Genewiz) was used to confirm the presence of the mutation(s) without any other unexpected mutation present in the genome (Figure 3.3). Confirmation of NP production by the virus mutants was performed via western blot analysis (Figure 3.3), with NP production by "Top" being significantly more pronounced than both wild-type virus and other mutants.

After the MuV mutants were established and verified, growth curve assays were performed to evaluate the phenotype of the mutants by growth kinetics at high (2.0) and low (0.01) multiplicities of infection (MOI). Mutant Y185P at both high (Figure 3.4A) and low (Figure 3.4B) MOI took longer than wild-type MuV to reach maximal titer, with it not being reached until hour 24 and day 2 post infection (respectively). Mutant A197Q grew similarly to MuV wild-type when infected at a low MOI (Figure 3.4C). However, when infected at a high MOI, A197Q grew one log lower than wild-type by the end of the 72-hour collection period (Figure 3.4D). Interestingly, "Top" grew approximately one log lower than wild-type by the end of the time collection period when infected at a low MOI (Figure 3.4E), and when infected at a high MOI was unable to grow well (Figure 3.4F). At 24 hpi, when peak PFU titer for high MOI infections is expected, "Top" grew only two logs higher from its initial titer at hour 0, decreasing thereafter to just above the same titer as the 0 hpi timepoint at the end of the experiment.

"Top" Virus Inhibits MuV Replication

To investigate whether "Top" virus has an inhibitory effect on MuV replication, a reduction of infectious yield assay was designed. The experimental design (Figure 3.5A) was based on a co-infection of Vero cells with a MuV expressing *Renilla* luciferase and either wild-type or mutant virus. While the MOI of MuV-*Renilla* Luciferase will be maintained the same for each co-infection, the wild-type or mutant virus was titrated from high to low MOIs. Additionally, a subset of wild-type or mutant virus was UV-treated to cross-link the viral RNA. The expectation was that should there be an effect on *Renilla* luciferase activity due to wild-type or mutant virus inhibition, UV-treatment would inactivate the wild-type or mutant virus, and therefore decreased MuV-*Renilla* Luciferase activity would not be observed. If the effect on MuV-*Renilla* Luciferase activity remained unchanged after the wild-type or mutant virus was inactivated, then the inhibition of viral replication by "Top" is more likely caused by something in the supernatant and not the virus itself.

For virus A197Q, at 24 hpi (Figure 3.5B) the mutant has a significant negative effect on the *Renilla* luciferase activity. However, at 48 hpi (Figure 3.5C), there appears to be no significant difference between the inhibition caused by wild-type MuV and A197Q, nor for the UV-treated group. On the contrary, "Top" virus 24 hpi (Figure 3.5D) showed increased inhibition of *Renilla* luciferase activity for all MOIs, but especially high MOI, compared to wild-type virus. At 48 hpi (Figure 3.5E) this trend continued, demonstrating that while especially at a high MOI, even at a low MOI, "Top" inhibits viral replication. This is further demonstrated by the "Top"-UV-treated virus having minimal inhibitory

activity compared to wild-type-UV-treated virus, thus confirming that the inhibition in viral growth by "Top" is due to the virus and not an extracellular component in the supernatant.

Only Infectious Virus Titer is Affected, not Binding Affinity

The peculiar growth curve kinetics of "Top", combined with the noticeably higher presence of NP in the viral supernatant at equivalent PFUs compared to other viruses, is remarkable, and warranted further investigation into this phenotype.

To investigate whether the PFU titer of "Top" was accurately representing the presence of total virus particles, a hemagglutination assay was performed. In Table 3.3, it is shown that compared to wild-type MuV, the amount of binding activity by hemagglutination activity is much higher than what should be expected of "Top" given its PFU titer. This information leads to the hypothesis that there are virus particles unaccounted for by the plaque titer that are capable of binding to cells but are incapable of plaque formation. A plausible explanation is that "Top" virus produces a significant amount of defective interfering (DI) particles compared to wild-type MuV, and therefore, the growth of plaque-inducing virus is negatively affected, while the ability of virus particles to assemble and bind to neighboring cells is not.

RT-PCR and Sequencing of "Top" Confirms Presence of Defective Interfering Particles

To definitively confirm the presence of DI particles and to characterize them, wild-type and "Top" virus was serial passaged at low MOI (0.01) for 4 passages. RNA was extracted from these viruses at each passage, and reverse transcribed with random

hexamers, and then PCR with leader and trailer primers (Table 3.4) was performed. The RT-PCRs were run on a 1% agarose gel and imaged. All viruses were positive for the F/HN junction control (Primer Set 7), indicating that the RT-PCR methodology was appropriate.

In general, DI genomes are generated by most negative-stranded RNA viruses during viral replication. These genomes are truncated forms of the original genome, and usually retain a few key pieces of information from its full-length parent genome: a suitable initiation site on the 3' end and its complement on the 5' end, the terminal sequence(s) recognized by the RdRp, and sequences for packaging and encapsulation into the NP (NN). Based on these parameters, primers were designed to capture potential DI genomes. The most common type of DI genome is Class III, or an internal deletion genome, which would be captured by primer sets 1 and 2. Class I includes "copy-back" or panhandle DI genomes, which arise when the polymerase carrying an incomplete strand switches back to transcribe the 5' end, forming a classic panhandle shape in the RNA sequence. Class II includes hairpin and "snapback" DI genomes, which are less complex in their secondary structure than copy-backs; in this case, the polymerase will transcribe part of one strand and then use it as a template, forming a hairpin structure (178, 179). Copy-back and hairpin DI genomes were intended to be captured by primer pairs 3, 4, 5, and 6. Primer set 6 would use the leader sequence and its complement to capture Class I and II DI genomes, while sets 3, 4, and 5, as single primers, would help discern copy-backs from hairpins. Typically, if there is a complex secondary structure, such as a panhandle, the polymerase during PCR will either skip over the structure and make shortened cDNA segments with internal deletions or will generate truncated products. Hairpins typically have fewer inner deletions with shorter segments. These structures are detailed further in Figure 3.6.

In Figure 3.7A, the wild-type MuV displayed PCR bands for Primer Sets 2, 4, and 6, which included leader and trailer, leader only, and leader with its reverse complement, respectively. This was consistently observed throughout passages 2, 3, and 4 (data not shown), establishing a qualitative "baseline" of DI particle genomes that may appear naturally in the wild-type MuV population.

"Top" (passage 2) presented bands for the same primer groups as wild-type MuV (2, 4, 6); however, it also had bands for groups 1, 3, and 5, which included primers for the full leader and trailer, the full leader alone, and the trailer alone, respectively (Figure 3.7). Interestingly, Primer Set 6 (leader with reverse complement) for "Top" showed a large DNA smear. This was likely due to when amplifying reverse-transcribed RNA from "Top" using complement leader primers, there was increased DNA of various length, indicating a high likelihood of the presence of copy-back genomes that could not be well-transcribed due to various secondary structures (180). Top" passage 3 appeared to have "lost" some of the PCR bands that hallmarked "Top" passage 2 (Figure 3.7), indicating that with serial passages, the viral population has a shift back to the wild-type genotype and thus becomes heterogeneous.

To elucidate these bands and their DI sequences, the bands from wild-type MuV and "Top" passages 2 and 3 were excised, and TOPO cloning performed. In Figure 3.8, Sanger sequencing analysis for bands consistent between wild-type and "Top" passage 2 showed an increased variety of deletion defections in the sequences, while sequences of bands unique to "Top" passage 2 revealed the presence of copy-back sequences. The copy-back sequences were determined by examining the repeated sections of nucleotides before

the beginning of a complemented region, indicating the RNA polymerase "stuttering", and then switching to the opposite or same strand.

Taken together, the sequencing and RT-PCR data suggests three main aspects regarding "Top" and its production of DI particles: (1) "Top" produces a greater number of DI particles compared to wild-type MuV, (2) "Top" produces a greater variety of DI particles, particularly copy-back, compared to wild-type MuV, and (3) as "Top" is passaged, the DI particle genotype becomes more representative of wild-type's DI particle profile in its increase of deletion and decrease of copy-back DI genomes.

Discussion

Here, we have shown that by changing MuV NP amino acid sites to PIV5 sites, MuV NP function is vastly affected. Here, we have shown that by changing MuV NP residues to those represented in PIV5, MuV NP function is markedly affected. Three of the mutations (200, "Tip", "Bottom") proved to be detrimental to replication and virus viability. The mutation at 185 showed comparable growth kinetics to wild-type MuV, but 197 showed decreased viral growth at high MOI infection. Interestingly, "Top", a MuV mutant where amino acid sites at 63, 139, and 197 were altered, showed less growth at low MOI infection, and displayed an inhibitory effect on its growth kinetics when infected at a high MOI (Figure 3.4). When investigating the possibility of "Top" alone being the culprit of these inhibitory effects seen in MuV growth, it was determined that not only at high MOI, but at low MOI, "Top" was able to inhibit viral replication of MuV-Renilla Luciferase. This thought was further verified by the fact that when "Top" is UV-inactivated, these inhibitory effects are no longer observed, minus minimal effects at high

MOI infection at 24 hpi likely due to not all of the virus particles being initially inactivated (Figure 3.5). Furthermore, “Top” displayed binding affinities by HN to sialic acid in titers comparable to wild-type virus, indicating that there are virus particles in the supernatant of “Top” that because they are uninfectious are being unaccounted for by plaque assay (Table 3.3). All this information taken together led to the hypothesis that the “Top” mutant inherently produces DI particles, without requiring induction by high MOI infection.

DI particles were first discovered in 1954 by Preben von Magnus while working with influenza. When he noticed a loss in viral yield after high multiplicity passage in eggs, he discovered an increase in the ratio of viral particles to infectious virus; von Magnus referred to these generated particles as “incomplete” virus (113). It was not until 1973, after more advanced analytical techniques became available, that these particles were fully characterized and named DI particles (128, 181). These particles have severely shortened viral genomes and are thus deficient in replication. While these genomes are truncated, they are still packaged by viral and cellular proteins due to the presence of signaling packaging sequences (178), often with higher affinity than full-length viral genome, and bud from host cells. Since these particles can still bind to cells but not replicate on their own, they are considered noninfectious. The production of more DI particle progeny relies on the replication machinery of infectious “helper” virus, which can be parasitized during co-infection of the cell, and thus a competition arises between DI and infectious particles (182). This phenomenon can often be induced by high multiplicity passages of virus, thus alluding to the nature of DI particles to be of a “check-and-balance” evolutionary benefit via triggering of innate immune responses (128, 181, 183). More recent characterizations of DI particles through sequencing and in different virus types has progressed the

knowledge of viral replication and has thus provided an opportunity for advancements in antiviral and vaccine development.

DI particles are a budding field of interest in the field of virology, especially since more non-influenza RNA viruses, along with specifically paramyxoviruses, are being found to produce DI segments and particles of potential inhibitory qualities (184-187). The reasoning behind this widespread characteristic of RNA viruses is due to the detection of DI genomes by innate immune system mechanisms that include multiple viral sensors independent of TLRs and type I IFN signaling can detect DI genomes, such as MDA5 and IRF3 (188). There is additional data that argues in favor of the adjuvant capacity of paramyxovirus DI particles in stimulating both mouse and human dendritic cells and have offered biological relevance to the reported inhibition of MDA5 by various paramyxovirus V proteins (49, 189).

To the best of our knowledge, there has not been a reported specific and intentional mutation to not only Mumps virus nucleoprotein by which the new virus mutant naturally produces DI particles. Further, this is the first report of a paramyxovirus that, after subsequent passages, presents a switch from a mutation-dominant population to that of wild-type, while still strongly exhibiting inhibitory and DI particle effects (sequencing data available upon request), this residue change of the "Top" region is critical to understanding key aspects of MuV RNA synthesis.

Due to "Top" being a domain, all three residues (63, 139, 197) were investigated using the minigenome system in singularity and duality combinations in order to verify that the entire "Top" domain is essential for this result to occur. The results of this investigation on both a minigenome and virus rescue scale showed that only the "Top"

combination exhibited the phenotype reported here – all three amino acid residue changes were required to maintain nucleoprotein formation and/or virus viability. While some individual and combinations of the "Top" amino acid mutations could produce either correctly formed nucleoprotein or virus, the viruses that could be rescued grew to dismal titers that could not be used for further characterization (data not shown).

Preliminary data has suggested that the "Top" domain of the nucleoprotein assists in its ability to properly interact with P-CTD, thus affecting the chaperoning and adherence of the polymerase to the RNA template. When this site was exchanged with the residues present in PIV5 NP, which does not interact with the CTD of its P, the phenotype inhibited viral growth while still producing DI particles. It is possible that since this "Top" domain has changed, it now has decreased efficiency in its ability to properly interact with P. This could help explain why the sequences from "Top" using primers to "capture" copy-back and hairpin DI genomes had repeated sections, as the inability for the L to properly secure to the template within the NP could cause a "stuttering" effect and inability to successfully replicate the genome to completion and accuracy. Most of the data suggests an inability of the "Top" nucleoprotein to interact fully with the carboxy domain of P; however, this interaction needs to be further investigated. It is also of interest to investigate how the "Top" nucleoprotein interacts with that of PIV5's P, because "Top" NP now exhibits PIV5 amino acid residues within a critical domain.

Conclusively, this research provides insight into the mechanics and functions of MuV NP's role in replication where crystallization could not. Through the exchange of residues between similar paramyxoviruses, insight was gained into how MuV's NP is essential for replication and assists in deciphering the function of specific sites and domains

of the protein's structure. MuV NP's role in viral RNA synthesis on a structural level can directly affect the viral polymerase's ability to access the genome successfully, either through the polymerase having difficulty in binding to NP, or NP being unable to conformationally change to reveal the RNA template. We have also learned that by manipulating the structure of one protein, DI particles can be produced in excess without high MOI infection. This could also be applied to other paramyxoviruses to not only discern how NP structure affects replicative function, but how to potentially manipulate other viruses to produce DI particles without using a high amount of virus particles. This development can help in developing further understanding of paramyxovirus replication and potential antiviral production using DI particles.

Acknowledgements

We greatly appreciate the helpful discussions and technical assistance from all members of Biao He's laboratory. This work was supported by grant R01AI106307 from the National Institutes of Health.

Figures and Figure Legend

A

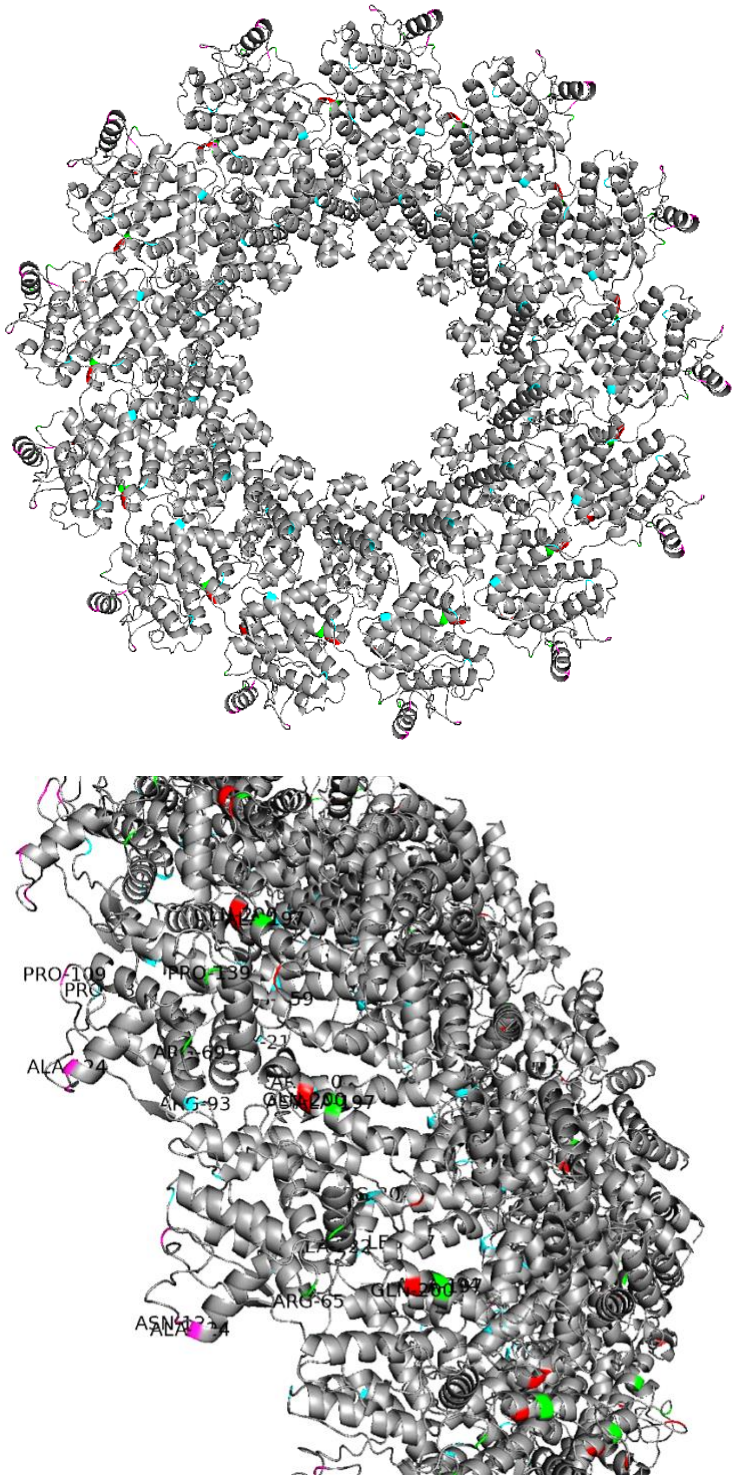

B

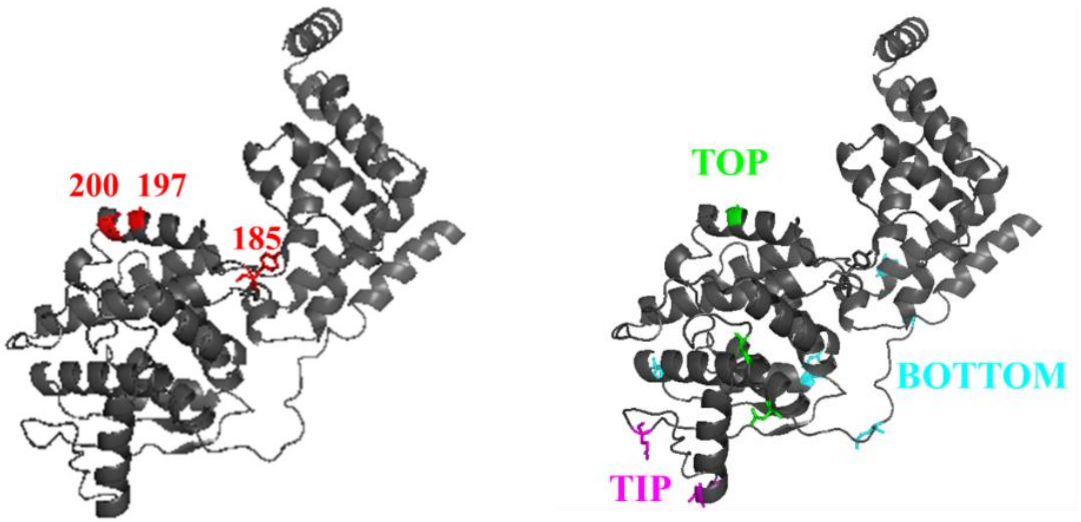

Figure 3.1. Model of MuV nucleoprotein. (A) The resulting theoretical 3D model of MuV NP built upon a PIV5 NP crystal structure. The image(s) shown depict the ring structure composed with 13 NP subunits. Red sites are 185 and 200, while green, magenta, and cyan residues are "Top", "Tip", and "Bottom" domains, respectively. (B) Depicts a singular NP NP subunit. Sites 185, 197, and 200 are marked and highlighted in red, and domains "Top", "Tip", and "Bottom" are denoted in green, magenta, and cyan, respectively, within the NP subunit model. Images were designed in PyMOL software.

Mutant	Site of Mutation
185 (Individual)	Y185P
197 (Individual)	A197Q
200 (Individual)	Q200R
Top	N063G/P139D/A197Q
Tip	P109E/N121G/A124R
Bottom	G021S/S029T/P043N/R093Q/R304Q

Table 3.1. Construct names and mutations made to the NP protein.

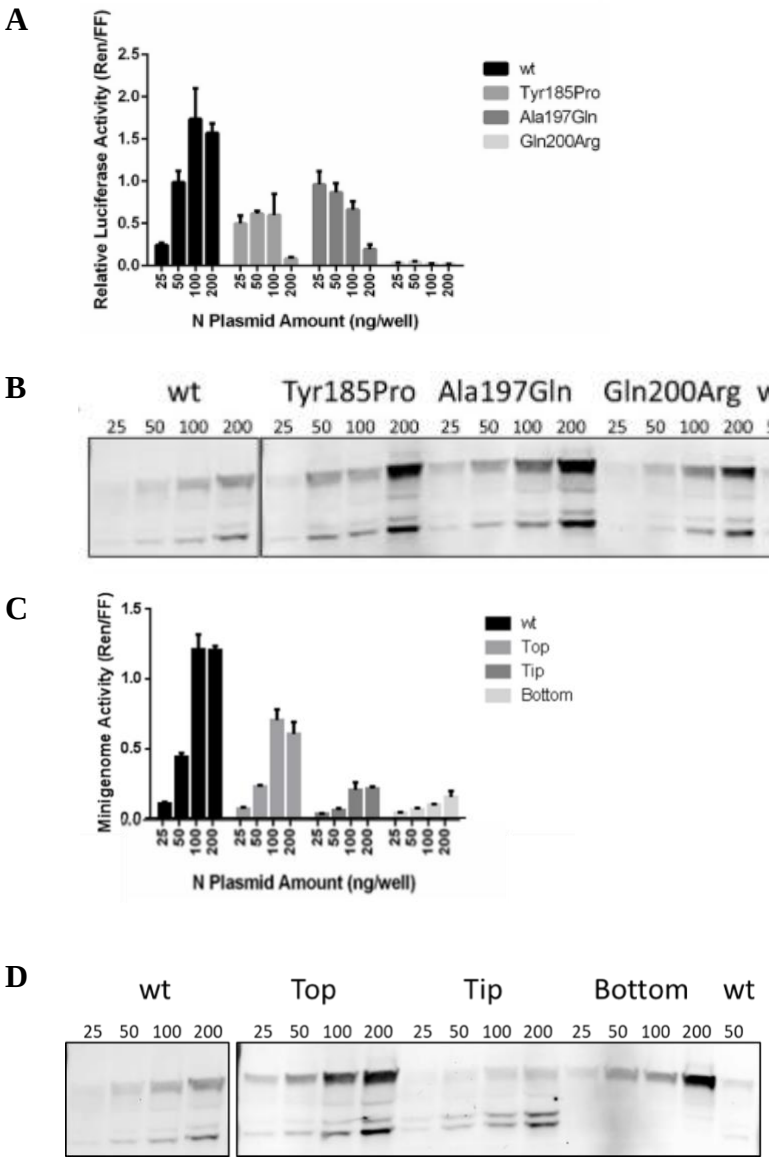

Figure 3.2. Effects of mutations in NP in a minigenome system. (A) Relative minigenome activity for NP mutants 185, 197, and 200, accompanied with their expression using a western blot analysis for NP protein (B). (C) Relative minigenome activity for NP mutants "Top", "Tip", and "Bottom", alongside a western blot of their protein expression levels, including protein degradation product (D).

Plasmid	Alias	Mutation(s)	Successful Rescue Attempt(s)	Plaques with Crystal Violet Staining	Positive (+) Immuno-staining	Colony Purified	Viral Titer
pJR01	MuV NP 185	Y185P	1/1	YES	YES	YES	3.25E+07
pJR02	MuV NP 197	A197Q	1/2	YES	YES	YES	4.70E+07
pJR03	MuV NP 200	Q200R	0/4	NO	NO	NO	____
pJR04	MuV NP TOP	N63G/P139D/A197Q	1/1	YES	YES	YES	2.67E+06
pJR05	MuV NP TIP	P109E/N121G/A124R	0/4	NO	NO	NO	____
pJR06	MuV NP BOTTOM	G21S/S29T/P43N/R93Q/R304Q	0/4	NO	NO	NO	____

Table 3.2. Rescue Status of MuV Mutants with NP mutations.

A **185Y (TAC) → P (CCA)**

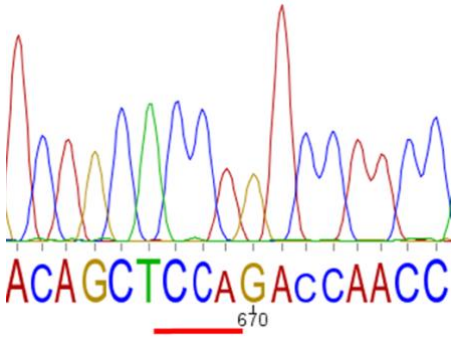

B **197A (GCG) → Q (CAA)**

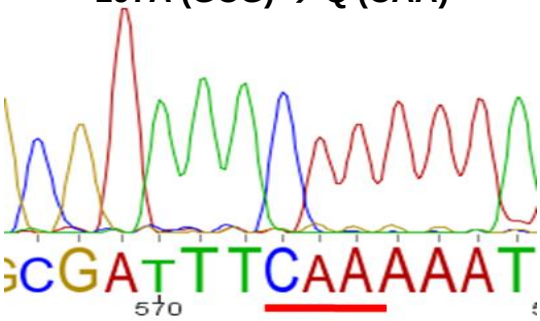

C **“Top” 63N (AAT) → G (GGT)**

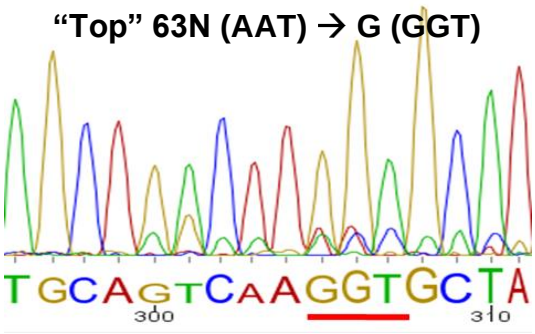

D **“Top” 139P (CCA) → D (GAC)**

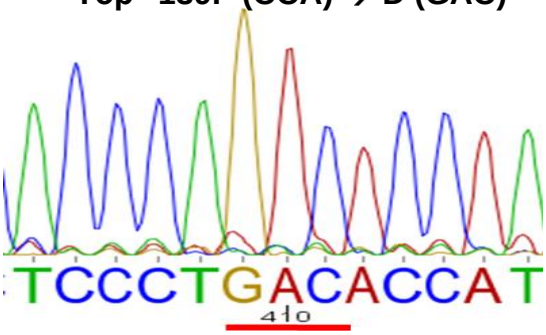

E

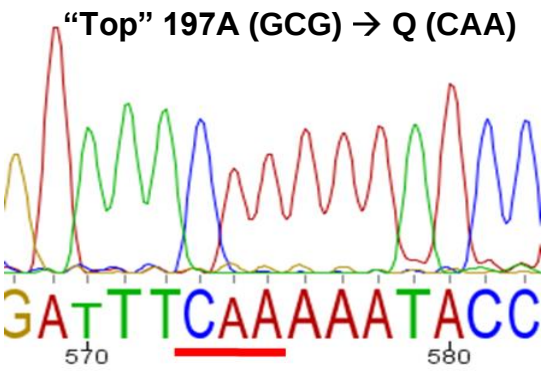

F

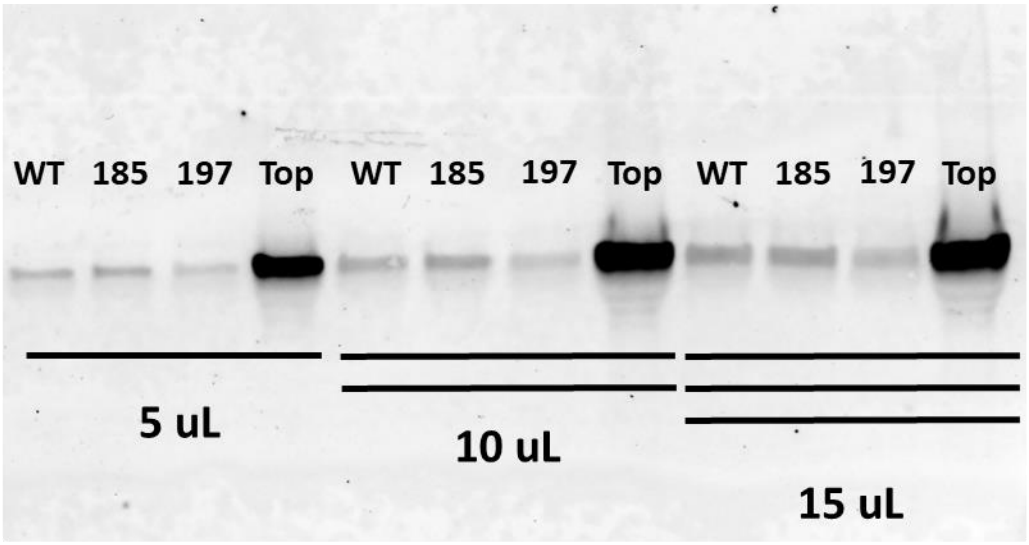

Figure 3.3: Confirmation of MuV mutant genomes and NP expression. Chromatograms of sequencing data using Geneious R11.1.5 software for (A) Y185P, (B) A197Q, and "Top" mutations N63G/P139D/A197Q (C, D, E, respectively). The red line underlines the nucleic acid mutation site of interest. Viruses MuV-IA (WT), "185", "197", and "Top" were diluted to $3.0x10^6$ PFU/mL, and either 5, 10, or 15 uL of virus supernatant were loaded onto a gel to perform SDS-PAGE and western blotting for nucleoprotein (NP) expression (F).

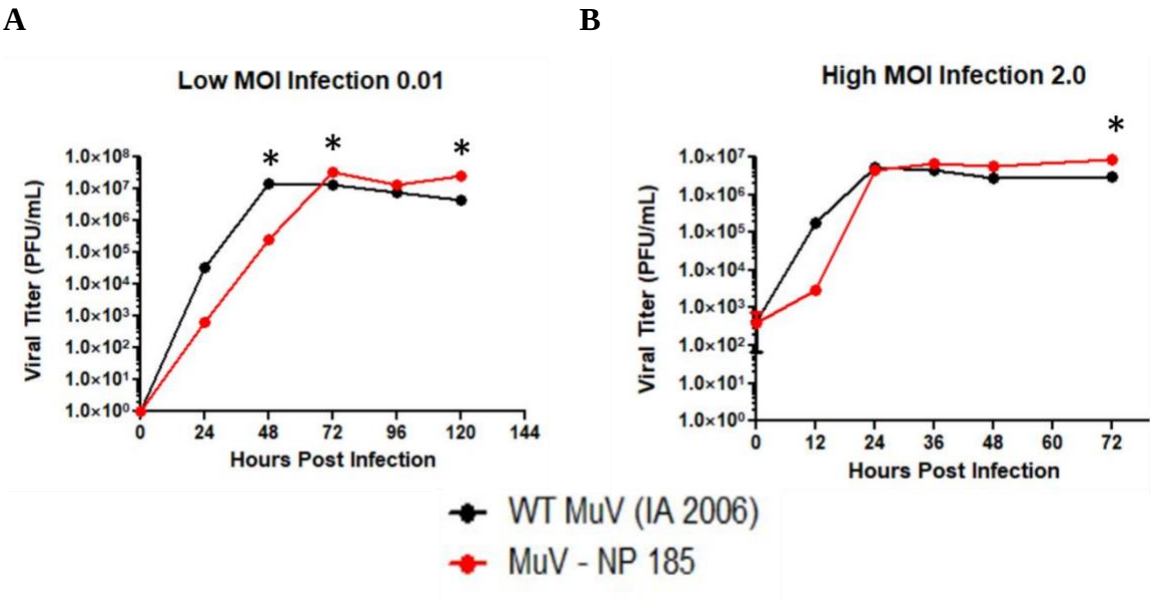
A
B
Low MOI Infection 0.01
High MOI Infection 2.0
Viral Titer (PFU/mL)
Hours Post Infection
WT MuV (IA 2006)
MuV - NP 185

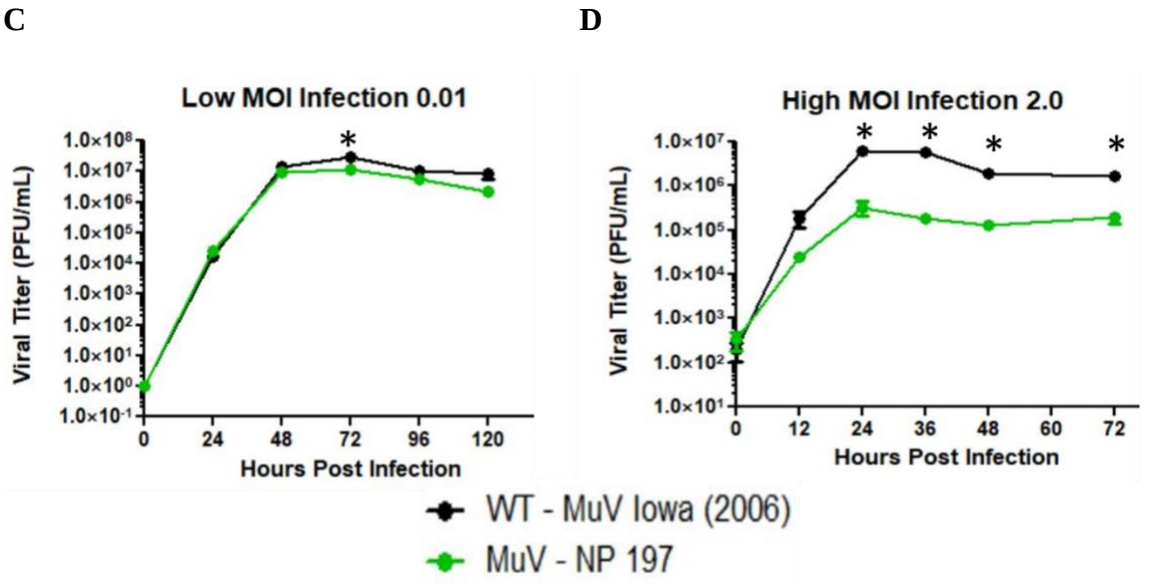
C
D
Low MOI Infection 0.01
High MOI Infection 2.0
Viral Titer (PFU/mL)
Hours Post Infection
WT - MuV Iowa (2006)
MuV - NP 197

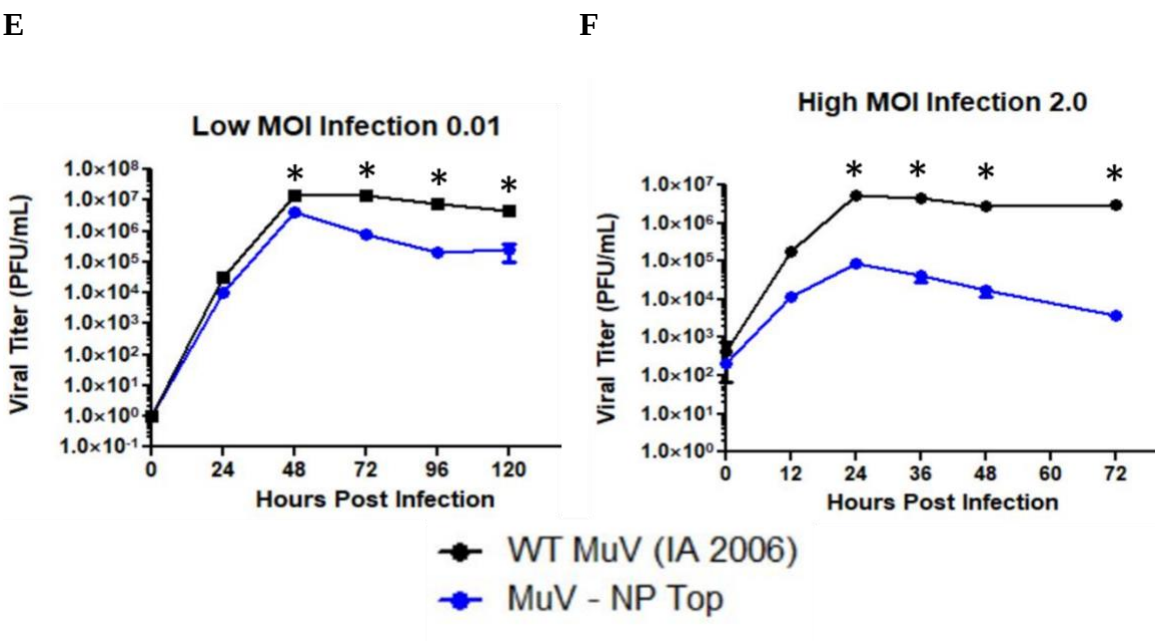

Figure 3.4. Growth curve kinetics of MuV mutants compared to wild-type. Low MOI growth curves (A, C, E) for 185, 197, and "Top", respectively, are based on samples taken every 24 hours post infection for 72 hours of a MOI of 0.01 infection of Vero cells. High MOI growth curves (B, D, F) for 185, 197, and "Top", respectively, are based on samples taken every 12 hours post infection for 60 hours of a MOI of 2 infection of Vero cells. Each MOI infection was verified by back titration. Asterisk denotes statistical significance of $p<0.05$ between groups at the same time point.

A

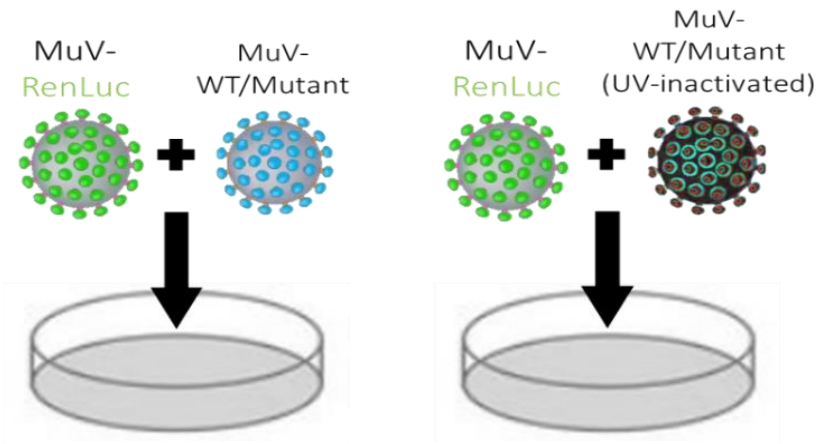

MuV-RenLuc = MOI 5
MuV WT = MOI 2, 0.1, 0.01, 0.001

B

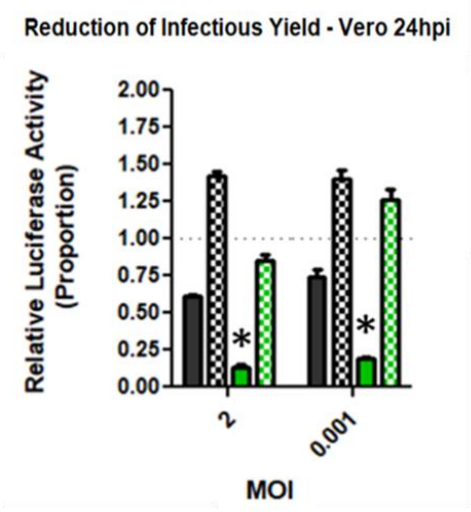

C

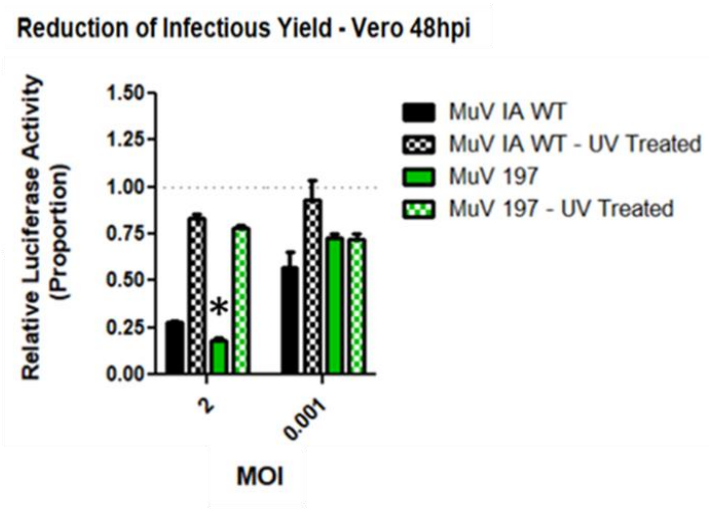

D

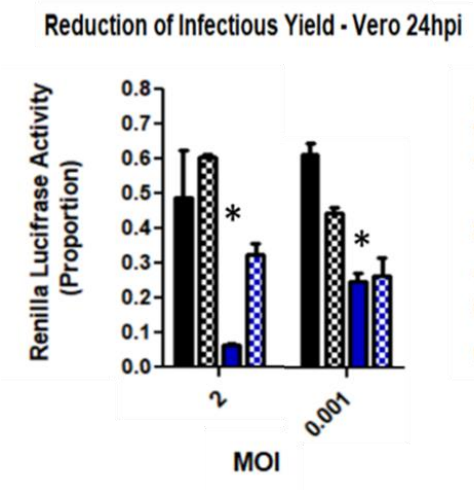

E

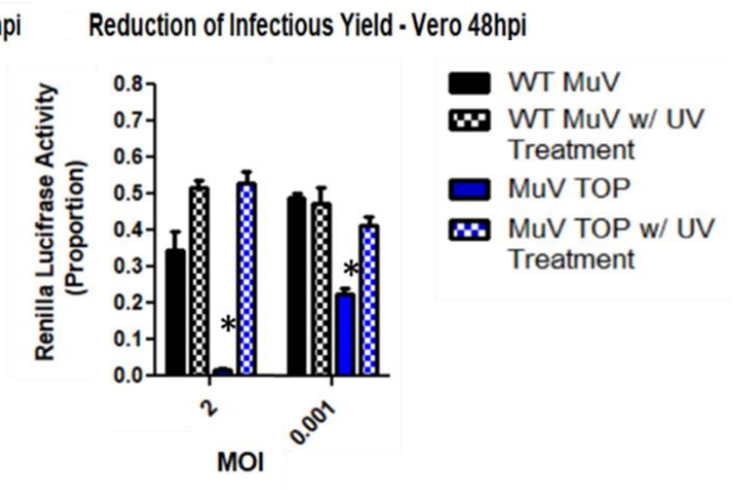

Figure 3.5. Reduction of Infectious Yield (RIY) assay. A diagram of the experimental set up and design of the reduction of infectious yield experiments (A). The Renilla luciferase activity for wild-type and 197 MuV, as well as wild-type and 197 MuV that was UV inactivated, is shown at 24 hours (B) and 48 hours (C) post infection at various MOIs. The same experiment was done for "Top" MuV, and the Renilla luciferase activity is shown at 24 hours (D) and 48 hours (E) post infection. Asterisk denotes statistical significance of $p<0.05$ when compared to a like-group (WT to mutant, or WT-UV-treated to mutant-UV-treated).

Virus	Passage	PFU/mL Titer	HA Titer	PFU to HA Ratio (per mL) ($x10^3$)	Normalized to Wild type
MuV-WT	5	1.63E+7	128	6.37	1
MuV-WT*	6	3.78E+7	256	7.38	1.159
MuV-RenLuc	5	4.38E+7	256	8.55	1.34
MuV-Y185P	2	3.25E+7	128	12.70	1.99
MuV-A197Q	2	4.70E+7	256	9.18	1.44
MuV-A197Q*	4	8.68E+5	64	0.678	0.106
MuV-Top	2	3.00E+6	128	1.17	0.18
MuV-Top	3	7.77E+5	256	0.15	0.02
MuV-Top*	4	6.00E+4	64	0.047	0.0074

* = Purified

Table 3.3. Hemagglutination titers compared to infectious virus (PFU) titer of MuV wild-type and mutants. The * denotes virus purified by ultracentrifugation on a sucrose gradient cushion.

Primer Set	Forward Primer	Reverse Primer	Description	RT-PCR Bands Present in MuV-WT Pass 2?	RT-PCR Bands Present in MuV-Top Pass 2?	RT-PCR Bands Present in MuV-Top Pass 3?
1	JR236F: 5′-ACC AAG GGG AAA ATG AAG ATG GGA TAT TGG TAG AAC AAA TAG TGT AAG AAA CAG T-3′	JR234R: 5′-ACC AAG GGG AGA AAG TAA AAT CAA T-3′	Entire leader sequence with trailer sequence	No	Yes (2)	Yes (1)
2	JR232F: 5′-ACC AAG GGG AAA ATG AAG ATG GGA TAT T-3′	JR234R: 5′-ACC AAG GGG AGA AAG TAA AAT CAA T-3′	First half of leader sequence with trailer sequence	Yes (4)	Yes (3)	Yes (5)
3	JR236F: 5′-ACC AAG GGG AAA ATG AAG ATG GGA TAT TGG TAG AAC AAA TAG TGT AAG AAA CAG T-3′	N/A	Entire leader sequence only	No	Yes (1)	No
4	JR232F: 5′-ACC AAG GGG AAA ATG AAG ATG GGA TAT T-3′	N/A	First half of leader sequence only	Yes (3)	Yes (3)	Yes (6)
5	N/A	JR234R: 5′-ACC AAG GGG AGA AAG TAA AAT CAA T-3′	Trailer sequence only	No	Yes (1)	No
6	JR232F: 5′-ACC AAG GGG AAA ATG AAG ATG GGA TAT T-3′	JR238R: 5′-AAT ATC CCA TCT TCA TTT TCC CCT TGG T-3′	First half of leader sequence with its reverse complementary primer.	Yes (1)	Yes (smear)	No
7	MuV_4939F: 5′-ACA AAT GCA CGC GCA ATA GC-3′	MuV_8550R: 5′-AAC TGA CAG GCA AGC CAA AC-3′	3.6kb region within F and HN genes	Yes (1)	Yes (1)	Yes (1)

Table 3.4. Defective Interfering (DI) particle primers pairs list for RT-PCR of mumps viruses. Seven primer pairs were used in all, with three being single primers and pair "7" being a positive control for the F and HN gene region of the MuV genome. Primer descriptions and sequences are included.

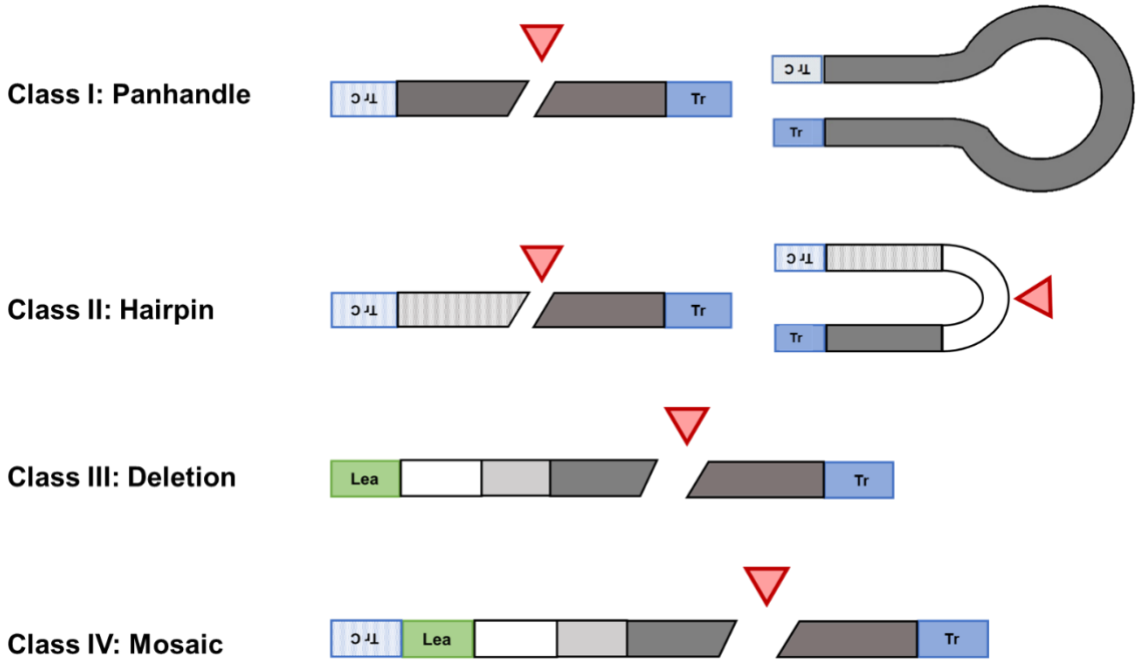

Figure 3.6. Diagram of types of defective interfering particle genomes. The diagram shows four main categories of DI particle genomes: Class I and Class II are referred to often as copy- and snap-backs, respectively, and share similar inherent properties in that the leader/trailer sequences are complementary, representing the skipping of the polymerase between positive and negative RNA strands. Class III is a common type of DI particle, where the polymerase skips large sections of the genome, but reattaches on the same strand and direction, causing minor to major deletions in the final replicated genome. The last class, mosaic, represents a combination of the classes within the same DI particle, and does not occur often.

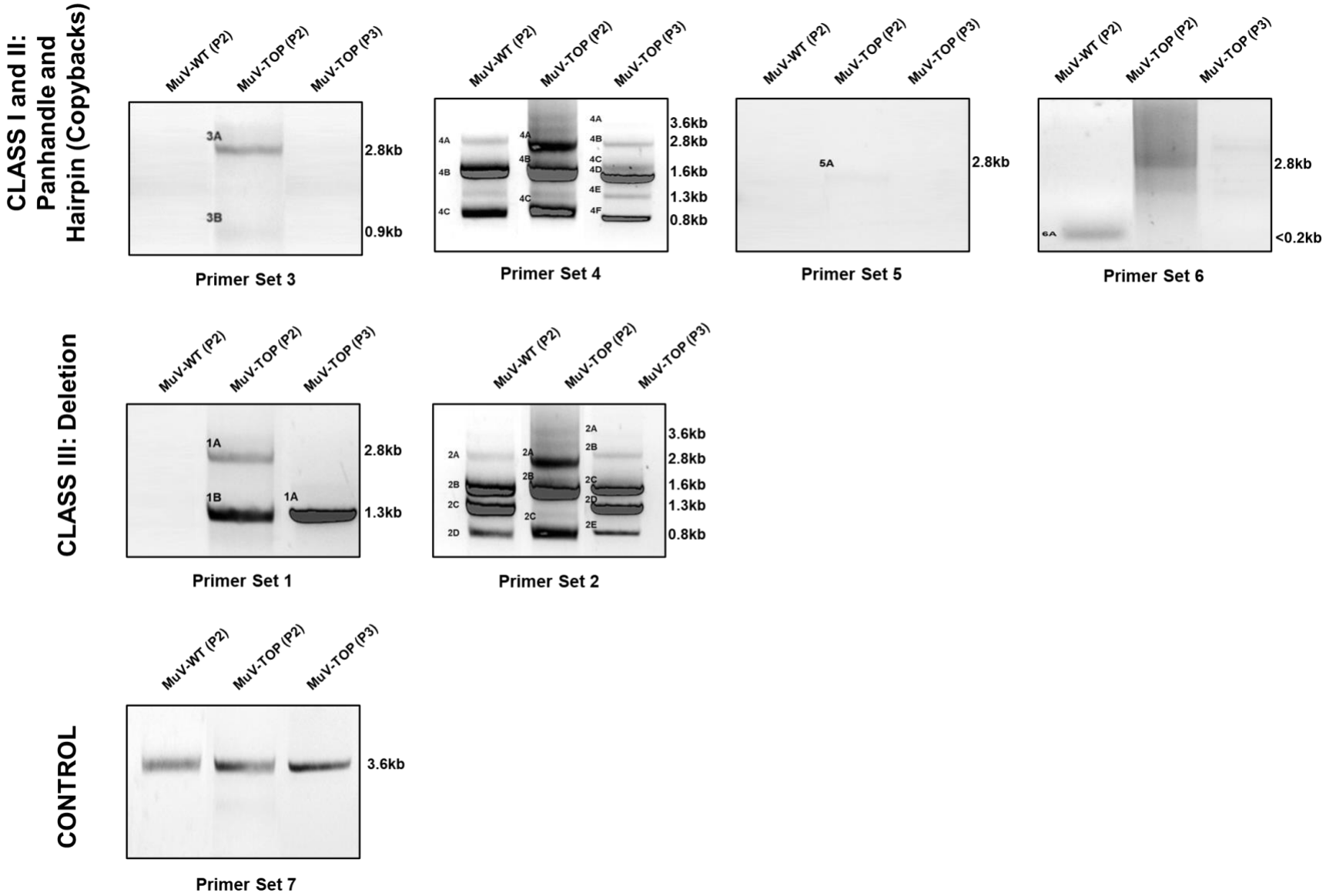
CLASS I and II: Panhandle and Hairpin (Copybacks)
MuV-WT (P2)
MuV-TOP (P2)
MuV-TOP (P3)
3A
3B
2.8kb
0.9kb
Primer Set 3
4A
4B
4C
3.6kb
2.8kb
1.6kb
1.3kb
0.8kb
Primer Set 4
5A
2.8kb
Primer Set 5
6A
2.8kb
<0.2kb
Primer Set 6
CLASS III: Deletion
1A
1B
Primer Set 1
2A
2B
2C
2D
2E
Primer Set 2
CONTROL
3.6kb
Primer Set 7

Figure 3.7. RT-PCR of MuV using primers designed for detecting Defective Interfering (DI) particles. Included are images of the gel electrophoresis of the RT-PCR products of extracted viral RNA from passage 2 of MuV wild-type and "Top" mutant passages 2 and 3. Primer sets are organized by their "class" of DI particles and labeled at the bottom of the image. Bands are labeled starting with their primer set number and then with a letter of the alphabet in order of size (largest to smallest). Bands are also labeled with relative sizes to the right of each gel image.

A

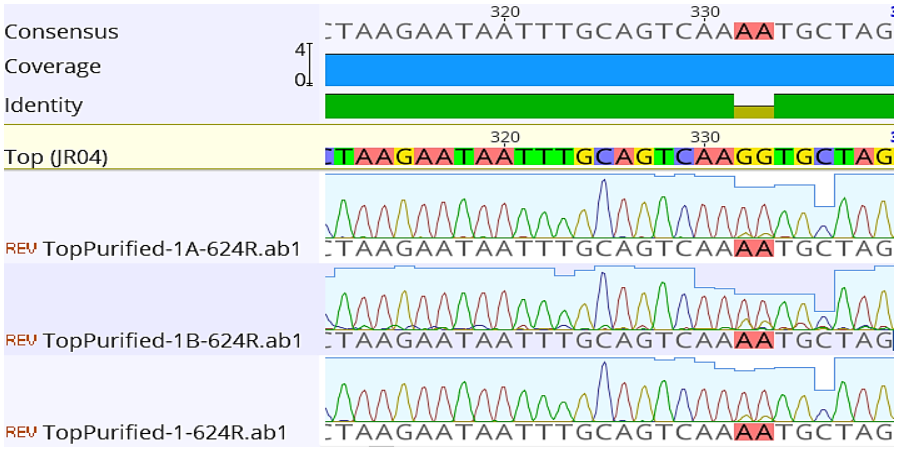
Consensus
Coverage
Identity
Top (JR04)
REV TopPurified-1A-624R.ab1
REV TopPurified-1B-624R.ab1
REV TopPurified-1-624R.ab1

B

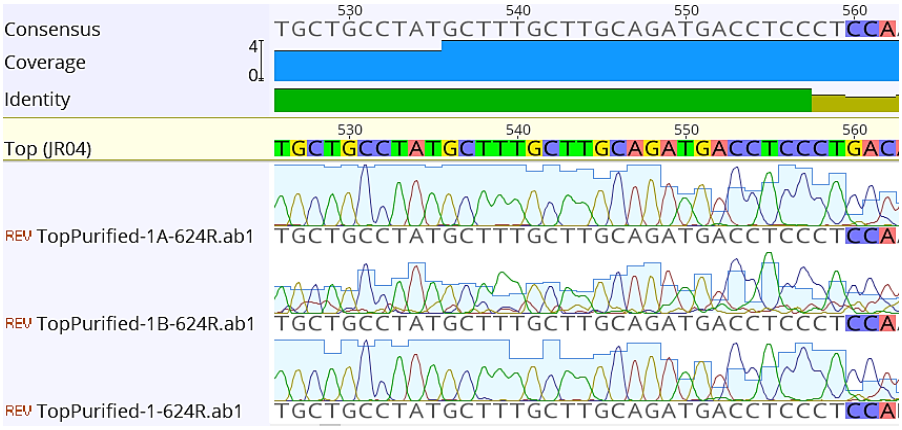
Consensus
Coverage
Identity
Top (JR04)
REV TopPurified-1A-624R.ab1
REV TopPurified-1B-624R.ab1
REV TopPurified-1-624R.ab1

C

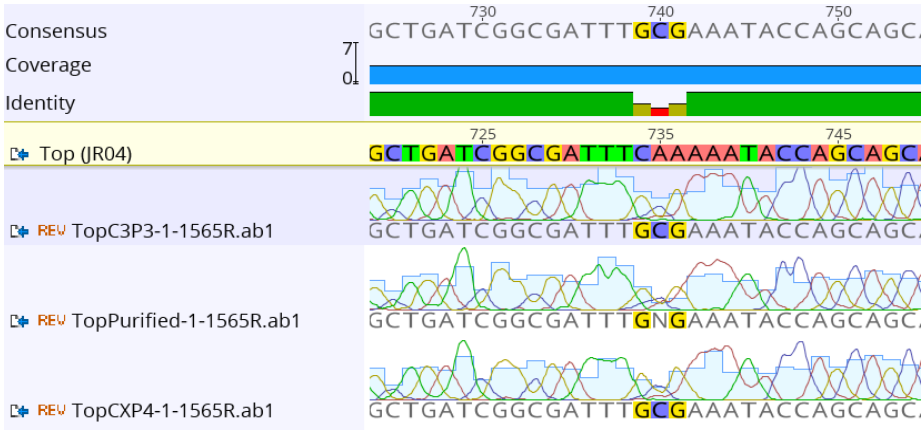
Consensus
Coverage
Identity
Top (JR04)
REV TopC3P3-1-1565R.ab1
REV TopPurified-1-1565R.ab1
REV TopCXP4-1-1565R.ab1

Figure 3.8. Sanger sequencing results from TOPO cloning of excised RT-PCR DI Particle gel electrophoresis products. As seen in Figure 3.7, "Top's" population becomes more heterogeneous and reverts to a predominantly wild-type genotype. Through TOPO cloning of excised gel fragments of the RT-PCR products, Sanger sequencing was able to be performed on these unknown band sequences captured by the DI primer sets. This qualitatively observed variability from the gel electrophoresis results is further supported by the variance of peak height and quality surrounding the base pairs, which should be mutated in passage 4 of the "Top" virus, for amino acid sites 63 (A), 139 (B), and 197 (C). A collection of sequencing samples is shown and are aligned to the sequence for "Top" virus.

CHAPTER 4

THE STRUCTURAL AND FUNCTIONAL ANALYSIS OF THE MUMPS PHOSPHOPROTEIN TRANS-COMPLEMENTARY N- AND C-TERMINAL DOMAINS[2]

[2] Risalvato J, Oliver AP, Luo M, He B. Submitted to Journal of Virology XX/XX/20XX.

Abstract

Mumps virus (MuV) is a negative-stranded RNA virus that encapsidates its genomic RNA within the nucleocapsid protein (NP). To make the viral genome accessible to viral RNA-dependent RNA polymerase (L) for viral RNA synthesis, the phosphoprotein (P) binds to NP to initiate the conformational change necessary for exposing the replication template and helps to bring the RNA polymerase to NP and genomic RNA. Together, NP, L, and P form the ribonucleoprotein (RNP) complex that is essential for viral transcription and replication. MuV is the only known paramyxovirus for which both the N-terminal domain (NTD) and C-terminal domain (CTD) of P bind to NP. It is thought that the unique structure of MuV P, an anti-parallel tetramer, could be attributed to this distinctive interaction. Each domain of P plays a different role in replication through the binding to the nucleocapsid; the NTD uncoils the helical nucleocapsid, while the CTD assists in directing the RNA polymerase to the nucleocapsid RNA template. To determine which sites within the NTD and CTD of P are the precise binding sites to NP, an alanine scan was performed on MuV P truncation mutants and full-length P, and their activities were examined using a minigenome reporter system. Interestingly, our results indicate that the NTD likely possesses a “positive” motif, while the CTD possesses a “negative” motif in regulating viral RNA synthesis.

Significance

As an important reemerging human pathogen, MuV requires greater understanding regarding its protein interactions in viral replication. The MuV phosphoprotein is a critical component of viral RNA synthesis. In this work, a novel minigenome system was utilized

to allow the NTD and CTD of P to be paired trans-complementary to aid in the verification of MuV P's protein conformation and better characterize its structural stability. This understanding of protein structure in replicative function will allow the design of improved antivirals and vaccines.

Introduction

A human disease, mumps causes acute infection with symptoms that range from fatigue and parotitis to severe meningitis and permanent deafness (1). Mumps virus (MuV), the causative agent of mumps, is a virus in the genus *Rubulavirus* and family *Paramyxoviridae*. The MuV genome is a nonsegmented, negative-stranded RNA genome with 15,384 nucleotides with seven genes encoding for nine viral proteins (6). The RNA genome of mumps virus is encapsidated by the nucleoprotein (NP) within a helical nucleocapsid (RNP) – this NP-RNA structural conformation serves as a template for MuV RNA synthesis (99). The large protein (L) and the phosphoprotein (P) together form the viral RNA-dependent RNA polymerase (vRdRp) complex which replicates the RNA genome and performs transcription. L protein enzymatic activities include initiation, elongation, and termination of RNA synthesis, but it is also capable of post-transcriptional modifications such as mRNA capping and the addition of a 3' poly(A) tail (6, 147). P is the critical cofactor of the polymerase – it acts as a chaperone and anchor for L to the NP-RNA template for all its essential enzymatic functions (98, 133, 190). As it is capable of self-oligomerization and forming various complexes with L, NP, and RNP, P's role in MuV replication is vital.

Across the paramyxoviruses, the P proteins are modular and consist primarily of three main domains: the N-terminal, oligomerization, and C-terminal domains, all with flexible linkers between the adjoining regions (135, 136). P is observed to self-oligomerize in many negative-stranded RNA viruses (NSVs) (135). The first paramyxovirus to have its oligomerization domain of P crystallized was Sendai virus (SeV), which revealed a parallel coiled-coil tetramer (all monomers in the same polar orientation) (137, 191-193). The tetrameric structure of phosphoprotein has been found among other paramyxoviruses, including mumps virus, but the orientation of the monomers within the tetramer differs among them. The previously mentioned self-association of P is necessary for transcriptional activity, and in the case of SeV, the region also serves as a binding site for SeV L (47, 194-200).

The tetrameric structure of P does not appear to be a hallmark of all NSVs. For example, the P protein of vesicular stomatitis virus (VSV) from the family *Rhabdoviridae* forms a singular dimer of α-helices held together via hydrophobic interactions in parallel orientation (141). As the VSV P is also capable of self-oligomerization, as seen in a VSV minigenome assay, characterizing how VSV P's dimer structure affects viral replication compared to the paramyxovirus tetrameric structure can assist in understanding how these P interactions are affected by structure (140, 201, 202). For example, the N-terminal of rabies virus P, another rhabdovirus, interacts with nascent NP and L, while the C-terminal domain binds to the RNP (143-145). However, this difference could be due to the N-terminal and C-terminal domains of rabies P being positioned on the same poles, while the domains are at opposite ends of oligomerization domains for MuV.

For paramyxovirus P proteins, the nucleocapsid-binding domain (NBD) is mainly found within the C-terminal domain for most viruses (148, 203, 204). Particularly in MuV P, the last 49 amino acid residues of P directly mediate binding to the NP, although the precise residues remain unknown (34). While the NBD within the C-terminal domain is conserved, MuV P uniquely also binds to the NP within its N-terminal domain (47). This NP interaction within the N-terminal of MuV P was confirmed by electron microscopy, which revealed uncoiling of the helical nucleocapsid and resulted in increased viral RNA synthesis within a minigenome system (39).

The MuV P oligomerization domain (defined as amino acid residues 213-277) has been crystalized and revealed a tetrameric formation with two pairs of parallel α-helices oriented in antiparallel to each other (47). This orientation means that both poles of the P tetramer have two copies each of the N-terminal and C-terminal domains. This specific orientation has been found to be unique among P proteins of nonsegmented NSVs.

In this work, we used a novel minigenome system for MuV in which the C-terminal and N-terminal domains of P could be studied using different ratios of trans-complementation. Furthermore, this system allowed for the testing of mutant P domains for the determination of structural parameters of P's stability and function in NP binding interactions for viral replication.

Materials and Methods

Molecular cloning

Plasmids constructed in this work were done using standard molecular techniques – details and sequence files of plasmids constructed and used are available upon request.

The MuV NP, P, and L genes of the MuV strain Iowa/US/2006 were cloned into a pCAGGS expression vector as previously described (75). P truncations with Flag and MetMetMetFlag (mmmFlag) epitope tags are defined as P_{NO} (residues 1-277 + mmmFlag) and P_{OC} (Flag + residues 213-391) throughout this work (48). A MuV minigenome plasmid (pBH276/pMG-RLuc) containing the *Renilla* luciferase expression gene was used, along with a plasmid containing the firefly-luciferase gene (pFF-Luc) (44). Both the firefly-luciferase and minigenome plasmid expression plasmids were constructed using a pCAGGS vector as the backbone.

Cell culture

BSR-T7 cells were maintained in Dulbecco's modified Eagle medium (DMEM) with 10% fetal bovine serum (FBS), 10% tryptose phosphate broth (TPB), and 1% penicillin-streptomycin solution (P/S) (Mediatech Inc. Manassas, VA). 293T cells were maintained DMEM supplemented with 5% FBS and 1% P/S (Mediatech Inc., Manassas, VA). Both cell lines were incubated at 37°C and 5% CO_2.

Transfections

BSR-T7 or 293T cells were passed at an appropriate dilution one day prior to use in order to achieve approximately 80% confluency upon transfection the following day. Cells were transfected using a JetPRIME (Polyplus Transfection Inc., New York, NY) transfection reagent kit following the manufacturer's protocols.

MuV minigenome system and dual-luciferase assay

The MuV minigenome system used in this work was described previously (39, 44, 48). Total P, P domain truncations, or P domain truncation mutants were transfected at increasing amounts (10, 20, 40, 80, or 160 ng) along with NP (25 ng), L (500 ng), pMG-RLuc (100 ng), and pFF-Luc (1 ng) held at steady state in BSR-T7 cells. pCAGGS expressing green fluorescent protein (GFP) was used to normalize the mass of transfected DNA per sample. After 48 hours, the cells were lysed and the lysate was used to perform a dual-luciferase assay according to the manufacturer's protocol (Promega, Madison, WI). Light intensity of firefly and *Renilla* luciferase was detected and measured using a GloMax 96 Microplate Luminometer (Promega). Relative luciferase activity was defined and calculated as the ratio of Renilla luciferase to firefly luciferase activity. Three replicates of each sample were used to compare the peak relative luciferase activity of each P mutant to that of wild-type P. Aliquots of the cell lysates were used for Western blot analysis.

Western Blot analysis of minigenome lysates

Minigenome lysate aliquots were diluted 3:1 with 4X Laemmli Sample Buffer (Bio-Rad Laboratories, Hercules, CA) plus β-mercaptoethanol at 9:1, and then heated at 95ºC for 5 minutes. Samples were loaded into a 4-20% Mini-PROTEAN® TGX (Bio-Rad Laboratories, Hercules, CA) polyacrylamide gel, and proteins were size-separated by gel electrophoresis. The proteins were then transferred to a polyvinylidene difluoride (PVDF) membrane (GE Healthcare, Piscataway, NJ). The membrane was then incubated with mouse anti-MuV-NP antibody (1:2000 dilution) and either anti-MuV-P antibody (1:1000 dilution) or anti-Flag antibody (1:2500 dilution) (ThermoFisher Scientific) or both anti-MuV-P and anti-Flag antibody. Primary incubation was followed by secondary incubation

with Cy3-conjugated goat anti-mouse IgG antibody (1:2500 dilution) (Jackson ImmunoResearch, West Grove, PA), and scanned using a Typhoon 9700 imager (GE Healthcare Life Sciences, Piscataway, NJ).

Results

MuV P domains exhibit trans-complementarity

As previously mentioned, the MuV P has three key domains: a N-terminal domain (NTD), an oligomerization domain (OD), and a C-terminal domain (CTD). These domains are connected via flexible linker regions. For the purpose of this work, P_{NO} and P_{OC} proteins were used. P_{NO} is a truncated P protein including only the NTD and OD, while P_{OC} includes only the OD and CTD of the phosphoprotein. Both P_{NO} and P_{OC} are tagged with a flag tag on the carboxy terminus and the amino terminus, respectively. When truncated, it is known that MuV P can form parallel dimers, and it is even capable of forming antiparallel dimers (Figure 4.1). The presence of the oligomerization domain is essential for this dimerization and tetramerization of the phosphoprotein and is also necessary for MuV genome replication, so it was included in the truncated protein constructs (39, 44, 48). Additionally, both the NTD and CTD of MuV must be present for the MuV genome to be replicated and proteins expressed (Figure 4.2A).

Previous work had detailed use of P_{NO} and P_{OC} at a ratio of 1:1 (39, 48). Before pursuing further experiments, other ratios of P_{NO}:P_{OC} were investigated in order to determine if a ratio of 1:1 was suitable for our applications on the basis of P_{NO} and P_{OC} being different molecular sizes (~31 and 21 kDa, respectively) and having different roles during MuV replication. When holding the amount of POC static and adding increasing

amounts of P_{NO}, the ratio of P_{NO}:P_{OC} determined to yield the highest minigenome activity was at those higher than 1:2, consistently 1:4 (Figure 4.2B). This was also seen when holding the mass of P_{NO} while adding increasing amounts of POC – the best P_{NO}:P_{OC} ratio determined to yield increased minigenome activity was 1:2 to 1:4 (Figure 4.2C). The data displayed that a P_{NO}:P_{OC} ratio at a minimum of 1:2 yielded significantly increased minigenome results. However, since previous work was done using a P_{NO}:P_{OC} ratio of 1:1, which also showed a trend of increased minigenome activity compared to wild-type P, these parameters were not changed in order to not potentially introduce confounding variables such as extraneous activity that could overshadow noteworthy results.

Truncations of the N- and C-terminal domains of P to isolate interacting regions

The initial goal of this work was to isolate the specific binding domains of NP to the amino and carboxy termini of P. To do this, P_{NO} and P_{OC} were fractioned into fifths of their original domains, denoted as $P_{0.8NO/OC}$, $P_{0.6NO/OC}$, $P_{0.4NO/OC}$, and $P_{0.2NO/OC}$ to represent how much of the original domain was left after fractionation. Figure 4.3A shows a visual representation of the fractioning of P_{NO}'s N-terminal domain into fifths. MuV minigenome data concluded no minigenome activity for these mutants (Figure 4.3B). However, since expression was noted on the immunoblot for these fractioned P_{NO} truncates (Figure 4.3C), it was deduced that the first forty amino acids of the N-terminal domain of P was critical for protein tetramerization and dimerization stability and replication functions.

The same process was repeated for P_{OC}. Figure 4.4A shows a visual representation of the fractioning of P_{OC}'s C-terminal domain into fifths. The MuV minigenome data for this fractionation determined that there was no minigenome activity for any of these

mutants (Figure 4.4B). When immunoblotted, expression was present for the P_{OC} truncates (Figure 4.4C); thus, it was deduced that the last twenty amino acids of the C-terminal domain of P was critical for protein tetramerization and dimerization stability and replication functions.

Further fractionations and alanine substitutions in groups of five or four residues were performed on the N-terminal and C-terminal of P. The data from these fractionations further isolated the regions of interest for the N- and C-terminal domains to be the first twenty and last twenty residues (data not shown).

Alanine scan of N- and C-terminal domains of P to find points of interaction

Once these regions of interest were narrowed down, an alanine scan was performed within these regions and their minigenome activity observed. For the N-terminal domain, the first eight (Figure 4.5A) and second eight (Figure 4.5B) amino acid residues were replaced with alanine and minigenomes performed. For the C-terminal domain, two alanine residues were "skipped" – aa390 and 378. Due to this, the last nine (except aa390) and second-to-last nine (except aa378) amino acid residues were replaced with alanine, and their minigenome activities observed (Figures 4.5C and D respectively). After performing the minigenomes, it was noted that there appeared to be a "reflection" of activity, with the N-terminal and C-terminal domains of P exhibiting chiral properties of minigenome replication activity.

The observed chirality of minigenome replication activity between N-terminal and C-terminal domain alanine mutants was further investigated by transfecting the chiral domains in pairs, and the same minigenome activity pattern was observed (Figure 4.6).

Taken one step further, full-length P was also mutated so that chiral alanine substitutions in both the N- and C-terminal domains were present in P simultaneously. Transfecting full-length P mutants with single alanine substitutions in either its amino or carboxy terminus, along with "double knock-out" mutants with mutations reflected in both termini, exhibited a similar pattern of minigenome activity (Figure 4.7 and 4.8, respectively). A summary of the amino acid residues substituted, their chemical properties, and subjective minigenome activities per experiment can be seen in Table 4.1.

"Rescue" N- and C-terminus truncates with low activity with high activity termini

Based on the information gathered in Table 4.1, it was hypothesized that termini with "low" minigenome activity might be "rescued", or have some of their minigenome activity return, if transfected with a "high" activity complementary terminus. To test this, one "high" minigenome activity mutant representing the N- and C-termini, respectively, were transfected with their opposing terminus mutants classified as having "low" minigenome activity. The high performing P_{NO} mutant selected to test in this instance was $P_{NO\text{-}15A}$ against the low P_{OC} performers $P_{OC\text{-}391A}$, $P_{OC\text{-}388A}$, $P_{OC\text{-}387A}$, $P_{OC\text{-}384A}$, $P_{OC\text{-}383A}$, $P_{OC\text{-}382A}$, $P_{OC\text{-}379A}$, and $P_{OC\text{-}377A}$. The high performing P_{OC} mutant selected to test in this instance was $P_{OC\text{-}376A}$ against the low P_{NO} performers $P_{NO\text{-}2A}$, $P_{NO\text{-}4A}$, $P_{NO\text{-}5A}$, $P_{NO\text{-}8A}$, $P_{NO\text{-}9A}$, $P_{NO\text{-}10A}$, $P_{NO\text{-}13A}$, and $P_{NO\text{-}14A}$. It should be noted that both the "high" performing N- and C-terminus P truncation mutants are chiral in their placement to one another.

As shown in Figure 4.9, $P_{NO\text{-}15A}$ was able to "rescue" $P_{OC\text{-}387A}$ and $P_{OC\text{-}377A}$, and $P_{OC\text{-}376A}$ was able to "rescue" $P_{NO\text{-}8A}$. $P_{NO\text{-}15A}$ was originally a Glutamine residue, which is polar and charged, while $P_{OC\text{-}387A}$ and $P_{OC\text{-}377A}$ were Isoleucine and Aspartic Acid, hydrophobic

and charged residues, respectively. $P_{OC\text{-}376A}$ was also originally a Glutamine residue, and it was able to "rescue" $P_{NO\text{-}8A}$, originally Aspartic Acid. This data suggests that these residues are critical to P structure and MuV replication ability. The replacement of critical residues with Alanine within one terminus can be potentially offset or "repaired" by the replacement of specific residues on the opposing terminus, indicating that a structural interaction between the N- and C- termini of P is essential to its replicative function.

From this point on in the study, the focus of the work became deducing why there appeared to be identical minigenome activities among alanine scanned N-terminal and C-terminal domains in chiral.

Heptad repeat in MuV P N- and C-terminal domains

Due to the repeating patterns seen in alanine-scanned P_{NO} and P_{OC} mutants separately (Figure 4.5) and together (Figure 4.6), a similar pattern of minigenome activity seen in P single-point and "double knock-out" mutants (Figures 4.7 and 4.8), and the ability for "high" activity domains to "rescue" "low" activity opposite domains (Figure 4.9), it was hypothesized that a heptad repeat for structural stability and possible maintenance of viral replication activity was present. Heptad repeats are structural motifs that consist of a repeating pattern of seven residues – *abcdefg*. Typically, "a" and "d" are hydrophobic residues that reside towards the inside of a protein dimer, trimer, or tetramer, whereas "b", "c", "e", "f", and "g" are polar residues and face the outer surface of the protein structure. Additionally, "e" and "g" are often, but not always, charged amino acids (205). Heptad repeats are essential for the structural basis of coiled coils and stabilizing their reactions

and can have functional applications to allow for secondary structures as can be seen in paramyxovirus fusion glycoproteins.

Due to the published crystal structure of the oligomerization domain of MuV P (47), the antiparallel P_{NTD} and P_{CTD} helical pairs are approximately offset by ~0.25 heptad in respect to each other, while the helical offset is zero in parallel homodimer structures (206). This tetramer in which two dimers in parallel are oriented antiparallel to one another provides a unique interdigitation at the nonpolar interface. The "d" side chains of P_{NTD1} are hypothesized to intercalate into pockets formed by the "a" residues of the P_{CTD2} and the "g" residues of the P_{CTD1} helices. P_{CTD1} "d" residues are thought to interact with both the P_{NTD1} and P_{NTD2} helices at the "a" and "g" residues, respectively. A similar structural relation pattern can be seen where the "a" side chains of P_{NTD2} fit into grooves formed by residues "d" and "e" of helices P_{CTD1} and P_{CTD2}, respectively. The proposed model can be seen in Figure 4.10 and is supported by coiled-coil predictive software PredictProtein (207) and Coiled-Coils Prediction (208, 209) (see Appendix).

Discussion

Paramyxovirus P proteins are believed to be capable of domain modification without affecting the function of other P domains due to their modular structure and nature. MuV P's domains have been mapped and its oligomerization domain crystallized (47, 135). Here, we generated MuV P N- and C-terminal domain truncations in order to examine how mutations within the N- and C-terminal domains affect P structure and function in viral RNA synthesis. It was previously found that transfecting increased amounts of N terminal domain would result in enhanced activity in the minigenome system due to increased

uncoiling of the nucleocapsid (39). This study confirmed that increasing the ratio of P_{NTD}:P_{CTD} from 1:1 to 1:2-4 would result in enhanced MuV minigenome replicative function. The necessity of the oligomerization domain and presence of both the N- and C-termini of P was also confirmed. Thus, not only is the multimerization of P through a central oligomerization domain required for MuV RNA synthesis, but the trans-complementation of the N- and C-terminal domains of P as well. Furthermore, increasing the amount of P_{OC} two- to four-fold compared to P_{NO} resulted in enhanced minigenome activity. This is likely because P_{OC} is both smaller in size than P_{NO} and possesses a binding site for NP and L polymerase within its domain.

Knowing that there is a binding site for NP in both the N- and C-termini of P, truncations were made to narrow down this region. The first and last twenty amino acids of P are thought to be the regions of highest likelihood for this interaction (Figure 4.3 and 4.4). However, in pursuing the binding site of NP within P domains, an alanine scan of the termini revealed a pattern of activity between P_{NO} and P_{OC}. As mutations were made going inwards starting at the beginning of the N-terminal of P, a similar minigenome activity pattern could be seen when mutating inwards starting at the end of the C-terminus. This observation held true for sixteen amino acid substitutions (Figure 4.5) and when transfecting matching mutant P_{NO} and P_{OC} plasmids (Figure 4.6) as well as full-length P single-point and "double knock-out" mutants (Figures 4.7 and 4.8). Not only does MuV P exhibit trans-complementary properties of its amino and carboxy terminal domains, but there is a chiral characteristic for approximately the first twenty amino acids. This chirality is important for the function of P in MuV replication and is a hallmark of how P structure can affect protein and viral replication functions.

The chirality was further explored by using "high" minigenome activity P_{NO} mutants to "rescue" "low" minigenome activity P_{OC} mutants, and vice a versa (Figure 4.9). What was observed was a "high" activity P_{NO} and P_{OC} mutant, which had the same residues replaced (Glutamine), were able to "rescue" two P_{OC} and one P_{NO} mutants, respectively. This information helped guide the construction of a theoretical protein model for the N- and C-termini of MuV P.

Heptad repeats have been documented thoroughly in paramyxoviruses, primarily for glycoproteins F and HN. It has been found that heptad repeats are essential for structural stability and transition from pre- to post-fusion states of the F protein (67-69). While the research available for heptad repeats within glycoproteins of paramyxoviruses is extensive, the same cannot easily be said for phosphoproteins. In 2000, Tarbouriech *et al.* published a detailed characterization of an X-ray crystallized coiled coil structure of the Sendai virus (SeV) phosphoprotein tetramer. The research documented the need for more diverse heptad repeat models due to the unique nature of this viral phosphoprotein's structural stability. Using a traditional canonical hydrophobic heptad repeat model, the authors were unable to consistently disrupt structural stability of SeV P when implementing point mutations (136). Heptad repeats have been noted in Nipah virus and other Henipaviruses (Hendra virus, Cedar virus, Ghanian bat henipavirus) but in the C-terminal domain of phosphoprotein only, and the phosphoprotein of these viruses are parallel tetramers (210).

To understand the diversity of heptad repeats, new methods need to be researched to demonstrate how different tetrameric orientations can affect protein stability and function. While the traditional heptad repeat utilizes a 3-1 (a-d) hydrophobic core, this only

mostly holds true for dimers, trimers, or tetramers in parallel and are best exhibited in the GCN4 leucine zipper motif (206, 210, 211). Anti-parallel tetramers have been identified to have at least five different types of interaction patterns defined by hydrophobic repeats: 3-1 (a-d), 3-3-1 (a-d-e), and 3-3-2 (a-d-g) to name a few (212, 213). When tetramers are in tetramer, the classic knob-into-hole packaging interactions vary based on interdigitated packing arrangements and offsets between helices. This can be further exacerbated when working with a tetramer that is composed of two homodimers in anti-parallel – said structures often follow a combination of classical knob-in-hole packaging and 3-1 hydrophobic interactions, as well as 3-3-1, 3-3-2, or other triad combinations switching between differing helices within the tetramer (214-216).

In this work, a MuV minigenome system was used to estimate viral replication activity and was applicable to understanding how alanine substitutions affected P coiled-coil tetramerization and function. A replication activity pattern was observed when mutations were performed in chiral orientation between the amino and carboxy termini of P. This pattern held true when chiral pairs were transfected together and chiral mutations were placed into full-length MuV P. With this minigenome system and activity pattern, a heptad repeat coiled-coil structure was hypothesized and residues suggested (Figure 4.10). By examining minigenome activity and comparing residue substitution characteristics, this system was used in an innovative fashion to examine complex heptad repeats between helices in the MuV P tetramer.

As heptad repeats are often important for protein structure and function via interactions with other proteins, it is important to note that there is evidence to suggest that the residues affected within this heptad repeat model had variable effect on NP binding

activity (data not shown). Further experimentation would be useful in determining the extent by which the structure of the N- and C-termini of P affect binding to NP during viral replication.

The minigenome system for viruses, while typically used to characterize impacts of replication protein differences on viral genome replication efficiency, proposes other applications into improving our understanding of viral protein structure and their functions. Our studies suggest that MuV P is trans-complementary, has chiral properties due to its unique orientation, and has a heptad repeat present in the N- and C-terminal domains that are critical to its stability and function in viral replication.

Acknowledgements

We greatly appreciate the helpful discussions and technical assistance from all current and past members of Biao He's laboratory. This work was supported by grant R01AI106307 from the National Institutes of Health.

Figures and Figure Legend

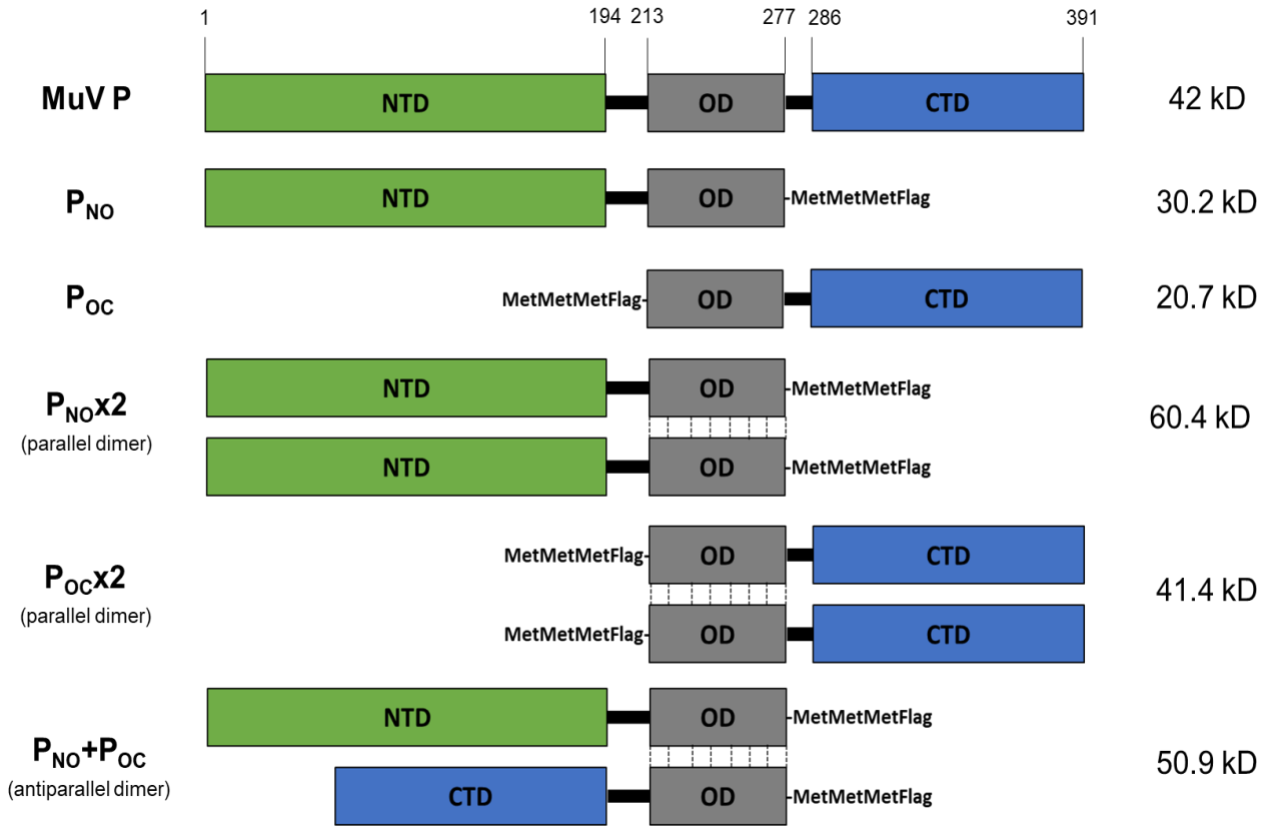

Figure 4.1. MuV P and domain truncation orientations. The amino acid residues and relative sizes in kiloDaltons (kD) for the MuV P domains are provided, along with the nomenclature of the truncation mutants. The orientations of the truncations (parallel or antiparallel dimers) are presented along with the Flag tag locations for the domain truncation mutants. Green represents the N-terminal domain (NTD), gray represents the oligomerization domain (OD), and blue represents the C-terminal domain (CTD) of P.

A

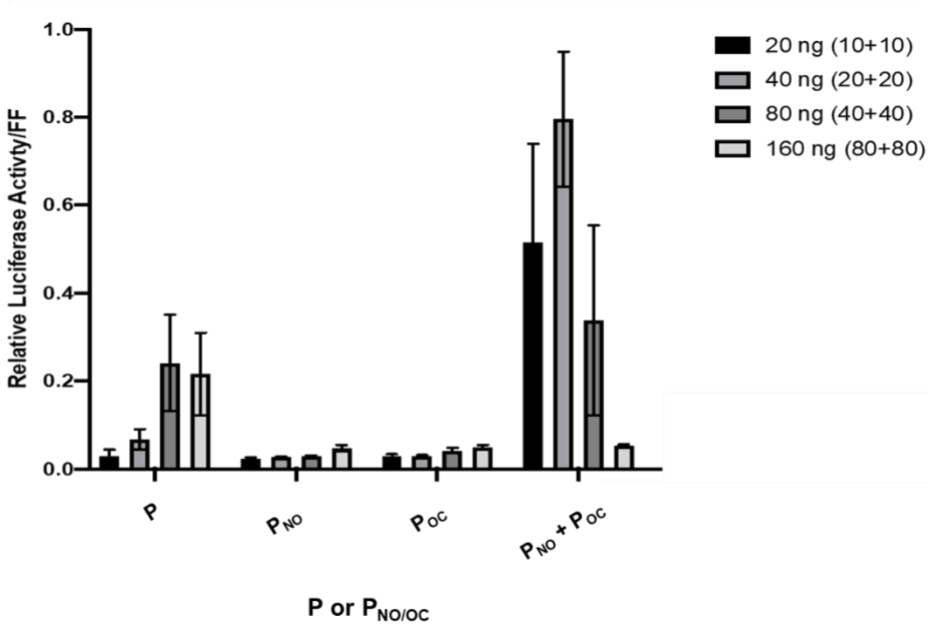
Relative Luciferase Activity/FF
1.0
0.8
0.6
0.4
0.2
0.0
20 ng (10+10)
40 ng (20+20)
80 ng (40+40)
160 ng (80+80)
P
P NO
P OC
P NO + P OC
P or P NO/OC

B

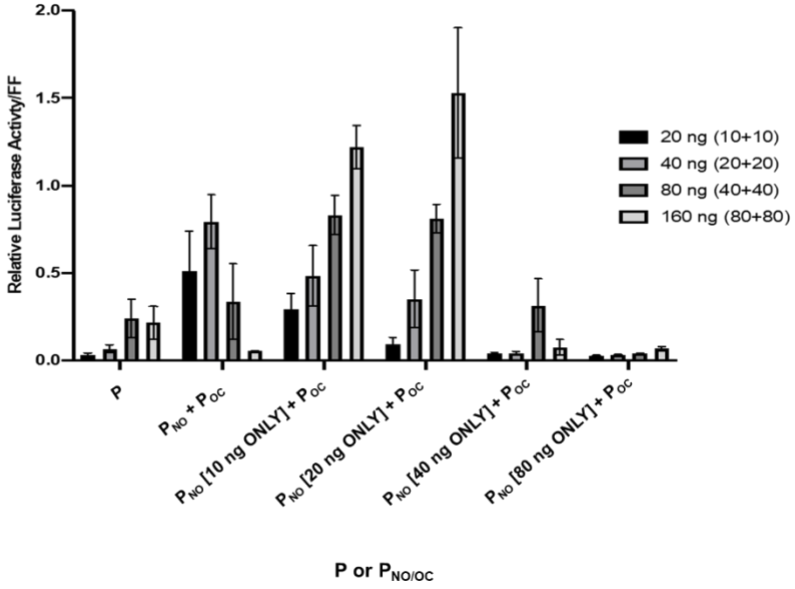
Relative Luciferase Activity/FF
2.0
1.5
1.0
0.5
0.0
20 ng (10+10)
40 ng (20+20)
80 ng (40+40)
160 ng (80+80)
P
P NO + P OC
P NO [10 ng ONLY] + P OC
P NO [20 ng ONLY] + P OC
P NO [40 ng ONLY] + P OC
P NO [80 ng ONLY] + P OC
P or P NO/OC

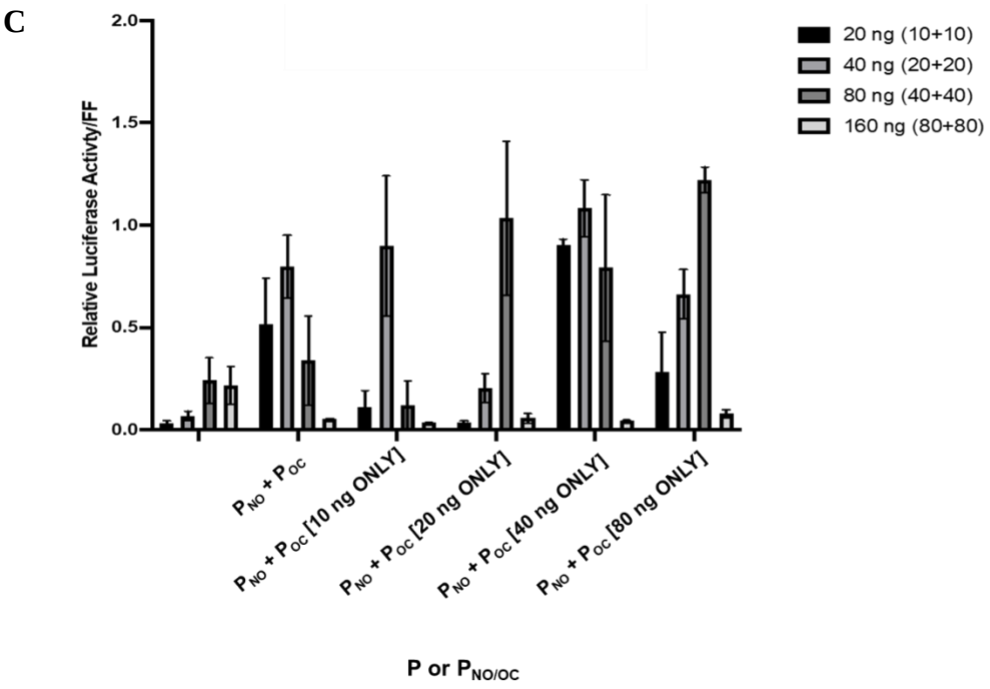

Figure 4.2. Ratios of trans-complementation of P in the minigenome system. Minigenomes were performed with wild-type phosphoprotein (P), PNO, POC, and PNO and POC in different ratios in combination. Differing mass amounts are depicted by the different shades of grey. Mass descriptions, for example "20 ng (10+10)", indicates 20 ng of full-length P, or 10 ng of P_{NO} and 10 ng of P_{OC} used together for a total of 20 ng of plasmid transfected. (A) Minigenome activity of P, P_{NO}, P_{OC}, and P_{NO} with P_{OC} in increasing amounts. P, P truncations alone, or P truncations together were transfected with other MuV replication plasmids as described in the Materials and Methods section. The transfection amounts of P_{NO} + P_{OC} truncations were each one-half of the total transfected wild-type P, so that the total mass P protein would be equivalent. (B) Minigenome activity of P_{NO} held static at either 10, 20, 40, or 80 ng with P_{OC} in increasing amounts for each N-terminal mass condition. (C) Minigenome activity of P_{OC} held static at either 10, 20, 40, or 80 ng with P_{NO} in increasing amounts for each C-terminal mass condition.

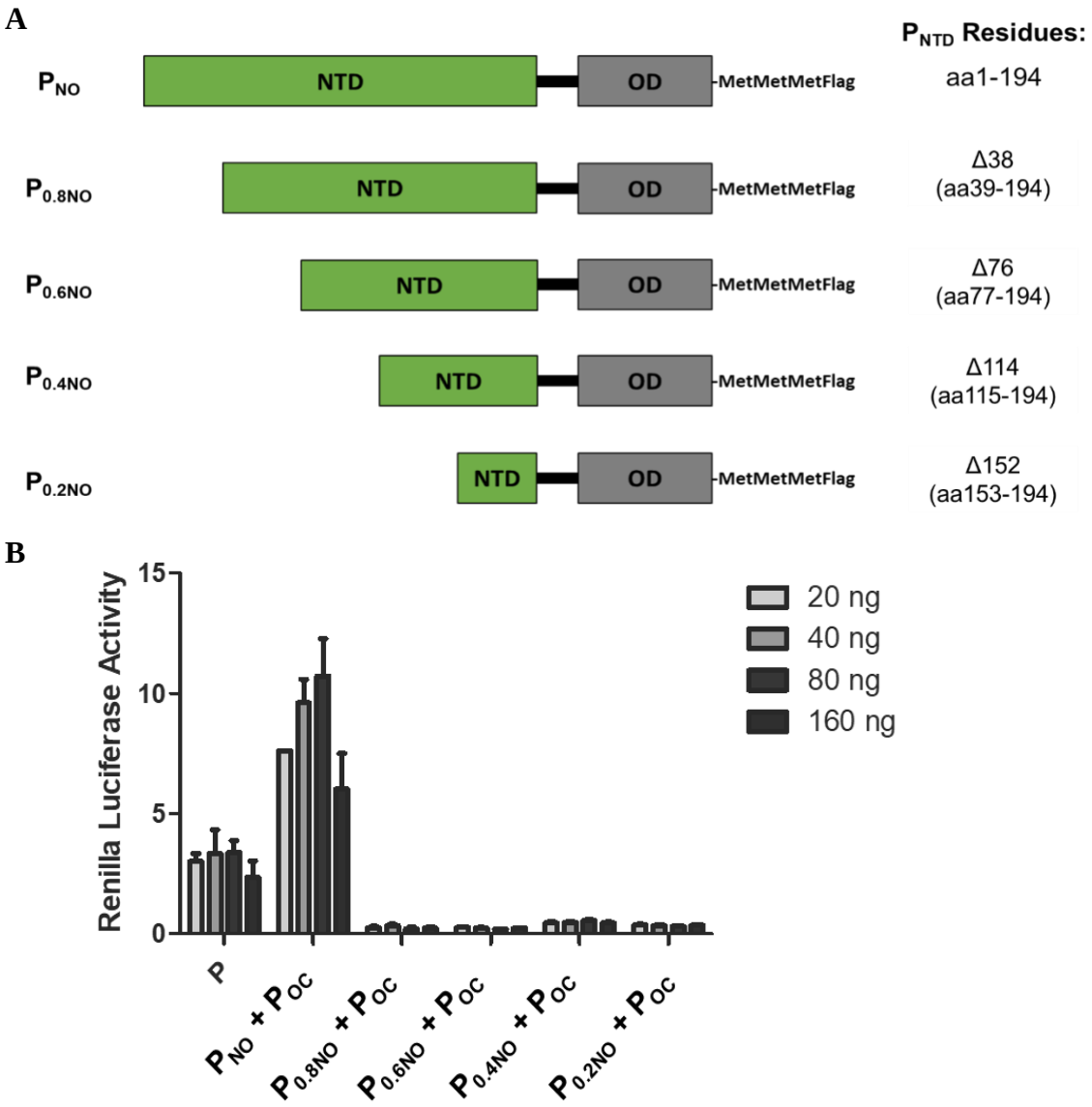
A
P_NTD Residues:
P_NO
NTD
OD
MetMetMetFlag
aa1-194
P_0.8NO
Δ38
(aa39-194)
P_0.6NO
Δ76
(aa77-194)
P_0.4NO
Δ114
(aa115-194)
P_0.2NO
Δ152
(aa153-194)
B
Renilla Luciferase Activity
15
10
5
0
20 ng
40 ng
80 ng
160 ng
P
P_NO + P_OC
P_0.8NO + P_OC
P_0.6NO + P_OC
P_0.4NO + P_OC
P_0.2NO + P_OC
C
P
P_NO+P_OC
P_0.8NO+P_OC
P_0.6NO+P_OC
P_0.4NO+P_OC
P_0.2NO+P_OC
NP
P
P_NO
P_OC
P_0.8NO
P_OC
P_0.6NO
P_OC
P_0.4NO
P_OC
P_0.2NO
P_OC

Figure 4.3. MuV P Truncations to isolate N-interacting domains. (A) A diagram depicting the fractionation of P_{NO} to isolate regions of utmost importance for replication activity. (B) Minigenome activity of the P_{NO} fractioned mutants and their respective immunoblots (C). Note the shift in size down the immunoblot of P_{NO} due to fractionation, especially in the $P_{0.4NO}$ and $P_{0.2NO}$ groups – the size in kDa for these two mutants is comparable to P_{OC} (~19 kDa, 16 kDa, and 20 kDa, respectively). This made visualization of these two P_{NO} mutants difficult to differentiate from P_{OC}. The expression of the flag epitope in P_{NO} was also found to be lesser than P_{OC} during experimentation, making the appearance of P_{NO} bands lighter by comparison.

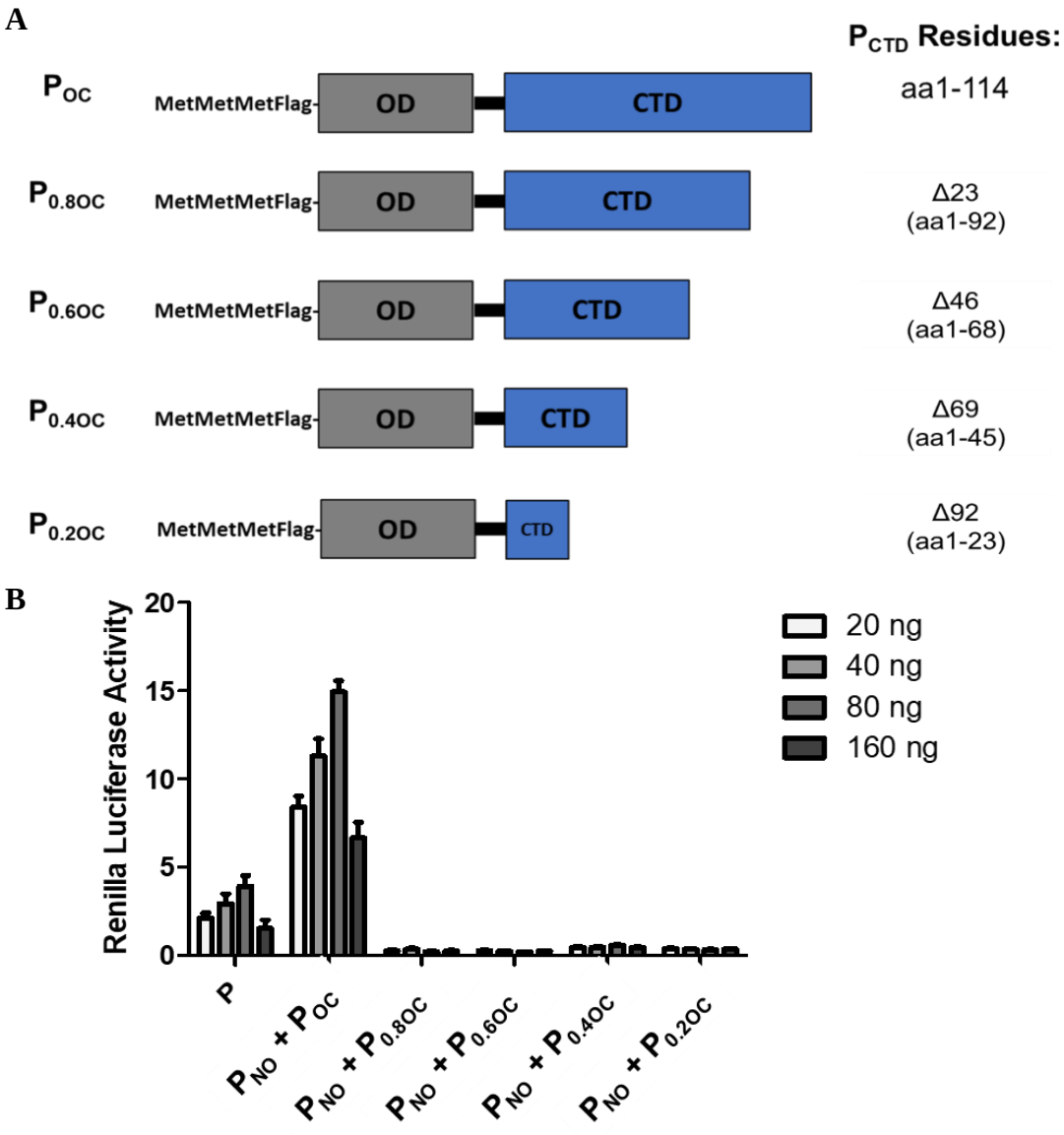
A
P_CTD Residues:
P_OC
MetMetMetFlag-
OD
CTD
aa1-114
P_0.8OC
Δ23
(aa1-92)
P_0.6OC
Δ46
(aa1-68)
P_0.4OC
Δ69
(aa1-45)
P_0.2OC
Δ92
(aa1-23)
B
Renilla Luciferase Activity
20 ng
40 ng
80 ng
160 ng
P
P_NO + P_OC
P_NO + P_0.8OC
P_NO + P_0.6OC
P_NO + P_0.4OC
P_NO + P_0.2OC
C
NP
P
P_NO
P_OC

Figure 4.4. MuV P Truncations to isolate C-interacting domains. (A) A diagram depicting the fractionation of P_{OC} to isolate regions of utmost importance for replication activity. (B) Minigenome activity of the P_{OC} fractioned mutants and their respective immunoblots (C). Note the shift in size down the immunoblot of P_{OC} due to fractionation. The expression of the flag epitope in P_{OC} was satisfactory. $P_{0.2OC}$ was barely detectable on the immunoblot most likely due to its small size.

A

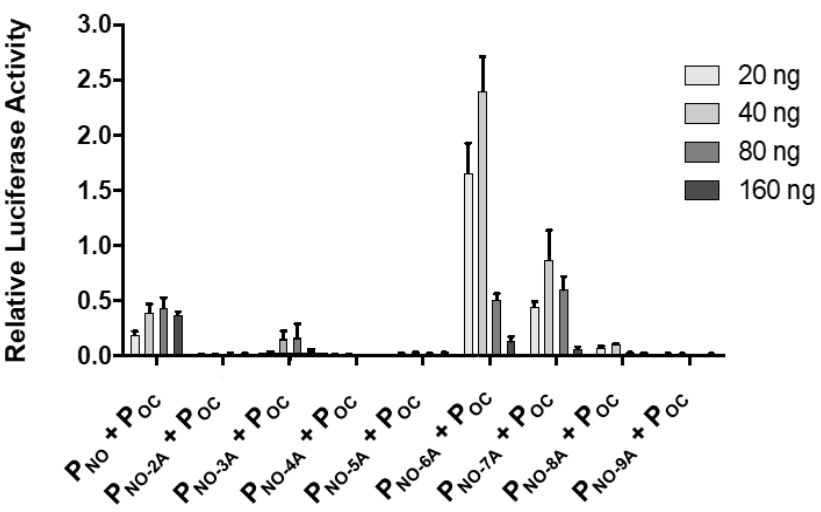
Relative Luciferase Activity
3.0
2.5
2.0
1.5
1.0
0.5
0.0
20 ng
40 ng
80 ng
160 ng
P NO + P OC
P NO-2A + P OC
P NO-3A + P OC
P NO-4A + P OC
P NO-5A + P OC
P NO-6A + P OC
P NO-7A + P OC
P NO-8A + P OC
P NO-9A + P OC

B

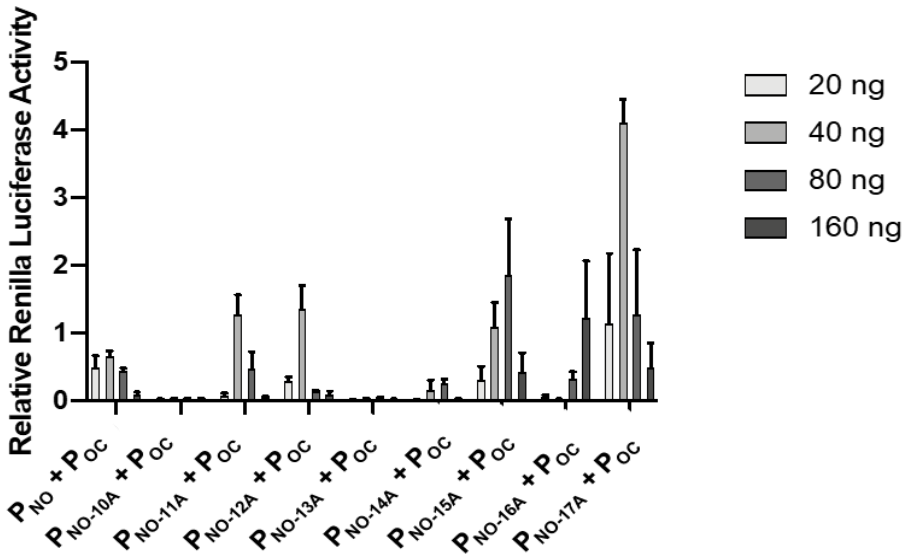
Relative Renilla Luciferase Activity
5
4
3
2
1
0
20 ng
40 ng
80 ng
160 ng
P NO + P OC
P NO-10A + P OC
P NO-11A + P OC
P NO-12A + P OC
P NO-13A + P OC
P NO-14A + P OC
P NO-15A + P OC
P NO-16A + P OC
P NO-17A + P OC

C

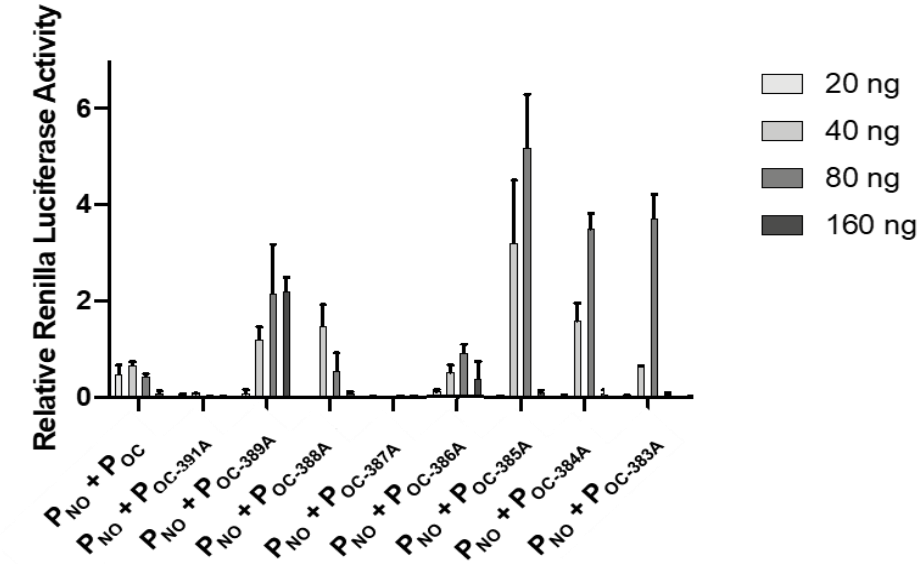
Relative Renilla Luciferase Activity
6
4
2
0
20 ng
40 ng
80 ng
160 ng
P NO + P OC
P NO + P OC-391A
P NO + P OC-389A
P NO + P OC-388A
P NO + P OC-387A
P NO + P OC-386A
P NO + P OC-385A
P NO + P OC-384A
P NO + P OC-383A

D

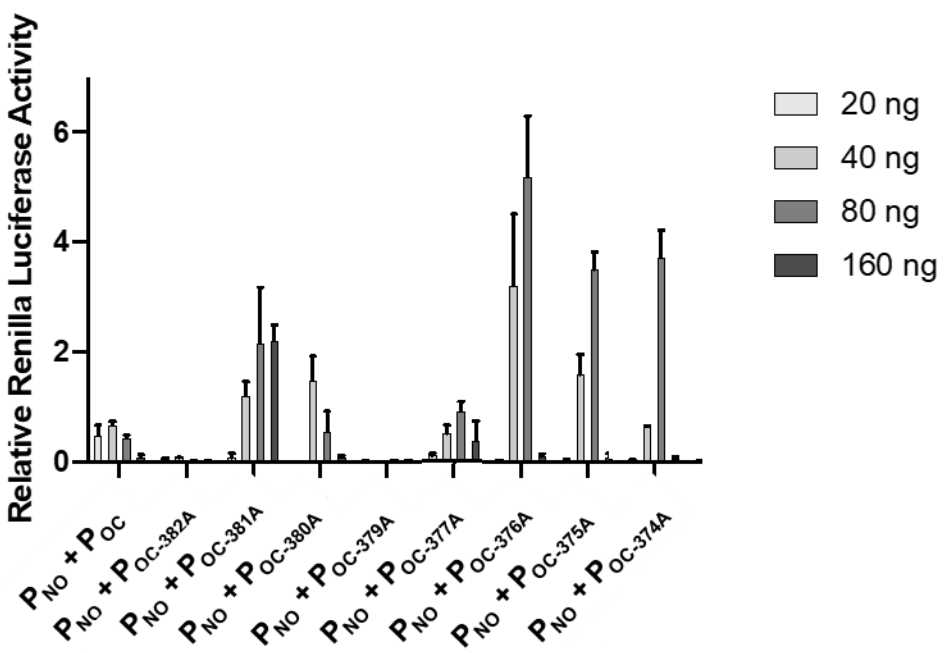

Figure 4.5. Minigenome activity of Alanine scanned P_{NO} and P_{OC} truncation mutants. Minigenome of an alanine scan of the first eight (A) and second eight (B) amino acid residues of the N-terminus of P_{NO}. Minigenomes were also performed for the last eight (C) and the second-to-last eight (D) amino acid residues of the C-terminus of P_{OC}. For P_{OC}, residues were also replaced with alanine unless alanine was already present – the residue was skipped if this was the case.

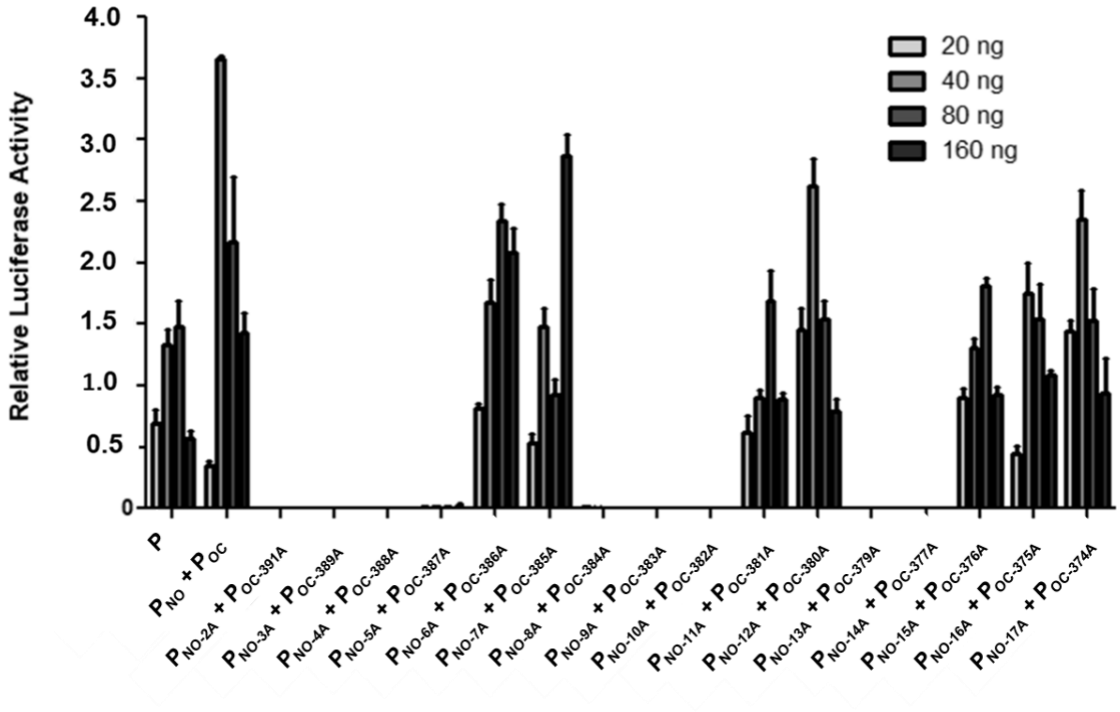

Figure 4.6. Minigenome activity of chiral P_{NO} and P_{OC} truncation mutants in conjunction.

A minigenome using chiral P_{NO} and P_{OC} alanine scanned truncation mutants.

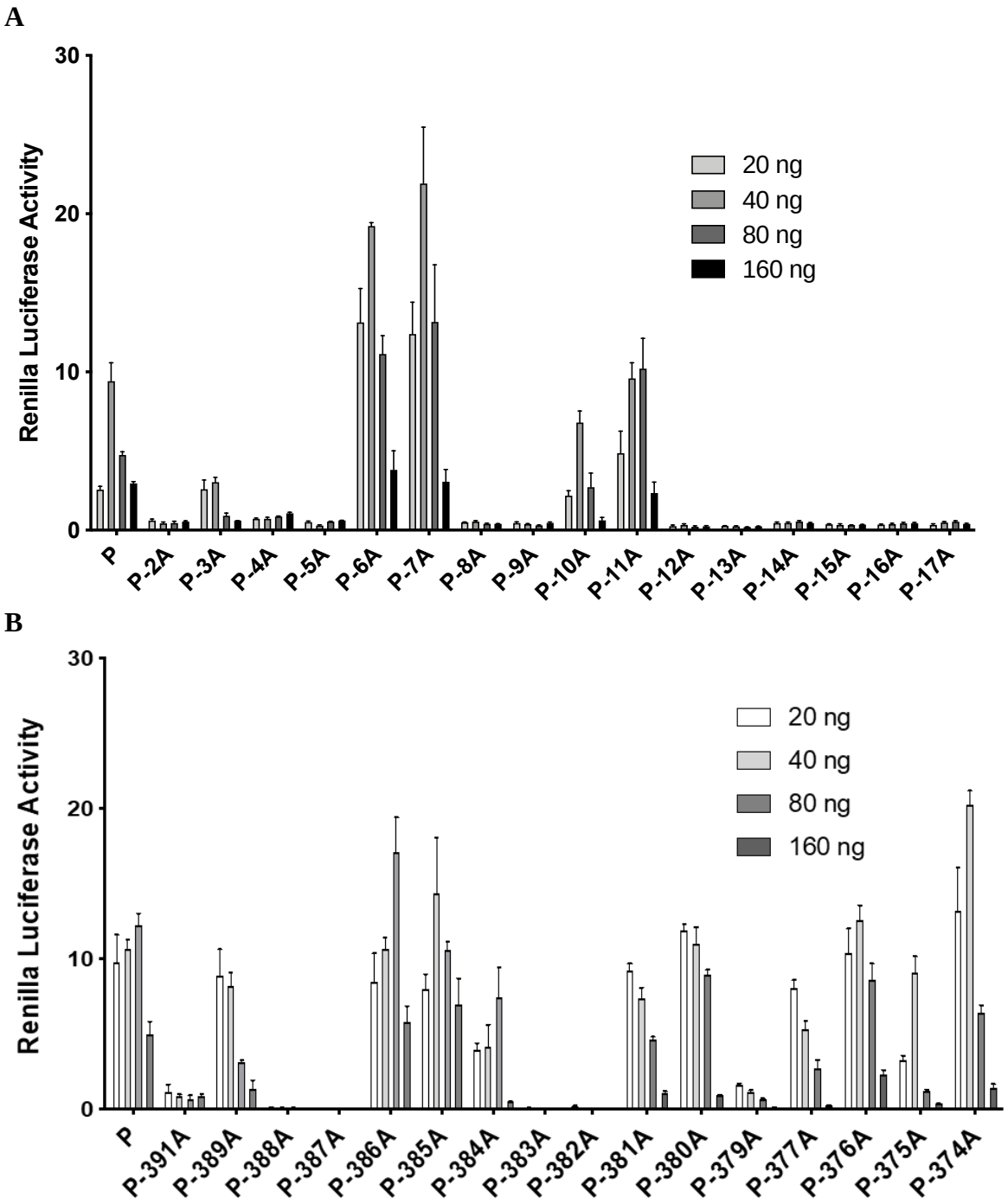

Figure 4.7. Minigenome activity full-length P single point mutations. Minigenome activity of full-length MuV mutants with point alanine substitutions in either the N- (A) or C-terminus (B).

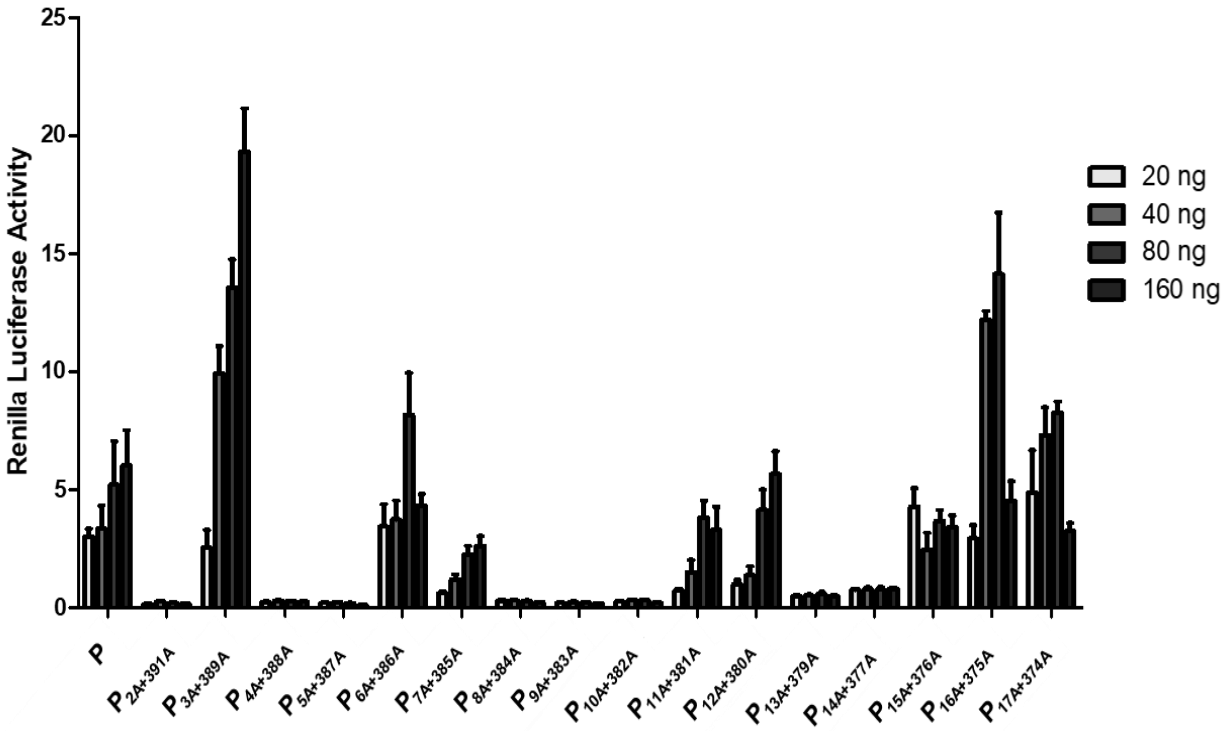

Figure 4.8. Minigenome activity of full-length P double knock-out mutants. Minigenome activity of full-length MuV P mutants with double alanine substitutions in the N- and C-terminal domains representative of their chiral residue pairs as demonstrated in Figures 5 and 6.

Residue				Activity				
Residue No.	Residue Code	Residue Letter	Polar (P)/ Charged (C+ or C-)/ Hydrophobic (H)?	P_{NO}	P_{OC}	$P_{NO}+P_{OC}$	P Single Mutation	P Double Knock-out
2	Asp	D	P,C-	Low	–	Low	Low	Low
3	Gln	Q	P	High	–	Low	High	High
4	Phe	F	H	Low	–	Low	Low	Low
5	Ile	I	H	Low	–	Low	Low	Low
6	Lys	K	P,C+	High	–	High	High	High
7	Gln	Q	P	High	–	High	High	High
8	Asp	D	P,C-	Low	–	Low	Low	Low
9	Glu	E	P,C-	Low	–	Low	Low	Low
10	Thr	T	P	Low	–	Low	High	Low
11	Gly	G	neutral	High	–	High	High	High
12	Asp	D	P,C-	High	–	High	Low	High
13	Leu	L	H	Low	–	Low	Low	Low
14	Ile	I	H	Low	–	Low	Low	Low
15	Glu	E	P,C-	High	–	High	Low	High
16	Thr	T	P	Low	–	High	Low	High
17	Gly	G	neutral	High	–	High	Low	High
391	Ile	I	H	–	Low	Low	Low	Low
389	Ser	S	P	–	High	Low	High	High
388	Arg	R	P,C+	–	Low	Low	Low	Low
387	Ile	I	H	–	Low	Low	Low	Low
386	Ile	I	H	–	High	High	High	High
385	Asp	D	P,C-	–	High	High	High	High
384	Arg	R	P,C+	–	Low	Low	High	Low
383	Lys	K	P,C+	–	Low	Low	Low	Low
382	Ile	I	H	–	Low	Low	Low	Low
381	Asp	D	P,C-	–	High	High	High	High
380	Asn	N	P	–	High	High	High	High
379	Leu	L	H	–	Low	Low	Low	Low
377	Asp	D	P,C-	–	Low	Low	High	Low
376	Glu	E	P,C-	–	High	High	High	High
375	Thr	T	P	–	High	High	High	High
374	Ser	S	P	–	Low	High	High	High

Table 4.1. Summary of minigenome activity of residues in the N- and C-terminal domains of P. "Low" indicates little to no minigenome activity while "High" indicates some to high minigenome activity. Note that for the "P_{NO}+P_{OC}" and "P Double Knock-out" column the activities are repeated for both the N- and C-terminal domain residues.

A

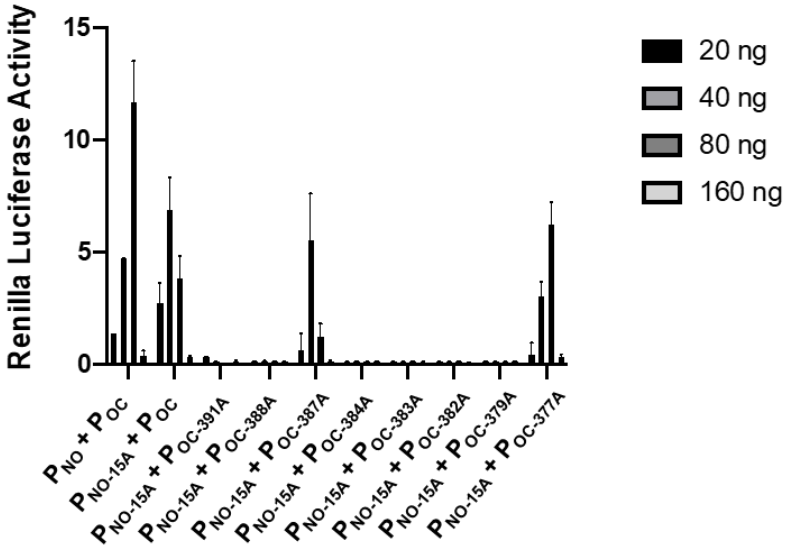

B

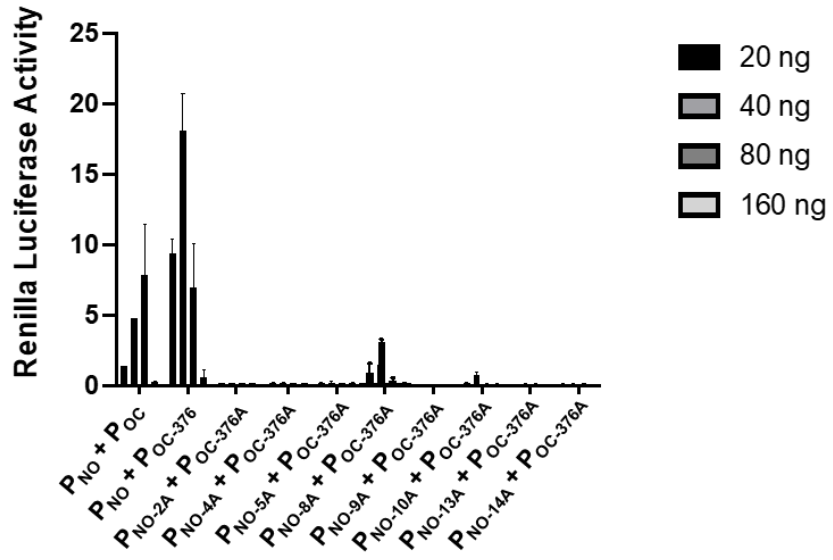

Figure 4.9. Rescue of "low" activity terminal truncation mutants with "high" activity opposite mutant termini. The figures depict the minigenome activity seen when transfecting a "high" activity P_{NO} (A) or P_{OC} (B) mutant with P_{OC} or P_{NO} "low" performing mutants, respectively. The purpose of this was to see if minigenome activity with "low" performing mutants could be restored.

A

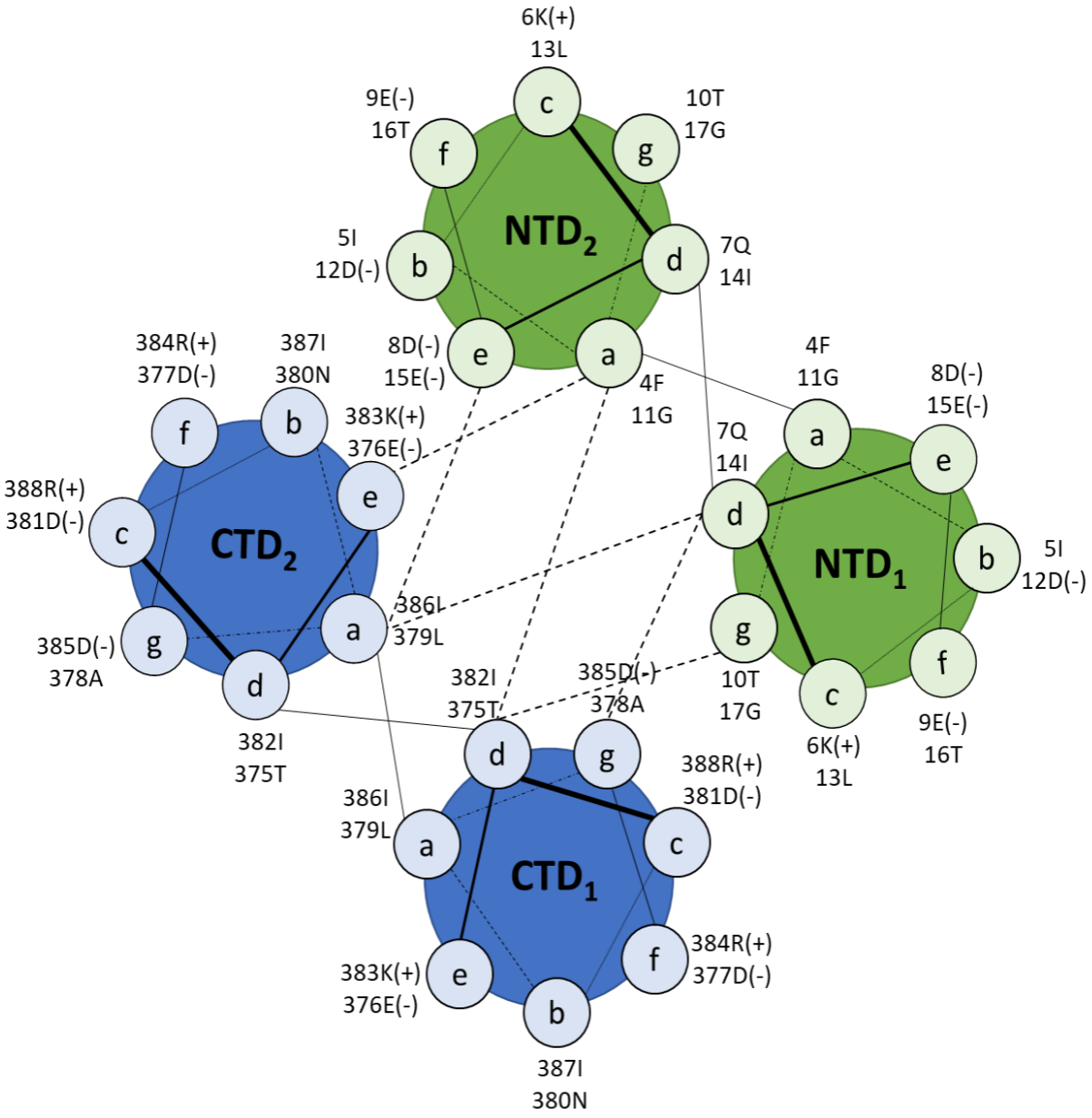
NTD2
6K(+)
13L
9E(-)
16T
10T
17G
5I
12D(-)
7Q
14I
8D(-)
15E(-)
4F
11G
CTD2
384R(+)
377D(-)
387I
380N
383K(+)
376E(-)
388R(+)
381D(-)
386I
379L
385D(-)
378A
382I
375T
NTD1
CTD1

B

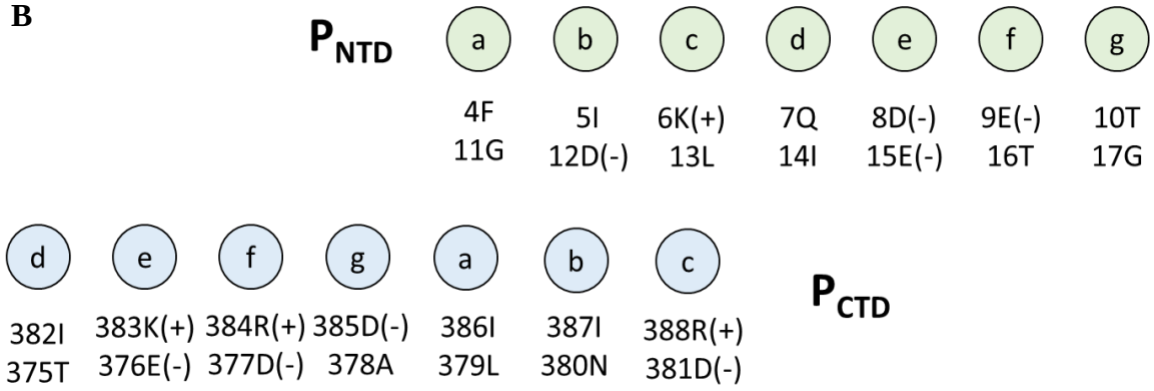
PNTD
a
4F
11G
b
5I
12D(-)
c
6K(+)
13L
d
7Q
14I
e
8D(-)
15E(-)
f
9E(-)
16T
g
10T
17G
PCTD
d
382I
375T
e
383K(+)
376E(-)
f
384R(+)
377D(-)
g
385D(-)
378A
a
386I
379L
b
387I
380N
c
388R(+)
381D(-)

Figure 4.10. Heptad repeat and coiled-coil structure for MuV P. (A) This is a diagram of the coiled-coil interactions between residues of the heptad repeat within P_{NTD} and P_{CTD} as parallel homodimers and between homodimers in antiparallel. (B) A visual representation of the amino acid residues assigned to their heptad repat residue "letter" in the N-terminal and C-terminal domains of P.

CHAPTER 5

CONCLUSIONS

Mumps virus is a highly infectious and neurotropic paramyxovirus – over 40% of the US population were infected by the age of 10 years before mass vaccination campaigns in the 1960s (217). Since widespread vaccination, there has been over a 99% reduction of mumps disease incidence in the US reported. With an efficacious vaccine widely available, research interest in MuV declined and became stagnant until large outbreaks in the US were reported in 2006 (2, 3, 5, 7, 157, 158, 218). While researchers work to deduce precisely what is the cause of this resurgence, it is evident that a greater understanding of MuV infection, pathogenicity, and correlates of protection is needed to conquer this problem. At the core of this understanding of MuV is the need to better characterize MuV proteins and their roles in the viral life cycle, primarily viral replication. Viral RNA replication and transcription is a process that can be exploited by evolving antiviral therapies and vaccine platform development. The goal of this research endeavor was to characterize how the structure of nucleoprotein and phosphoprotein impact MuV replication. The importance of these two proteins in genome replication and transcription has been documented in numerous paramyxoviruses, but there are still facets of these proteins in MuV-specific replication processes that remain to be elucidated. Previous work from our lab has highlighted the importance of the MuV NP structure and how it unravels the RNA genome for viral replication (27, 110, 171). Other work by our lab has detailed the role of P in bridging the L polymerase and NP-RNA template for successful replication

and transcription (39, 44, 47, 48). To address how NP and P structure impact replicative functions, the following specific aims were proposed and addressed:

Specific Aim 1: To determine how structure modulates function of MuV NP by mutating amino acid sites to those found similarly in PIV5 (parainfluenza virus 5). The hypothesis was that by exchanging amino acid sites between similar paramyxovirus NP, the structure and function of specific domains of MuV NP may be determined. In these studies, the results in Chapter 3 show that of the six isolated domains, only mutants Y185P, A197Q, and "Top" were viable in virus form. Minigenome and western blot data also supported this notion. Furthermore, mutations to the domains "Top", "Tip", and "Bottom" individually or in combination did not yield viable virus, indicating that these domains in their entirety are essential for virus viability (data not shown).

The MuV mutant "185" had a substitution at Y185 for residue P, which is seen in PIV5's NP. This virus was able to be rescued and propagated. Interestingly, mutant 185 was consistently slow to grow, but by the end of the time frame would grow up to half a log higher than wildtype MuV. This was also seen during a two-week long persistent infection growth curve – MuV mutant 185 would be delayed in its initial titer, but throughout the time period would grow up to a log higher and maintain higher titers during persistent infection (data not shown). The reasoning behind this could be due to site 185 being right within the "hinge" region of the RNP that must move to allow access of the vRdRp to the viral RNA template. Should this hinge-effect be altered, decreased viral growth could be initially observed. Additionally, NP functions not only in protecting the RNA genome, but in helping to chaperone viral components to the inner cell surface for

eventual budding and egress. It is possible that residue 185 plays a role in binding to M for viral assembly and budding, and the process of viral release is delayed. Both scenarios are also not mutually exclusive and could together explain the viral growth kinetics observed. More investigation into why MuV 185 has initially delayed but increased viral growth and persistence is warranted.

MuV mutant "197" had decreased growth kinetics and grew to a lower titer than wildtype MuV. However, "197" is one of the three mutations found in the "Top" domain. When amino acid residues 63, 139, and 197 together were mutated to residues found in PIV5's NP, virus initially grew, but titers quickly plummeted within 24-48 hours to baseline levels. Thus, it was concluded that this "Top" domain was of critical importance to viral viability.

To determine how defective interfering particles can be innately developed by MuV due to structural changes to the MuV NP. Using binding affinity and interference assays, a novel MuV with a mutated NP domain is hypothesized to inherently produce high numbers of defective interfering (DI) particles that inhibit viral replication. In these studies, as detailed in Chapter 3, it was found that MuV mutant "Top" was capable of inherently producing DI particles without the assistance of high multiplicity of infection (MOI). This was observed in viral growth curve kinetics, particle formation was confirmed via a comparison of hemagglutination-assay (HA) titer and infectious titer (PFU), and interference by "Top" on MuV replication was determined using a reduction-of-infectious-yield (RIY) assay. At both high and low MOIs as low as 0.001, statistically significant reduction in MuV-*Renilla* infectious titer was observed when co-infected with MuV mutant "Top". This was further confirmed to not be due to any chemical substances secreted by

the cells into the media when the mutant "Top" was UV cross-linked and inactivated – MuV-*Renilla* when co-infected with sterilized "Top" was unaffected.

To characterize the DI particles, RT-PCR using primers designed to capture a variety of DI particles was utilized. Compared to wild-type MuV, mutant "Top" could produce a diverse repertoire of DI particles. TOPO-cloning of the RT-PCR products was also utilized in order to classify the DI particles, which noted the presence of copy-back and deletion DI genomes of higher variety of type when compared to wild-type MuV.

In conclusion, MuV mutant "Top" has a uniquely inherent ability to produce DI particles. One possible explanation is that PIV5's NP interacts with only the N-terminal domain of its P, whereas MuV's NP interacts with both the N- and C-terminal domains of its P. When performing radiolabeling, it was discovered that "Top" NP had a decreased ability to bind with the C-terminal domain of P in co-immunoprecipitation assays (data not shown). Further investigation into this mechanism would be of interest.

Specific Aim 2: To determine the role of the amino and carboxy terminal domains of MuV P (P_{NTD} and P_{CTD}, respectively) and how the structure of P affects viral replication function. A novel minigenome assay was developed to investigate effects of an alanine screen in theorized NP-P binding domains in P_{NTD} and P_{CTD}. The working hypothesis is that these amino acid substitutions will have impacts on replication protein interactions and structural stability of P, thus displaying how P's unique antiparallel tetramer structure affects MuV viral replication. In Chapter 4, P's trans-complementarity was shown as well as its diverse dynamics when the ratio of N- and C-terminal domains are transfected in different amounts. It was observed that transfecting two- to four-fold the amount of C-

terminal to N-terminal domain of P caused markedly increased MuV minigenome activity, which exhibited MuV P's unique ability to interact with NP and both termini.

After performing fractionation of the N- and C-terminal truncations and an alanine scan to deduce interaction sites of interest, a chiral property of P was noticed. When alanine scanning the N-terminus from beginning to end, the same minigenome activity pattern was seen when alanine scanning the C-terminus from its end to its beginning. This property showed the importance of the MuV P tetramer being a pair of homodimers in anti-parallel to one another – having two copies of both the N- and C-terminal domains on either end, as well as the ability for the MuV P to form either homo- or hetero-dimers, requires structural stability that allows for these functions. This chiral property of replication activity was observed when transfecting "matched pairs" of P_{NO} and P_{OC} together, and when transfecting full-length P with "double knock-outs" of these matched chiral residue pairs on either terminus.

These patterns of activity based on structural substitutions led to the hypothesis and modeling of a heptad repeat in the head and tail ends of P. This heptad repeat could provide an explanation as to how P can form stable dimers and tetramers in both parallel and anti-parallel, and still perform replication functions. Heptad repeats for fusion glycoproteins have been documented in many paramyxoviruses, including MuV (67-69), and recently SeV P has had a heptad repeat documented in the C-terminal domain of its P (136). This use of a MuV minigenome is a novel method and strategy for determining the heptad repeat structure of MuV P's unique tetramerization and dimerization states, and helps characterize the diversity of hydrophobic interactions between homodimers, heterodimers, and

tetramers with a pair of homodimers in antiparallel beyond the standard 3-1 motif (206, 210, 212).

Developing more effective vaccine platforms and strategies, as well as novel antivirals and therapeutics, is necessary for the control of MuV infection and future outbreaks. These studies provide insight into the roles that NP and P structure have on viral function. Developing MuV mutant "Top" into quantifiable DI particles could assist in antiviral therapy and inhibit viral replication in the human host. The discovery of a virus that can self-inhibit without high viral loads would also be useful in the development of antivirals in other negative-stranded RNA viruses. The characterization of a heptad repeat in MuV P can help in expanding the toolkit for pinpointing heptad repeats and other protein structural motifs, as well as assist in pinpointing residues or domains of interest for developing antiviral compounds. This research shows the importance of basic research in creating steppingstones for the development of translational research for disease prevention or cures in humans and animals.

REFERENCES

1. Carbone KM WJ. 2001. Mumps virus, p 1382-1441. *In* Knipe DM HP (ed), Fields Virology, 4 ed. Lippincott Williams and Wilkins, New York.
2. Dayan GH, Quinlisk MP, Parker AA, Barskey AE, Harris ML, Schwartz JM, Hunt K, Finley CG, Leschinsky DP, O'Keefe AL, Clayton J, Kightlinger LK, Dietle EG, Berg J, Kenyon CL, Goldstein ST, Stokley SK, Redd SB, Rota PA, Rota J, Bi D, Roush SW, Bridges CB, Santibanez TA, Parashar U, Bellini WJ, Seward JF. 2008. Recent resurgence of mumps in the United States. N Engl J Med 358:1580-9.
3. Dayan GH, Rubin S. 2008. Mumps outbreaks in vaccinated populations: are available mumps vaccines effective enough to prevent outbreaks? Clin Infect Dis 47:1458-67.
4. (CDC) CfDCaP. 2015. Epidemiology and Prevention of Vaccine-Preventable Diseases, 13th ed. Public Health Foundation, Washington DC.
5. Marin M, Quinlisk P, Shimabukuro T, Sawhney C, Brown C, Lebaron CW. 2008. Mumps vaccination coverage and vaccine effectiveness in a large outbreak among college students--Iowa, 2006. Vaccine 26:3601-7.
6. Lamb RA KD. 2001. Paramyxoviridae: The viruses and their replication, 4 ed. Lippincott Williams and Wilkins, Philadelphia.
7. Cortese MM, Jordan HT, Curns AT, Quinlan PA, Ens KA, Denning PM, Dayan GH. 2008. Mumps vaccine performance among university students during a mumps outbreak. Clin Infect Dis 46:1172-80.

8. Timani KA, Sun D, Sun M, Keim C, Lin Y, Schmitt PT, Schmitt AP, He B. 2008. A single amino acid residue change in the P protein of parainfluenza virus 5 elevates viral gene expression. J Virol 82:9123-33.

9. Chen M, Ogino T, Banerjee AK. 2007. Interaction of vesicular stomatitis virus P and N proteins: identification of two overlapping domains at the N terminus of P that are involved in N0-P complex formation and encapsidation of viral genome RNA. J Virol 81:13478-85.

10. Goodbourn S, Randall RE. 2009. The regulation of type I interferon production by paramyxoviruses. J Interferon Cytokine Res 29:539-47.

11. C. TE. 1967. HIPPOCRATES DESCRIBES MUMPS FOLLOWED BY ORCHITIS. Pediatrics 40:420-420.

12. Strauss JH, Strauss EG. 2002. Viruses and human disease. Academic Press, San Diego.

13. Hamilton R. 1790. An Account of a Distemper, by the Common People in England Vulgarly Called the Mumps. Lond Med J 11:190-211.

14. Prescott J, Feldmann H, Safronetz D. 2017. Amending Koch's postulates for viral disease: When "growth in pure culture" leads to a loss of virulence. Antiviral Res 137:1-5.

15. Anonymous. 2011. The Nature of Viruses. Fenner's Veterinary Virology:3-19.

16. Johnson CD, Goodpasture EW. 1934. An Investigation of the Etiology of Mumps. J Exp Med 59:1-19.

17. Johnson CD, Goodpasture EW. 1936. The Histopathology of Experimental Mumps in the Monkey, Macacus Rhesus. Am J Pathol 12:495-510 7.

18. Beveridge WI, Lind PE, Anderson SG. 1946. Mumps; isolation and cultivation of the virus in the chick embryo. Aust J Exp Biol Med Sci 24:15-9.

19. Enders JF. 1946. Mumps; techniques of laboratory diagnosis, tests for susceptibility, and experiments on specific prophylaxis. J Pediatr 29:129-42.

20. Enders JF, Levens JH, et al. 1946. Attenuation of virulence with retention of antigenicity of mumps virus after passage in the embryonated egg. J Immunol 54:283-91.

21. Henle G, Deinhardt F. 1955. Propagation and primary isolation of mumps virus in tissue culture. Proc Soc Exp Biol Med 89:556-60.

22. Smorodintsev AA, Klyatchko NS. 1958. Live anti-mumps vaccine. I. Results of tests of the immunogenic properties of live vaccine when administered intradermally to susceptible children. Acta Virol 2:137-44.

23. Klyatchko NS, Smorodintsev AA. 1958. Live anti-mumps vaccine. II. Epidemiological effectiveness of the immunization of children with a single intradermal injection of live anti-mumps vaccine. Acta Virol 2:145-51.

24. Duc-Nguyen H, Rosenblum EN. 1967. Immuno-electron microscopy of the morphogenesis of mumps virus. J Virol 1:415-29.

25. Rubin S, Eckhaus M, Rennick LJ, Bamford CG, Duprex WP. 2015. Molecular biology, pathogenesis and pathology of mumps virus. J Pathol 235:242-52.

26. Takeuchi K, Tanabayashi K, Hishiyama M, Yamada A. 1996. The mumps virus SH protein is a membrane protein and not essential for virus growth. Virology 225:156-62.

27. Cox R, Green TJ, Qiu S, Kang J, Tsao J, Prevelige PE, He B, Luo M. 2009. Characterization of a mumps virus nucleocapsidlike particle. J Virol 83:11402-6.

28. Calain P, Roux L. 1993. The rule of six, a basic feature for efficient replication of Sendai virus defective interfering RNA. J Virol 67:4822-30.

29. Peeters BP, Gruijthuijsen YK, de Leeuw OS, Gielkens AL. 2000. Genome replication of Newcastle disease virus: involvement of the rule-of-six. Arch Virol 145:1829-45.

30. Weik M, Enterlein S, Schlenz K, Muhlberger E. 2005. The Ebola virus genomic replication promoter is bipartite and follows the rule of six. J Virol 79:10660-71.

31. Elango N, Varsanyi TM, Kovamees J, Norrby E. 1988. Molecular cloning and characterization of six genes, determination of gene order and intergenic sequences and leader sequence of mumps virus. J Gen Virol 69 (Pt 11):2893-900.

32. Paterson RG, Lamb RA. 1990. RNA editing by G-nucleotide insertion in mumps virus P-gene mRNA transcripts. J Virol 64:4137-45.

33. McCarthy M, Lazzarini RA. 1982. Intracellular nucleocapsid RNA of mumps virus. J Gen Virol 58 Pt 1:205-9.

34. Kingston RL, Baase WA, Gay LS. 2004. Characterization of nucleocapsid binding by the measles virus and mumps virus phosphoproteins. J Virol 78:8630-40.

35. Kingston RL, Gay LS, Baase WS, Matthews BW. 2008. Structure of the nucleocapsid-binding domain from the mumps virus polymerase; an example of protein folding induced by crystallization. J Mol Biol 379:719-31.

36. Buchholz CJ, Retzler C, Homann HE, Neubert WJ. 1994. The carboxy-terminal domain of Sendai virus nucleocapsid protein is involved in complex formation between phosphoprotein and nucleocapsid-like particles. Virology 204:770-6.

37. Bourhis JM, Johansson K, Receveur-Brechot V, Oldfield CJ, Dunker KA, Canard B, Longhi S. 2004. The C-terminal domain of measles virus nucleoprotein belongs to the class of intrinsically disordered proteins that fold upon binding to their physiological partner. Virus Res 99:157-67.

38. Iseni F, Baudin F, Garcin D, Marq JB, Ruigrok RW, Kolakofsky D. 2002. Chemical modification of nucleotide bases and mRNA editing depend on hexamer or nucleoprotein phase in Sendai virus nucleocapsids. RNA 8:1056-67.

39. Cox R, Pickar A, Qiu S, Tsao J, Rodenburg C, Dokland T, Elson A, He B, Luo M. 2014. Structural studies on the authentic mumps virus nucleocapsid showing uncoiling by the phosphoprotein. Proc Natl Acad Sci U S A 111:15208-13.

40. Precious B, Young DF, Bermingham A, Fearns R, Ryan M, Randall RE. 1995. Inducible expression of the P, V, and NP genes of the paramyxovirus simian virus 5 in cell lines and an examination of NP-P and NP-V interactions. J Virol 69:8001-10.

41. Howard M, Wertz G. 1989. Vesicular stomatitis virus RNA replication: a role for the NS protein. J Gen Virol 70 (Pt 10):2683-94.

42. Masters PS, Banerjee AK. 1988. Resolution of multiple complexes of phosphoprotein NS with nucleocapsid protein N of vesicular stomatitis virus. J Virol 62:2651-7.

43. Masters PS, Banerjee AK. 1988. Complex formation with vesicular stomatitis virus phosphoprotein NS prevents binding of nucleocapsid protein N to nonspecific RNA. J Virol 62:2658-64.

44. Pickar A, Xu P, Elson A, Li Z, Zengel J, He B. 2014. Roles of serine and threonine residues of mumps virus P protein in viral transcription and replication. J Virol 88:4414-22.

45. Pickar A, Zengel J, Xu P, Li Z, He B. 2016. Mumps Virus Nucleoprotein Enhances Phosphorylation of the Phosphoprotein by Polo-Like Kinase 1. J Virol 90:1588-98.

46. Briggs K, Wang L, Nagashima K, Zengel J, Tripp RA, He B. 2020. Regulation of Mumps Virus Replication and Transcription by Kinase RPS6KB1. J Virol 94.

47. Cox R, Green TJ, Purushotham S, Deivanayagam C, Bedwell GJ, Prevelige PE, Luo M. 2013. Structural and functional characterization of the mumps virus phosphoprotein. J Virol 87:7558-68.

48. Pickar A, Elson A, Yang Y, Xu P, Luo M, He B. 2015. Oligomerization of Mumps Virus Phosphoprotein. J Virol 89:11002-10.

49. Andrejeva J, Childs KS, Young DF, Carlos TS, Stock N, Goodbourn S, Randall RE. 2004. The V proteins of paramyxoviruses bind the IFN-inducible RNA helicase, mda-5, and inhibit its activation of the IFN-beta promoter. Proc Natl Acad Sci U S A 101:17264-9.

50. Kubota T, Yokosawa N, Yokota S, Fujii N. 2001. C terminal CYS-RICH region of mumps virus structural V protein correlates with block of interferon alpha and

gamma signal transduction pathway through decrease of STAT 1-alpha. Biochem Biophys Res Commun 283:255-9.

51. Takeuchi K, Tanabayashi K, Hishiyama M, Yamada YK, Yamada A, Sugiura A. 1990. Detection and characterization of mumps virus V protein. Virology 178:247-53.

52. Precious B, Childs K, Fitzpatrick-Swallow V, Goodbourn S, Randall RE. 2005. Simian virus 5 V protein acts as an adaptor, linking DDB1 to STAT2, to facilitate the ubiquitination of STAT1. J Virol 79:13434-41.

53. Xu P, Luthra P, Li Z, Fuentes S, D'Andrea JA, Wu J, Rubin S, Rota PA, He B. 2012. The V protein of mumps virus plays a critical role in pathogenesis. J Virol 86:1768-76.

54. Yang Y, Zengel J, Sun M, Sleeman K, Timani KA, Aligo J, Rota P, Wu J, He B. 2015. Regulation of Viral RNA Synthesis by the V Protein of Parainfluenza Virus 5. J Virol 89:11845-57.

55. Sauder CJ, Zhang CX, Ngo L, Werner K, Lemon K, Duprex WP, Malik T, Carbone K, Rubin SA. 2011. Gene-specific contributions to mumps virus neurovirulence and neuroattenuation. J Virol 85:7059-69.

56. Shaw ML, Cardenas WB, Zamarin D, Palese P, Basler CF. 2005. Nuclear localization of the Nipah virus W protein allows for inhibition of both virus- and toll-like receptor 3-triggered signaling pathways. J Virol 79:6078-88.

57. Elango N. 1989. Complete nucleotide sequence of the matrix protein mRNA of mumps virus. Virology 168:426-8.

58. Mottet-Osman G, Miazza V, Vidalain PO, Roux L. 2014. Patchwork structure-function analysis of the Sendai virus matrix protein. Virology 464-465:330-340.

59. Naim HY, Ehler E, Billeter MA. 2000. Measles virus matrix protein specifies apical virus release and glycoprotein sorting in epithelial cells. EMBO J 19:3576-85.

60. Li M, Schmitt PT, Li Z, McCrory TS, He B, Schmitt AP. 2009. Mumps virus matrix, fusion, and nucleocapsid proteins cooperate for efficient production of virus-like particles. J Virol 83:7261-72.

61. Pei Z, Bai Y, Schmitt AP. 2010. PIV5 M protein interaction with host protein angiomotin-like 1. Virology 397:155-66.

62. Pei Z, Harrison MS, Schmitt AP. 2011. Parainfluenza virus 5 m protein interaction with host protein 14-3-3 negatively affects virus particle formation. J Virol 85:2050-9.

63. Schmitt AP, Leser GP, Morita E, Sundquist WI, Lamb RA. 2005. Evidence for a new viral late-domain core sequence, FPIV, necessary for budding of a paramyxovirus. J Virol 79:2988-97.

64. Merz DC, Server AC, Waxham MN, Wolinsky JS. 1983. Biosynthesis of mumps virus F glycoprotein: non-fusing strains efficiently cleave the F glycoprotein precursor. J Gen Virol 64 (Pt 7):1457-67.

65. Waxham MN, Server AC, Goodman HM, Wolinsky JS. 1987. Cloning and sequencing of the mumps virus fusion protein gene. Virology 159:381-8.

66. Chang A, Dutch RE. 2012. Paramyxovirus fusion and entry: multiple paths to a common end. Viruses 4:613-36.

67. Liu Y, Xu Y, Lou Z, Zhu J, Hu X, Gao GF, Qiu B, Rao Z, Tien P. 2006. Structural characterization of mumps virus fusion protein core. Biochem Biophys Res Commun 348:916-22.

68. Liu Y, Xu Y, Zhu J, Qiu B, Rao Z, Gao GF, Tien P. 2005. Crystallization and preliminary X-ray diffraction analysis of central structure domains from mumps virus F protein. Acta Crystallogr Sect F Struct Biol Cryst Commun 61:855-7.

69. Liu Y, Zhu J, Feng MG, Tien P, Gao GF. 2004. Six-helix bundle assembly and analysis of the central core of mumps virus fusion protein. Arch Biochem Biophys 421:143-8.

70. Bose S, Heath CM, Shah PA, Alayyoubi M, Jardetzky TS, Lamb RA. 2013. Mutations in the parainfluenza virus 5 fusion protein reveal domains important for fusion triggering and metastability. J Virol 87:13520-31.

71. Lamb RA, Paterson RG, Jardetzky TS. 2006. Paramyxovirus membrane fusion: lessons from the F and HN atomic structures. Virology 344:30-7.

72. Elango N, Kovamees J, Varsanyi TM, Norrby E. 1989. mRNA sequence and deduced amino acid sequence of the mumps virus small hydrophobic protein gene. J Virol 63:1413-5.

73. Hiebert SW, Richardson CD, Lamb RA. 1988. Cell surface expression and orientation in membranes of the 44-amino-acid SH protein of simian virus 5. J Virol 62:2347-57.

74. Wilson RL, Fuentes SM, Wang P, Taddeo EC, Klatt A, Henderson AJ, He B. 2006. Function of small hydrophobic proteins of paramyxovirus. J Virol 80:1700-9.

75. Xu P, Li Z, Sun D, Lin Y, Wu J, Rota PA, He B. 2011. Rescue of wild-type mumps virus from a strain associated with recent outbreaks helps to define the role of the SH ORF in the pathogenesis of mumps virus. Virology 417:126-36.

76. Kunkel U, Driesel G, Henning U, Gerike E, Willers H, Schreier E. 1995. Differentiation of vaccine and wild mumps viruses by polymerase chain reaction and nucleotide sequencing of the SH gene: brief report. J Med Virol 45:121-6.

77. Yeo RP, Afzal MA, Forsey T, Rima BK. 1993. Identification of a new mumps virus lineage by nucleotide sequence analysis of the SH gene of ten different strains. Arch Virol 128:371-7.

78. Waxham MN, Merz DC, Wolinsky JS. 1986. Intracellular maturation of mumps virus hemagglutinin-neuraminidase glycoprotein: conformational changes detected with monoclonal antibodies. J Virol 59:392-400.

79. Yuan P, Thompson TB, Wurzburg BA, Paterson RG, Lamb RA, Jardetzky TS. 2005. Structural studies of the parainfluenza virus 5 hemagglutinin-neuraminidase tetramer in complex with its receptor, sialyllactose. Structure 13:803-15.

80. Colman PM, Hoyne PA, Lawrence MC. 1993. Sequence and structure alignment of paramyxovirus hemagglutinin-neuraminidase with influenza virus neuraminidase. J Virol 67:2972-80.

81. Crennell S, Takimoto T, Portner A, Taylor G. 2000. Crystal structure of the multifunctional paramyxovirus hemagglutinin-neuraminidase. Nat Struct Biol 7:1068-74.

82. Reyes-Leyva J, Banos R, Borraz-Arguello M, Santos-Lopez G, Rosas N, Alvarado G, Herrera I, Vallejo V, Tapia-Ramirez J. 2007. Amino acid change 335

E to K affects the sialic-acid-binding and neuraminidase activities of Urabe AM9 mumps virus hemagglutinin-neuraminidase glycoprotein. Microbes Infect 9:234-40.

83. Sanchez-Betancourt JI, Santos-Lopez G, Alonso R, Doporto JM, Ramirez-Mendoza H, Mendoza S, Hernandez J, Reyes-Leyva J, Trujillo ME. 2008. Molecular characterization of the hemagglutinin-neuraminidase gene of porcine rubulavirus isolates associated with neurological disorders in fattening and adult pigs. Res Vet Sci 85:359-67.

84. Scheid A, Hsu M, Choppin PW. 1980. Role of paramyxovirus glycoproteins in the interactions between viral and cell membranes. Soc Gen Physiol Ser 34:119-30.

85. Merz DC, Wolinsky JS. 1983. Conversion of nonfusing mumps virus infections to fusing infections by selective proteolysis of the HN glycoprotein. Virology 131:328-40.

86. Liang B. 2020. Structures of the Mononegavirales Polymerases. J Virol doi:10.1128/JVI.00175-20.

87. Grdzelishvili VZ, Smallwood S, Tower D, Hall RL, Hunt DM, Moyer SA. 2005. A single amino acid change in the L-polymerase protein of vesicular stomatitis virus completely abolishes viral mRNA cap methylation. J Virol 79:7327-37.

88. Hercyk N, Horikami SM, Moyer SA. 1988. The vesicular stomatitis virus L protein possesses the mRNA methyltransferase activities. Virology 163:222-5.

89. Ogino T, Kobayashi M, Iwama M, Mizumoto K. 2005. Sendai virus RNA-dependent RNA polymerase L protein catalyzes cap methylation of virus-specific mRNA. J Biol Chem 280:4429-35.

90. Poch O, Blumberg BM, Bougueleret L, Tordo N. 1990. Sequence comparison of five polymerases (L proteins) of unsegmented negative-strand RNA viruses: theoretical assignment of functional domains. J Gen Virol 71 (Pt 5):1153-62.

91. Poch O, Sauvaget I, Delarue M, Tordo N. 1989. Identification of four conserved motifs among the RNA-dependent polymerase encoding elements. EMBO J 8:3867-74.

92. Li J, Rahmeh A, Morelli M, Whelan SP. 2008. A conserved motif in region v of the large polymerase proteins of nonsegmented negative-sense RNA viruses that is essential for mRNA capping. J Virol 82:775-84.

93. Feller JA, Smallwood S, Horikami SM, Moyer SA. 2000. Mutations in conserved domains IV and VI of the large (L) subunit of the sendai virus RNA polymerase give a spectrum of defective RNA synthesis phenotypes. Virology 269:426-39.

94. Cevik B, Smallwood S, Moyer SA. 2003. The L-L oligomerization domain resides at the very N-terminus of the sendai virus L RNA polymerase protein. Virology 313:525-36.

95. Cevik B, Holmes DE, Vrotsos E, Feller JA, Smallwood S, Moyer SA. 2004. The phosphoprotein (P) and L binding sites reside in the N-terminus of the L subunit of the measles virus RNA polymerase. Virology 327:297-306.

96. Horikami SM, Smallwood S, Bankamp B, Moyer SA. 1994. An amino-proximal domain of the L protein binds to the P protein in the measles virus RNA polymerase complex. Virology 205:540-5.

97. Holmes DE, Moyer SA. 2002. The phosphoprotein (P) binding site resides in the N terminus of the L polymerase subunit of sendai virus. J Virol 76:3078-83.

98. Emerson SU, Yu Y. 1975. Both NS and L proteins are required for in vitro RNA synthesis by vesicular stomatitis virus. J Virol 15:1348-56.

99. Abraham G, Banerjee AK. 1976. Sequential transcription of the genes of vesicular stomatitis virus. Proc Natl Acad Sci U S A 73:1504-8.

100. Ball LA, White CN. 1976. Order of transcription of genes of vesicular stomatitis virus. Proc Natl Acad Sci U S A 73:442-6.

101. Iverson LE, Rose JK. 1982. Sequential synthesis of 5'-proximal vesicular stomatitis virus mRNA sequences. J Virol 44:356-65.

102. Bernard JP, Northrop RL. 1974. RNA polymerase in mumps virion. J Virol 14:183-6.

103. Emerson SU. 1982. Reconstitution studies detect a single polymerase entry site on the vesicular stomatitis virus genome. Cell 31:635-42.

104. Bhella D, Ralph A, Murphy LB, Yeo RP. 2002. Significant differences in nucleocapsid morphology within the Paramyxoviridae. J Gen Virol 83:1831-1839.

105. Fuentes SM, Sun D, Schmitt AP, He B. 2010. Phosphorylation of paramyxovirus phosphoprotein and its role in viral gene expression. Future Microbiol 5:9-13.

106. Schmitt AP, Lamb RA. 2004. Escaping from the cell: assembly and budding of negative-strand RNA viruses. Curr Top Microbiol Immunol 283:145-96.

107. Tanabayashi K, Takeuchi K, Okazaki K, Hishiyama M, Yamada A. 1992. Expression of mumps virus glycoproteins in mammalian cells from cloned cDNAs: both F and HN proteins are required for cell fusion. Virology 187:801-4.

108. Paterson RG, Hiebert SW, Lamb RA. 1985. Expression at the cell surface of biologically active fusion and hemagglutinin/neuraminidase proteins of the paramyxovirus simian virus 5 from cloned cDNA. Proc Natl Acad Sci U S A 82:7520-4.

109. Alayyoubi M, Leser GP, Kors CA, Lamb RA. 2015. Structure of the paramyxovirus parainfluenza virus 5 nucleoprotein-RNA complex. Proc Natl Acad Sci U S A 112:E1792-9.

110. Severin C, Terrell JR, Zengel JR, Cox R, Plemper RK, He B, Luo M. 2016. Releasing the Genomic RNA Sequestered in the Mumps Virus Nucleocapsid. J Virol 90:10113-10119.

111. Gard S, Von Magnus P, Svedmyr A, Birch-Andersen A. 1952. Studies on the sedimentation of influenza virus. Arch Gesamte Virusforsch 4:591-611.

112. Manzoni TB, Lopez CB. 2018. Defective (interfering) viral genomes re-explored: impact on antiviral immunity and virus persistence. Future Virol 13:493-503.

113. Beale AJ, Finter NB. 1956. The infectivity of chorio-allantoic membrane influenza virus and incomplete influenza virus by the six-hour soluble antigen production test. J Hyg (Lond) 54:68-78.

114. Bellett AJ, Cooper PD. 1959. Some properties of the transmissible interfering component of vesicular stomatitis virus preparations. J Gen Microbiol 21:498-509.

115. Cooper PD, Bellett AJ. 1959. A transmissible interfering component of vesicular stomatitis virus preparations. J Gen Microbiol 21:485-97.

116. Mims CA. 1956. Rift Valley Fever virus in mice. IV. Incomplete virus; its production and properties. Br J Exp Pathol 37:129-43.

117. Sokol F, Neurath AR, Vilcek J. 1964. Formation of Incomplete Sendai Virus in Embryonated Eggs. Acta Virol 8:59-67.

118. Huang AS, Baltimore D. 1970. Defective viral particles and viral disease processes. Nature 226:325-7.

119. Bruton CJ, Porter A, Kennedy SI. 1976. Defective-interfering particles of Semliki Forest virus: intracellular events during interference. J Gen Virol 31:397-416.

120. Wiktor TJ, Dietzschold B, Leamnson RN, Koprowski H. 1977. Induction and biological properties of defective interfering particles of rabies virus. J Virol 21:626-35.

121. Hall WW, Martin SJ, Gould E. 1974. Defective interfering particles produced during the replication of measles virus. Med Microbiol Immunol 160:155-64.

122. Kolakofsky D. 1976. Isolation and characterization of Sendai virus DI-RNAs. Cell 8:547-55.

123. Murphy DG, Dimock K, Kang CY. 1987. Defective interfering particles of human parainfluenza virus 3. Virology 158:439-43.

124. Salinas Y, Roux L. 2005. Replication and packaging properties of short Paramyxovirus defective RNAs. Virus Res 109:125-32.

125. Genoyer E, Lopez CB. 2019. The Impact of Defective Viruses on Infection and Immunity. Annu Rev Virol 6:547-566.

126. Ziegler CM, Botten JW. 2020. Defective Interfering Particles of Negative-Strand RNA Viruses. Trends Microbiol 28:554-565.

127. Schubert M, Lazzarini RA. 1981. Structure and origin of a snapback defective interfering particle RNA of vesicular stomatitis virus. J Virol 37:661-72.

128. Dimmock NJ, Easton AJ. 2014. Defective interfering influenza virus RNAs: time to reevaluate their clinical potential as broad-spectrum antivirals? J Virol 88:5217-27.

129. Calain P, Curran J, Kolakofsky D, Roux L. 1992. Molecular cloning of natural paramyxovirus copy-back defective interfering RNAs and their expression from DNA. Virology 191:62-71.

130. Yoshida A, Kawabata R, Honda T, Sakai K, Ami Y, Sakaguchi T, Irie T. 2018. A Single Amino Acid Substitution within the Paramyxovirus Sendai Virus Nucleoprotein Is a Critical Determinant for Production of Interferon-Beta-Inducing Copyback-Type Defective Interfering Genomes. J Virol 92.

131. Baum A, Sachidanandam R, Garcia-Sastre A. 2010. Preference of RIG-I for short viral RNA molecules in infected cells revealed by next-generation sequencing. Proc Natl Acad Sci U S A 107:16303-8.

132. Yoshida A, Kawabata R, Honda T, Tomonaga K, Sakaguchi T, Irie T. 2015. IFN-beta-inducing, unusual viral RNA species produced by paramyxovirus infection accumulated into distinct cytoplasmic structures in an RNA-type-dependent manner. Front Microbiol 6:804.

133. Horikami SM, Curran J, Kolakofsky D, Moyer SA. 1992. Complexes of Sendai virus NP-P and P-L proteins are required for defective interfering particle genome replication in vitro. J Virol 66:4901-8.

134. Myers TM, Pieters A, Moyer SA. 1997. A highly conserved region of the Sendai virus nucleocapsid protein contributes to the NP-NP binding domain. Virology 229:322-35.

135. Curran J, Boeck R, Lin-Marq N, Lupas A, Kolakofsky D. 1995. Paramyxovirus phosphoproteins form homotrimers as determined by an epitope dilution assay, via predicted coiled coils. Virology 214:139-49.

136. Tarbouriech N, Curran J, Ruigrok RW, Burmeister WP. 2000. Tetrameric coiled coil domain of Sendai virus phosphoprotein. Nat Struct Biol 7:777-81.

137. Curran J, Marq JB, Kolakofsky D. 1995. An N-terminal domain of the Sendai paramyxovirus P protein acts as a chaperone for the NP protein during the nascent chain assembly step of genome replication. J Virol 69:849-55.

138. Curran J. 1996. Reexamination of the Sendai virus P protein domains required for RNA synthesis: a possible supplemental role for the P protein. Virology 221:130-40.

139. Kingston RL, Hamel DJ, Gay LS, Dahlquist FW, Matthews BW. 2004. Structural basis for the attachment of a paramyxoviral polymerase to its template. Proc Natl Acad Sci U S A 101:8301-6.

140. Chen M, Ogino T, Banerjee AK. 2006. Mapping and functional role of the self-association domain of vesicular stomatitis virus phosphoprotein. J Virol 80:9511-8.

141. Ding H, Green TJ, Lu S, Luo M. 2006. Crystal structure of the oligomerization domain of the phosphoprotein of vesicular stomatitis virus. J Virol 80:2808-14.

142. Chenik M, Schnell M, Conzelmann KK, Blondel D. 1998. Mapping the interacting domains between the rabies virus polymerase and phosphoprotein. J Virol 72:1925-30.

143. Schoehn G, Iseni F, Mavrakis M, Blondel D, Ruigrok RW. 2001. Structure of recombinant rabies virus nucleoprotein-RNA complex and identification of the phosphoprotein binding site. J Virol 75:490-8.

144. Mavrakis M, Mehouas S, Real E, Iseni F, Blondel D, Tordo N, Ruigrok RW. 2006. Rabies virus chaperone: identification of the phosphoprotein peptide that keeps nucleoprotein soluble and free from non-specific RNA. Virology 349:422-9.

145. Ivanov I, Crepin T, Jamin M, Ruigrok RW. 2010. Structure of the dimerization domain of the rabies virus phosphoprotein. J Virol 84:3707-10.

146. Abdella R, Aggarwal M, Okura T, Lamb RA, He Y. 2020. Structure of a paramyxovirus polymerase complex reveals a unique methyltransferase-CTD conformation. Proc Natl Acad Sci U S A 117:4931-4941.

147. Aggarwal M, Leser GP, Kors CA, Lamb RA. 2018. Structure of the Paramyxovirus Parainfluenza Virus 5 Nucleoprotein in Complex with an Amino-Terminal Peptide of the Phosphoprotein. J Virol 92.

148. De BP, Hoffman MA, Choudhary S, Huntley CC, Banerjee AK. 2000. Role of NH(2)- and COOH-terminal domains of the P protein of human parainfluenza virus type 3 in transcription and replication. J Virol 74:5886-95.

149. Richardson M, Elliman D, Maguire H, Simpson J, Nicoll A. 2001. Evidence base of incubation periods, periods of infectiousness and exclusion policies for the control of communicable diseases in schools and preschools. Pediatr Infect Dis J 20:380-91.

150. Wolinsky JS, Klassen T, Baringer JR. 1976. Persistence of neuroadapted mumps virus in brains of newborn hamsters after intraperitoneal inoculation. J Infect Dis 133:260-7.

151. Philip RN, Reinhard KR, Lackman DB. 1995. Observations on a mumps epidemic in a "virgin" population. 1958. Am J Epidemiol 142:233-53; discussion 231-2.

152. Marin M, Broder KR, Temte JL, Snider DE, Seward JF, Centers for Disease C, Prevention. 2010. Use of combination measles, mumps, rubella, and varicella vaccine: recommendations of the Advisory Committee on Immunization Practices (ACIP). MMWR Recomm Rep 59:1-12.

153. Buynak EB, Hilleman MR. 1966. Live attenuated mumps virus vaccine. 1. Vaccine development. Proc Soc Exp Biol Med 123:768-75.

154. Prevention CfDCa. 2020. Mumps Cases and Outbreaks. Accessed

155. Zengel J, Phan SI, Pickar A, Xu P, He B. 2017. Immunogenicity of mumps virus vaccine candidates matching circulating genotypes in the United States and China. Vaccine 35:3988-3994.

156. Soud FA, Cortese MM, Curns AT, Edelson PJ, Bitsko RH, Jordan HT, Huang AS, Villalon-Gomez JM, Dayan GH. 2009. Isolation compliance among

university students during a mumps outbreak, Kansas 2006. Epidemiol Infect 137:30-7.

157. Nelson GE, Aguon A, Valencia E, Oliva R, Guerrero ML, Reyes R, Lizama A, Diras D, Mathew A, Camacho EJ, Monforte MN, Chen TH, Mahamud A, Kutty PK, Hickman C, Bellini WJ, Seward JF, Gallagher K, Fiebelkorn AP. 2013. Epidemiology of a mumps outbreak in a highly vaccinated island population and use of a third dose of measles-mumps-rubella vaccine for outbreak control--Guam 2009 to 2010. Pediatr Infect Dis J 32:374-80.

158. Date AA, Kyaw MH, Rue AM, Klahn J, Obrecht L, Krohn T, Rowland J, Rubin S, Safranek TJ, Bellini WJ, Dayan GH. 2008. Long-term persistence of mumps antibody after receipt of 2 measles-mumps-rubella (MMR) vaccinations and antibody response after a third MMR vaccination among a university population. J Infect Dis 197:1662-8.

159. Murphy F. 1976. vol 9.15 MB, Public Health Image Library, CDC.

160. Maiuri A, Eckert, A. 2016. vol 18.04 MB. Public Health Image Library, CDC.

161. Karen C. Carroll SAM, Timothy Mietzner, Steve Miller. 2015. Jawetz, Melnick, & Adelberg's Medical Microbiology, 27 ed. McGraw-Hill Education.

162. White SJ, Boldt KL, Holditch SJ, Poland GA, Jacobson RM. 2012. Measles, mumps, and rubella. Clin Obstet Gynecol 55:550-9.

163. Werner CA. 1950. Mumps orchitis and testicular atrophy; occurrence. Ann Intern Med 32:1066-74.

164. Masarani M, Wazait H, Dinneen M. 2006. Mumps orchitis. J R Soc Med 99:573-5.

165. Mizushima N, Murakami Y. 1986. Deafness following mumps: the possible pathogenesis and incidence of deafness. Auris Nasus Larynx 13 Suppl 1:S55-7.

166. Rubin SA, Link MA, Sauder CJ, Zhang C, Ngo L, Rima BK, Duprex WP. 2012. Recent mumps outbreaks in vaccinated populations: no evidence of immune escape. J Virol 86:615-20.

167. McNabb SJ, Jajosky, R. A., Hall-Baker, P. A., Adams, D. A., Sharp, P., Anderson, W. J., Javier, A. J., Jones, G. J., Nitschke, D. A., Worshams, C. A., Richard, R. A. Jr. 2007. Summary of notifiable diseases - United States, 2005. Centers for Disease Control and Prevention (CDC),

168. Ortin J, Martin-Benito J. 2015. The RNA synthesis machinery of negative-stranded RNA viruses. Virology 479-480:532-44.

169. Waterhouse A, Bertoni M, Bienert S, Studer G, Tauriello G, Gumienny R, Heer FT, de Beer TAP, Rempfer C, Bordoli L, Lepore R, Schwede T. 2018. SWISS-MODEL: homology modelling of protein structures and complexes. Nucleic Acids Res 46:W296-W303.

170. Nayak D, Panda D, Das SC, Luo M, Pattnaik AK. 2009. Single-amino-acid alterations in a highly conserved central region of vesicular stomatitis virus N protein differentially affect the viral nucleocapsid template functions. J Virol 83:5525-34.

171. Zengel J, Pickar A, Xu P, Lin A, He B. 2015. Roles of Phosphorylation of the Nucleocapsid Protein of Mumps Virus in Regulating Viral RNA Transcription and Replication. J Virol 89:7338-47.

172. Andzhaparidze OG, Boriskin Yu S, Bogomolova NN, Drynov ID. 1982. Mumps virus-persistently infected cell cultures release defective interfering virus particles. J Gen Virol 63:499-503.

173. Andzhaparidze OG, Boriskin Iu S, Bogomolova NN, Lotte VD. 1982. [Characteristics of mumps virus intracellular ribonucleoprotein during chronic infection of cell cultures]. Vopr Virusol 27:22-7.

174. Andzhaparidze OG, Boriskin Iu S, Bogomolova NN. 1982. [Defective interfering mumps virus produced by chronically infected cell cultures]. Vopr Virusol 27:405-8.

175. Bertoni M, Kiefer F, Biasini M, Bordoli L, Schwede T. 2017. Modeling protein quaternary structure of homo- and hetero-oligomers beyond binary interactions by homology. Sci Rep 7:10480.

176. Anonymous. 2016. Minor Variant Software v1.0 User Guide. Life Technologies, Carlsbad, CA.

177. Anonymous. 2013. Detection and Quantification of Sequence Variants from Sanger Sequencing Traces: Determination of minor alleles by analyzing peak height data. Life Technologies Corporation.

178. Yang Y, Lyu T, Zhou R, He X, Ye K, Xie Q, Zhu L, Chen T, Shen C, Wu Q, Zhang B, Zhao W. 2019. The Antiviral and Antitumor Effects of Defective Interfering Particles/Genomes and Their Mechanisms. Front Microbiol 10:1852.

179. Mura M, Combredet C, Najburg V, Sanchez David RY, Tangy F, Komarova AV. 2017. Nonencapsidated 5' Copy-Back Defective Interfering Genomes Produced

by Recombinant Measles Viruses Are Recognized by RIG-I and LGP2 but Not MDA5. J Virol 91.

180. Gould PS, Easton AJ, Dimmock NJ. 2017. Live Attenuated Influenza Vaccine contains Substantial and Unexpected Amounts of Defective Viral Genomic RNA. Viruses 9.

181. Huang AS. 1973. Defective interfering viruses. Annu Rev Microbiol 27:101-17.

182. Bdeir N, Arora P, Gartner S, Hoffmann M, Reichl U, Pohlmann S, Winkler M. 2019. A system for production of defective interfering particles in the absence of infectious influenza A virus. PLoS One 14:e0212757.

183. Killip MJ, Young DF, Gatherer D, Ross CS, Short JA, Davison AJ, Goodbourn S, Randall RE. 2013. Deep sequencing analysis of defective genomes of parainfluenza virus 5 and their role in interferon induction. J Virol 87:4798-807.

184. Lazzarini RA, Keene JD, Schubert M. 1981. The origins of defective interfering particles of the negative-strand RNA viruses. Cell 26:145-54.

185. G.G. R. 1991. Deletion Mutants of Paramyxoviruses doi:10.1007/978-1-4615-3790-8_10. Springer, Boston, MA.

186. Holland JJ, Doyle M. 1973. Attempts to detect homologous autointerference in vivo with influenza virus and vesicular stomatitis virus. Infect Immun 7:526-31.

187. Xu J, Sun Y, Li Y, Ruthel G, Weiss SR, Raj A, Beiting D, Lopez CB. 2017. Replication defective viral genomes exploit a cellular pro-survival mechanism to establish paramyxovirus persistence. Nat Commun 8:799.

188. Yount JS, Gitlin L, Moran TM, Lopez CB. 2008. MDA5 participates in the detection of paramyxovirus infection and is essential for the early activation of

dendritic cells in response to Sendai Virus defective interfering particles. J Immunol 180:4910-8.

189. Childs K, Stock N, Ross C, Andrejeva J, Hilton L, Skinner M, Randall R, Goodbourn S. 2007. mda-5, but not RIG-I, is a common target for paramyxovirus V proteins. Virology 359:190-200.

190. Banerjee AK, Barik S, De BP. 1991. Gene expression of nonsegmented negative strand RNA viruses. Pharmacol Ther 51:47-70.

191. Curran J, Pelet T, Kolakofsky D. 1994. An acidic activation-like domain of the Sendai virus P protein is required for RNA synthesis and encapsidation. Virology 202:875-84.

192. Smallwood S, Ryan KW, Moyer SA. 1994. Deletion analysis defines a carboxyl-proximal region of Sendai virus P protein that binds to the polymerase L protein. Virology 202:154-63.

193. Kolakofsky D, Le Mercier P, Iseni F, Garcin D. 2004. Viral DNA polymerase scanning and the gymnastics of Sendai virus RNA synthesis. Virology 318:463-73.

194. Rahaman A, Srinivasan N, Shamala N, Shaila MS. 2004. Phosphoprotein of the rinderpest virus forms a tetramer through a coiled coil region important for biological function. A structural insight. J Biol Chem 279:23606-14.

195. Asenjo A, Villanueva N. 2000. Regulated but not constitutive human respiratory syncytial virus (HRSV) P protein phosphorylation is essential for oligomerization. FEBS Lett 467:279-84.

196. Castagne N, Barbier A, Bernard J, Rezaei H, Huet JC, Henry C, Costa BD, Eleouet JF. 2004. Biochemical characterization of the respiratory syncytial virus P-P and P-N protein complexes and localization of the P protein oligomerization domain. J Gen Virol 85:1643-1653.

197. Chattopadhyay S, Banerjee AK. 2009. Phosphoprotein, P of human parainfluenza virus type 3 prevents self-association of RNA-dependent RNA polymerase, L. Virology 383:226-36.

198. Communie G, Crepin T, Maurin D, Jensen MR, Blackledge M, Ruigrok RW. 2013. Structure of the tetramerization domain of measles virus phosphoprotein. J Virol 87:7166-9.

199. Communie G, Habchi J, Yabukarski F, Blocquel D, Schneider R, Tarbouriech N, Papageorgiou N, Ruigrok RW, Jamin M, Jensen MR, Longhi S, Blackledge M. 2013. Atomic resolution description of the interaction between the nucleoprotein and phosphoprotein of Hendra virus. PLoS Pathog 9:e1003631.

200. Leyrat C, Renner M, Harlos K, Grimes JM. 2013. Solution and crystallographic structures of the central region of the phosphoprotein from human metapneumovirus. PLoS One 8:e80371.

201. Gao Y, Lenard J. 1995. Cooperative binding of multimeric phosphoprotein (P) of vesicular stomatitis virus to polymerase (L) and template: pathways of assembly. J Virol 69:7718-23.

202. Gao Y, Lenard J. 1995. Multimerization and transcriptional activation of the phosphoprotein (P) of vesicular stomatitis virus by casein kinase-II. EMBO J 14:1240-7.

203. Ryan KW, Kingsbury DW. 1988. Carboxyl-terminal region of Sendai virus P protein is required for binding to viral nucleocapsids. Virology 167:106-12.

204. Garcia-Barreno B, Delgado T, Melero JA. 1996. Identification of protein regions involved in the interaction of human respiratory syncytial virus phosphoprotein and nucleoprotein: significance for nucleocapsid assembly and formation of cytoplasmic inclusions. J Virol 70:801-8.

205. Chambers P, Pringle CR, Easton AJ. 1990. Heptad repeat sequences are located adjacent to hydrophobic regions in several types of virus fusion glycoproteins. J Gen Virol 71 (Pt 12):3075-80.

206. Deng Y, Zheng Q, Liu J, Cheng CS, Kallenbach NR, Lu M. 2007. Self-assembly of coiled-coil tetramers in the 1.40 A structure of a leucine-zipper mutant. Protein Sci 16:323-8.

207. Yachdav G KE, Kajan L, Hecht M, Goldberg T, Hamp T, Honigschmid P, Schafferhans A, Roos M, Bernhofer M. 2014. PredictProtein - an open resource for online prediction of protein structural and functional features. Nucleic acids research gku366.

208. Lupas A VDM, Stock J. 1991. Predicting Coiled Coils from Protein Sequences. Science 252:1162-1164.

209. Combet C BC, Geourjon C, Deleage G. March 2000. NPS@: Network Protein Sequence Analysis. PBIL (Pole Bioinformatique Lyonnais) 25:147-150.

210. Harbury PB, Zhang T, Kim PS, Alber T. 1993. A switch between two-, three-, and four-stranded coiled coils in GCN4 leucine zipper mutants. Science 262:1401-7.

211. Wagschal K, Tripet B, Lavigne P, Mant C, Hodges RS. 1999. The role of position a in determining the stability and oligomerization state of alpha-helical coiled coils: 20 amino acid stability coefficients in the hydrophobic core of proteins. Protein Sci 8:2312-29.

212. Ramos J, Lazaridis T. 2011. Computational analysis of residue contributions to coiled-coil topology. Protein Sci 20:1845-55.

213. Grigorian G KA. 2008. Structural specificity in coiled coil interactions. Current Opinions in Structural Biology 18:477-483.

214. Gernert KM, Surles MC, Labean TH, Richardson JS, Richardson DC. 1995. The Alacoil: a very tight, antiparallel coiled-coil of helices. Protein Sci 4:2252-60.

215. Liu J, Zheng Q, Deng Y, Li Q, Kallenbach NR, Lu M. 2007. Conformational specificity of the lac repressor coiled-coil tetramerization domain. Biochemistry 46:14951-9.

216. Hadley EB, Testa OD, Woolfson DN, Gellman SH. 2008. Preferred side-chain constellations at antiparallel coiled-coil interfaces. Proc Natl Acad Sci U S A 105:530-5.

217. SD C. 1929. Age Incidence of the Common Communicable Diseases of Children: A Study of Case Rates among All Children and among Children Not Previously Attacked and of Death Rates and the Estimated Case Fatality.

218. Bitsko RH, Cortese MM, Dayan GH, Rota PA, Lowe L, Iversen SC, Bellini WJ. 2008. Detection of RNA of mumps virus during an outbreak in a population with a high level of measles, mumps, and rubella vaccine coverage. J Clin Microbiol 46:1101-3.

APPENDIX

SUPPLEMENTARY FOR CHAPTER 4

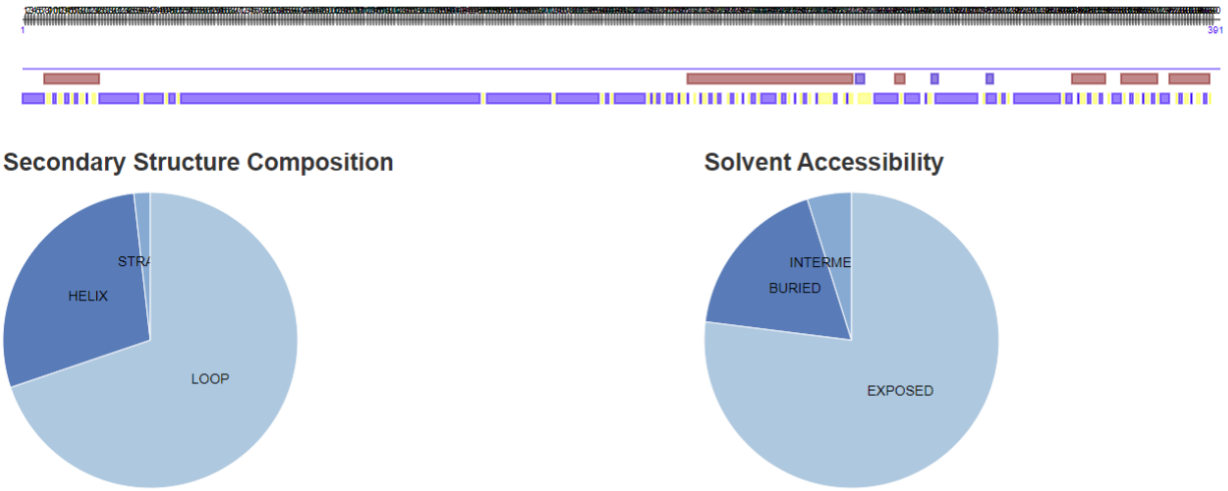

Figure A1. PredictProtein Software prediction for secondary structures and solvent accessibility of MuV P. Residues 1-391 of MuV phosphoprotein were entered into the PredictProtein Software and structural and solvent characteristics were predicted for each site. The purple regions denote areas that are exposed (outer surface of the protein) while yellow regions are predicted to be areas buried within the protein (inner surface). Red regions denote helix prediction regions of the protein (207).

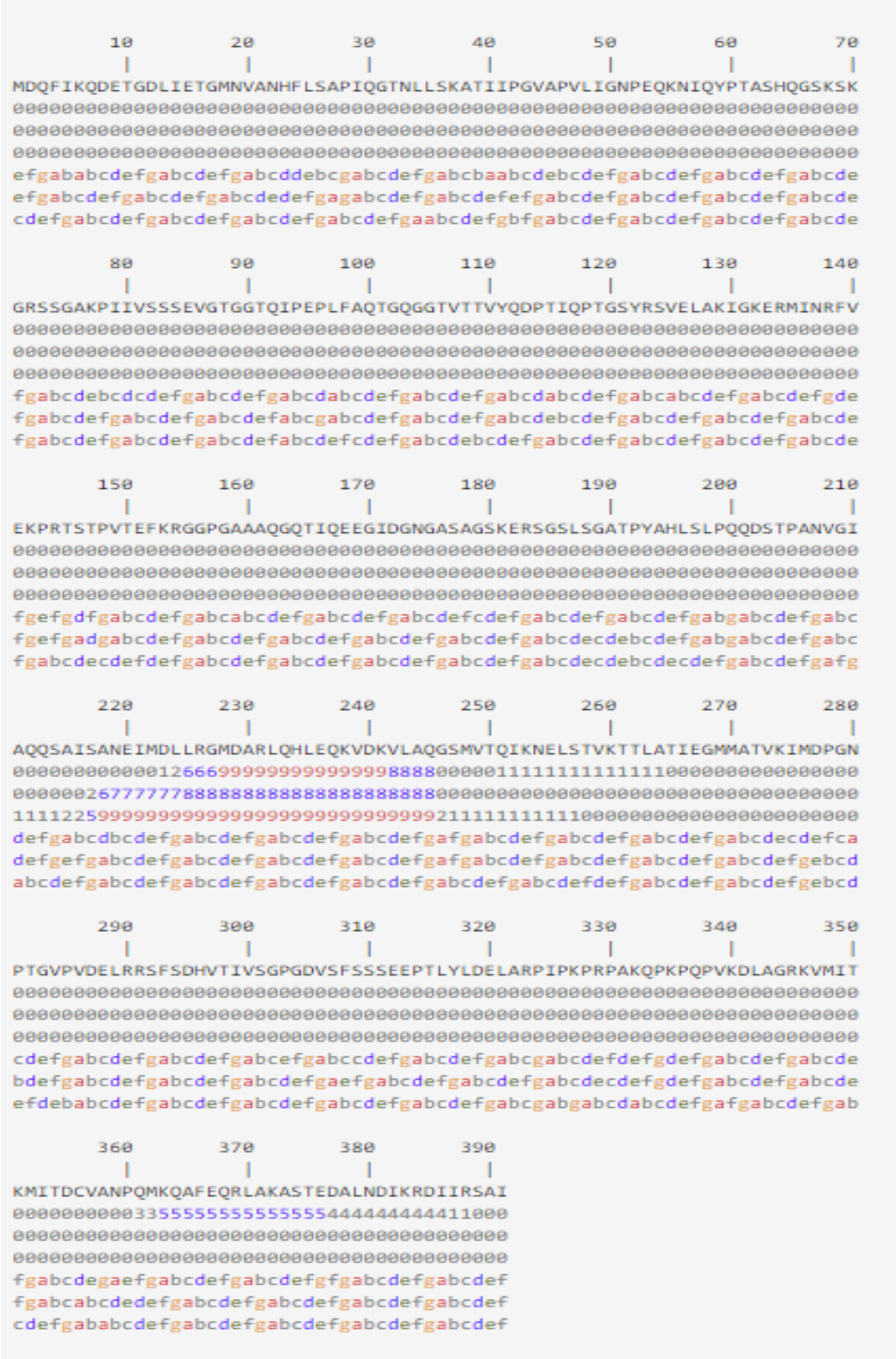

Figure A2. Coiled-Coils Software prediction for MuV P heptad repeat. The heptad repeat is denoted with various colored letters (abcdefg). Three output row iterations are provided with numbers 0-9 denoting likelihood for left-handed monomeric coils (208, 209).